THE NEUTRON-DEUTERON BREAKUP CROSS SECTION BETWEEN 8 AND 22 MeV

G. PAULETTA

A thesis submitted to the
University of Cape Town
for the degree of
Doctor of Philosophy

September 1973

ABSTRACT

The n-d breakup cross section has been measured at eleven energies between 8 and 22 MeV by integrating the energy distributions of breakup protons in a deuterated scintillator. The breakup protons were separated from the recoil deuterons by pulse shape discrimination. A comparison of these measurements with recent calculations favours those performed with local potentials.

ACKNOWLEDGEMENTS

The author wishes to thank the following.

His supervisor, Prof. F.D. Brooks for guidance, help and encouragement;

The staff of the Southern Universities Nuclear Institute for their cooperation;

Students and staff of the University of Cape Town for proof reading the manuscript;

Mrs. E.B. Prosser who typed this manuscript;

Mr. H. Schmidt who helped to prepare the diagrams;

The South African Council for Scientific and Industrial Research for financial assistance;

His parents for support and encouragement;

Miss Mandy Jerram for her selfless assistance during the writing and preparation of the manuscript.

CONTENTS

CONTENTS

LIST OF FIGURES

Fig.6.4(a) Proton energy spectra from $^{2}H(n,p)2n$ at 14.1 MeV for various angles of proton emission

Fig.6.4(b) Dalitz spectrum for the p+d → p+p+n reaction

Fig.6.4.(c) Angular distribution of d^{*}

Fig.6.5 A schematic diagram indicating the expected position of the enhancements due to various reaction mechanisms

Fig.6.6 Schematic diagram of an (LS) spectrum

Fig.6.7 An isometric representation of an (LS) spectrum obtained with deuterated anthracene

LIST OF TABLES

CHAPTER 1

INTRODUCTION

The system of three interacting nucleons belongs to the more general Nuclear Three-Body problem popularized by Faddeev's work (Fa61-63). Faddeev originated a formalism for describing such a system which is, in principle at least, exact. Subsequent to his work and the independent work of Mitra (Mi62) and Amado (Am63), who developed equivalent formalisms under the separable approximation, a renaissance of work with few nucleon systems was experienced which has often led people to ask whether the volume of work was commensurate with its physical significance.

In fact, the study of the system for its own sake is physically significant, for it is the simplest of the many body states and therefore an understanding of its mechanics is an important link between two widely differing approaches for handling two and many-body states. But it promises yet more exciting information concerning the nature of the nuclear forces which is not accessible to two-nucleon experiments, our most reliable windows on the nuclear interaction, namely the off-shell components of these interactions (Le73) and three-nucleon forces (No72).

There are many experimental observables in the three-nucleon system, ranging from bound-state parameters to particle correlations. They are sensitive in varying degrees to the details of nuclear forces. This work is concerned with the measurement of the n-d total breakup cross section in the energy range 8-22 MeV. It will be shown in section 1.3

that comparison of this quantity with theory could be significant.

To obtain a broader perspective, various ways in which the three-nucleon system is being employed to obtain information about nuclear forces are considered in the next section.

1.2 Nuclear Forces

Systems governed by a known interaction can be solved to an arbitrary degree of accuracy if sufficiently powerful numerical methods are used. An example of such a system is the atom, which is determined by the Coulomb interaction.

On the other hand, the nuclear interaction is not nearly as well established or well behaved. The study of nuclear matter therefore has a twofold purpose. On the one hand, we use our knowledge of the nuclear interaction to study dynamics and systematics of nuclear matter. On the other, we use simple nuclear systems, whose dynamics are well understood, to explore the nuclear interaction.

Until recently, an exact formalism existed only for the two-nucleon system. It could therefore be determined exactly once the nuclear interaction had been specified. The two-body system has been therefore, our principal window on the nuclear force.

Studies of the nuclear interaction fall into two categories: those which have some formal basis in field theory and those which are purely phenomenological. The former have succeeded in determining unambiguously, only the long range one pion exchange potential (OPEP) (Iw56). Phenomenological approaches seek to determine the interaction by testing it against the

full body of two-nucleon data, which is condensed in a number of partial wave phase parameters. The approach usually adopted is a semiphenomenological one, incorporating reliable theoretical components like the OPEP tail.

From such investigations we have learnt that the nuclear interaction is spin-dependent, isotopic spin-dependent, momentum-dependent, non-central and repulsive at short range (Si72).

Several potentials, incorporating all the known features of the nuclear forces, have been constructed to fit known phase parameters. Recent examples of these are the Reid soft core potentials (Re68) (Sp(70) and the Hamada-Johnston hard core potentials (Ha62) (Ha65). Nuclear matter has been shown to be sensitive to whether cores are "hard" (i.e. potential energy is infinite) or "soft" (i.e. Potential energy is near 1 GeV), but since the potentials are phase equivalent, one cannot distinguish between them on the basis of "on shell" two-nucleon data.

One therefore looks to the off-shell elements of the T-matrix (see Appendix A)to resolve such ambiguities.

Experimentally, one looks to processes like photo-disintegration of the deuteron and nucleon-nucleon bremsstrahlung. In these processes, energy is not conserved in the nucleon-nucleon system, since some of it belongs to the gamma radiation, which interacts weakly with the nucleons. The interpretation of these phenomena is confused however by the problem of correcting the electromagnetic Hamiltonian for mesonic exchange.

Another avenue of approach was emphasized by the formulation of a three-body theory (Fa61-63), which can, in

principle at least, determine the three-nucleon system exactly in terms of two-nucleon interactions, which are generally off-shell.

The application of such a theory to the three-nucleon system therefore provides an additional window on the nucleon-nucleon interactions. It is hoped that exact calculations of three-body observables will help to determine the off-shell structure, or form of the nuclear potential. In reality, the complexity of these calculations has, until recently, precluded the use of realistic potentials so that, with regard to bound state calculations at least, they have been matched by more conventional variational techniques. Their principle advantage lies in their ability to deal with the continuum state, for which purpose they were designed.

Nevertheless, bound-state calculations are easier and the most significant progress has been made in the application of sophisticated nucleon-nucleon interactions to the calculation of bound state parameters.

Recently, calculations for the triton bound-state have been reported for the Hamada-Johnston (De71) (Yu71) and the Reid (Ma70) (Tj70) (Ja71) (He72) (Bh72) using both variational methods and the Faddeev equations. The most recent of these yields triton binding energies of 7.75 ± .50 MeV for the Reid soft core (He72) potentials, and 6.5 - 6.7 MeV for the Hamada-Johnston hard core potentials (De71) (Yu71). It appears therefore, that the bound-state parameters are sensitive to the off-shell interactions, i.e. to the form of the potentials. However, discrepancies between the calculations using the Reid potential must be cleared up before any definite conclusions can be drawn (Am72). Other forms

of potential are also under investigation (Ha71)(Ha72).

The discrepancy between these calculations and the experimentally measured triton binding energy immediately suggests another way in which a three-nucleon system may reveal aspects of nuclear forces which are not observable in a two-nucleon system, namely three-nucleon forces.

These are forces which depend on the simultaneous presence of three nucleons. They have been the subject of much recent attention (No72) (Br72), but the evidence for their existence is inconclusive. One might naively suppose that the discrepancy in the calculated and measured binding energies is due to three-body forces, but one must first consider relativistic effects (Ja70) and a possible charge-dependence of nuclear forces (De71). These are, in principle, difficult to correct for since three-body forces, repulsive cores and relativistic corrections are theoretically inter-dependent (Am72), while the question of charge dependence (No72) and even charge symmetry of nuclear forces has still to be resolved.

A possible indication of charge asymmetry is given by the difference between the experimentally (0.77 MeV) and theoretically (0.6 MeV) determined Coulomb energy differences of ^{3}He and ^{3}H (Ok71).

The number of observables in the three-nucleon continuum state is greater than for the bound-state. However, owing to the difficulty of performing exact calculations in this state, progress in solving the scattering and breakup problems has been comparatively slower. Early calculations were characterised by S-wave, separable, central potentials (Aa65) (Aa66) (Du68) and have only recently been performed with S-wave

local potentials (Kl71) (Kl72) (Kl72a), and separable potentials including higher partial waves (Pi72) (Do73). Total cross sections, angular distributions and spin-observables show varying degrees of dependence on details of nuclear forces. These will be discussed in greater detail in the next section.

Three-nucleon scattering experiments can also be used to investigate the nuclear force by determining the kinematical configuration, so as to give prominence to some specific term of the interaction, thereby reducing its complexity.

The best known in this category of experiments are those performed to determine the n-n low-energy scattering parameters as a test of charge symmetry (Bo73). The kinematical configuration selected is such that two of the reaction products are in a state of low relative energy, so that the reaction is determined principally by their final-state interaction (FSI) (see Chapter 2). Energy and angular distributions can be compared with theory, e.g. (Wa52) to extract the low-energy scattering parameters (i.e. the scattering lengths and effective ranges) (Bo73).

Another example of such an experiment is the selection of kinematic configurations favouring quasi-free scattering (QFS) (Ch59) (Ku61). As implied by the terminology, this configuration corresponds to the incident nucleon interacting with one target nucleon, leaving the other unaffected. Such experiments can provide information about half-off-shell elements of N-N T-matrix.

1.3 n-d Scattering and Breakup

Since the spin S and isospin T of the deuteron are 1 and 0 respectively the 3-nucleon system can occur in either of two spin states, the doublet ($S = \frac{1}{2}$, $T = \frac{1}{2}$) and quartet ($S = \frac{3}{2}$, $T = \frac{1}{2}$) spin states. In the presence of non-central forces, transition amplitudes are not diagonal in L-S representation. These effects are, however, relatively small at our energies. The Pauli principle immediately suggests important characteristics for each channel.

The quartet state has an asymmetric spatial dependence. This means the nucleons cannot approach each other closely and this makes the interaction in this channel effectively repulsive (Am69). The doublet state, on the other hand, owing to the symmetry of the wave function, permits the nucleons to come closer together. One therefore expects this state to be more sensitive to details of the nuclear force.

A second characteristic of n-d scattering can be inferred from the structure of the deuteron, which is loosely bound and has an extended spatial distribution (Hu57). This leads one to expect exchange effects (Am69) in n-d scattering. Measurements of n-d elastic differential cross sections (see fig. 1.2) show strong forward and backward peaking. Early calculations (Ch53) use Born Approximation to obtain the starting points of phase analyses and correctly interpret this forward and backward peaking as being due to exchange effects. Another important observation made by these authors is that the elastic angular distributions are dominated by quartet phases and that they are not sensitive to details of

the nuclear interaction. This agrees well with the expected effect of the Pauli principle.

With regard to the doublet phases, the calculations once more bear out what is expected. These phases are sensitive to the nuclear interactions, but unfortunately contribute little to the elastic cross sections.

These early observations regarding the elastic differential cross section are corroborated by later "exact" calculations with separable S-wave potentials (see Chapter 3). Similar conclusions about the inelastic cross sections, however, were subsequently shown to be wrong by calculations of inelastic (Aa66) and elastic (Aa65) (Sl71) (Av69) cross sections in the "exact" formalism of Faddeev and Amado, as well as by various phase analyses (see Chapter 3).

These corroborate the sensitivity of doublet phase-shifts to the nuclear force and show that a large part of the absorption takes place in the doublet state (Sl71) (Aa66) (see Chapter 3). The breakup cross section is therefore expected to be sensitive to the details of the nuclear force.

An interesting relation between the doublet phase and the triton binding energy was discovered (Ph68). It was found that when all calculations of the binding energy and a_2 are plotted against each other, they fall on a straight line, which gives a scattering length of about 0.8 ± 2 fm for the known binding energy. This implies that the doublet scattering length ^2S is directly related to the triton binding energy and is therefore, equally sensitive to the details of the nuclear force. However, some doubt has been cast on this correlation by a new prediction of 0.15 ± 0.05 fm for the doublet scattering length (Va67a).

Early "exact" calculations reproduced the main features of the elastic differential cross sections but yielded zero vector polarizations since they incorporated only central forces. However, non-negligible polarizations were being observed. To account for these, efforts were made to include non-central components in the potentials. Separable tensor components (Ya54) as well as higher partial waves were included exactly (Aa72) (Do73), as well as by perturbation methods (Pi72) (Pi72a) (Pi73).

Meanwhile, exact calculations had been successfully performed using local potentials (Kl72) (Kl71) (Kl73). Total breakup cross sections were calculated with S-wave, spin dependent potentials of the Yukawa type. Repulsive cores were included in the singlet states for one set of calculations and in both the singlet and triplet in another. Soft cores of the Reid type were also considered. Doublet phase shifts and the total breakup cross section were found to be sensitive to the nature of the potential.

It is apparent from the fore-going account, that total breakup cross sections are sensitive to the details of the nuclear force and that we have now reached a stage where comparison of experiment with theory would be significant.

Direct measurements of the total n-d breakup cross section exist only up to 14.1 MeV (see Chapter 3). At energies above 23 MeV, the total p-d breakup cross section has recently been measured (Ca72). Between these energies, no direct measurements exist. Values have been obtained by integrating the differential n-d elastic cross section data and subtracting from the total (n-d) cross section at 18.55,

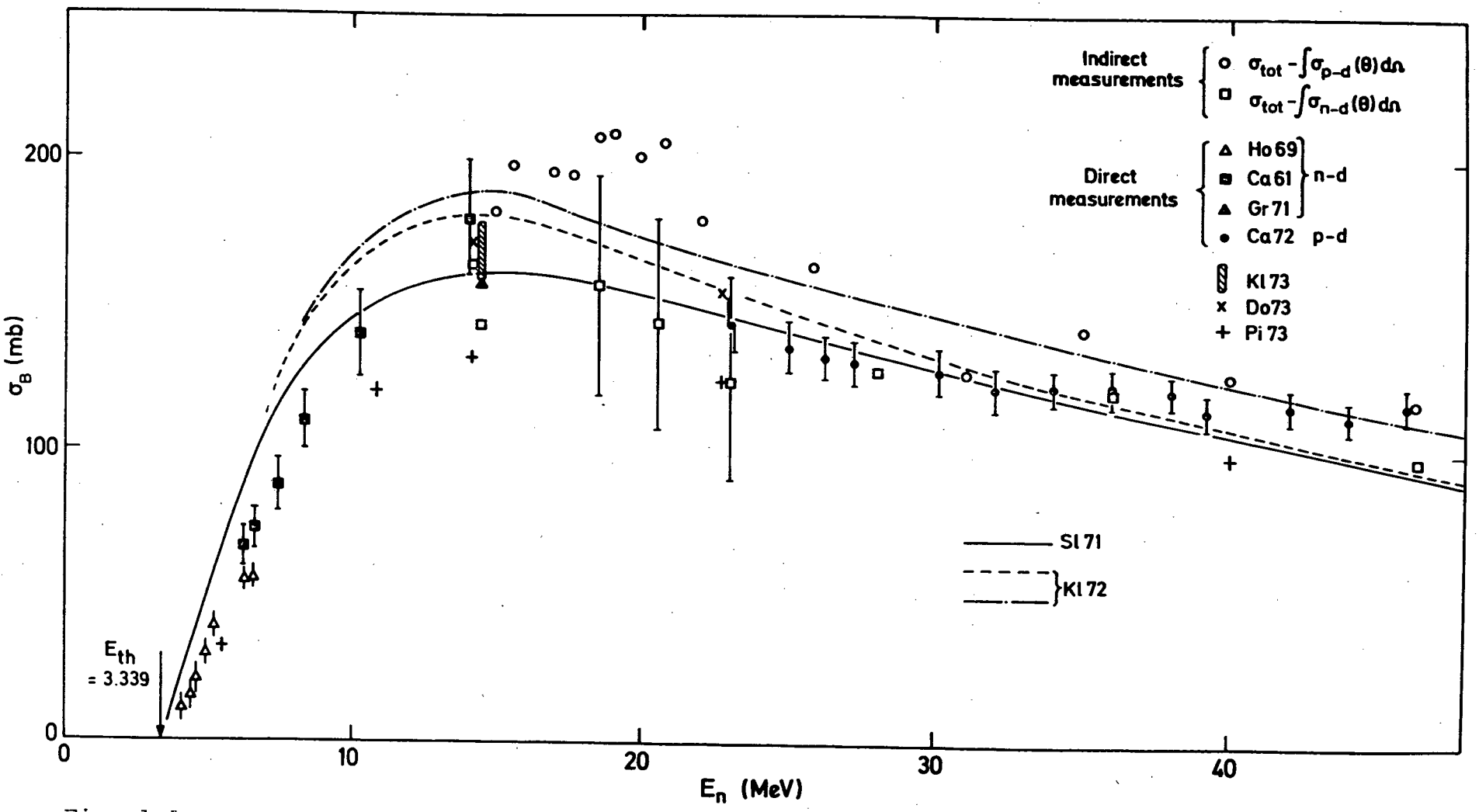

Fig. 1.1. Measurements and calculations of the total N-d breakup cross section below 50 MeV. Indirect measurements are included only for incident energies greater than 14 MeV.

20.50 and 23 MeV (Se72). These values, together with the p-d values, are considerably lower than values obtained by subtraction of integrated (p-d) elastic differential cross sections from the total n-d cross section after correction for Coulomb interference at forward angles (see Chapter 3).

We have seen above, that angular N-d differential cross sections, being dominated by the quartet phase, are very insensitive to details of the nuclear force. They can therefore be expected to be largely independent of any possible charge dependence of the nuclear force. In fact, (n-d) and (p-d) differential cross sections are found to agree very well above 14 MeV (see fig. I.2) and (Ho68)) except for Coulomb interference forward angles.

The reaction n+d → n+n+p offers a wide variety of observables because of the presence of three particles in the final state. To determine the reaction completely, one must define five variables, e.g. the angles of emission of two particles, and the energy of one. By performing such kinematically "complete" experiments, one can define kinematic conditions such that some desired reaction mechanism is dominant; for example, the final-state interaction (FSI) mechanism (see Chapter 2).

When all five kinematic variables are not determined, the experiment is termed "incomplete". These are not so exclusive as to isolate any particular mechanism. They afford, however, a view of how mechanisms combine, i.e. they permit us to study the mechanisms together with their interference.

An example of such an incomplete experiment is the measurement of the energy spectrum of some particle emitted

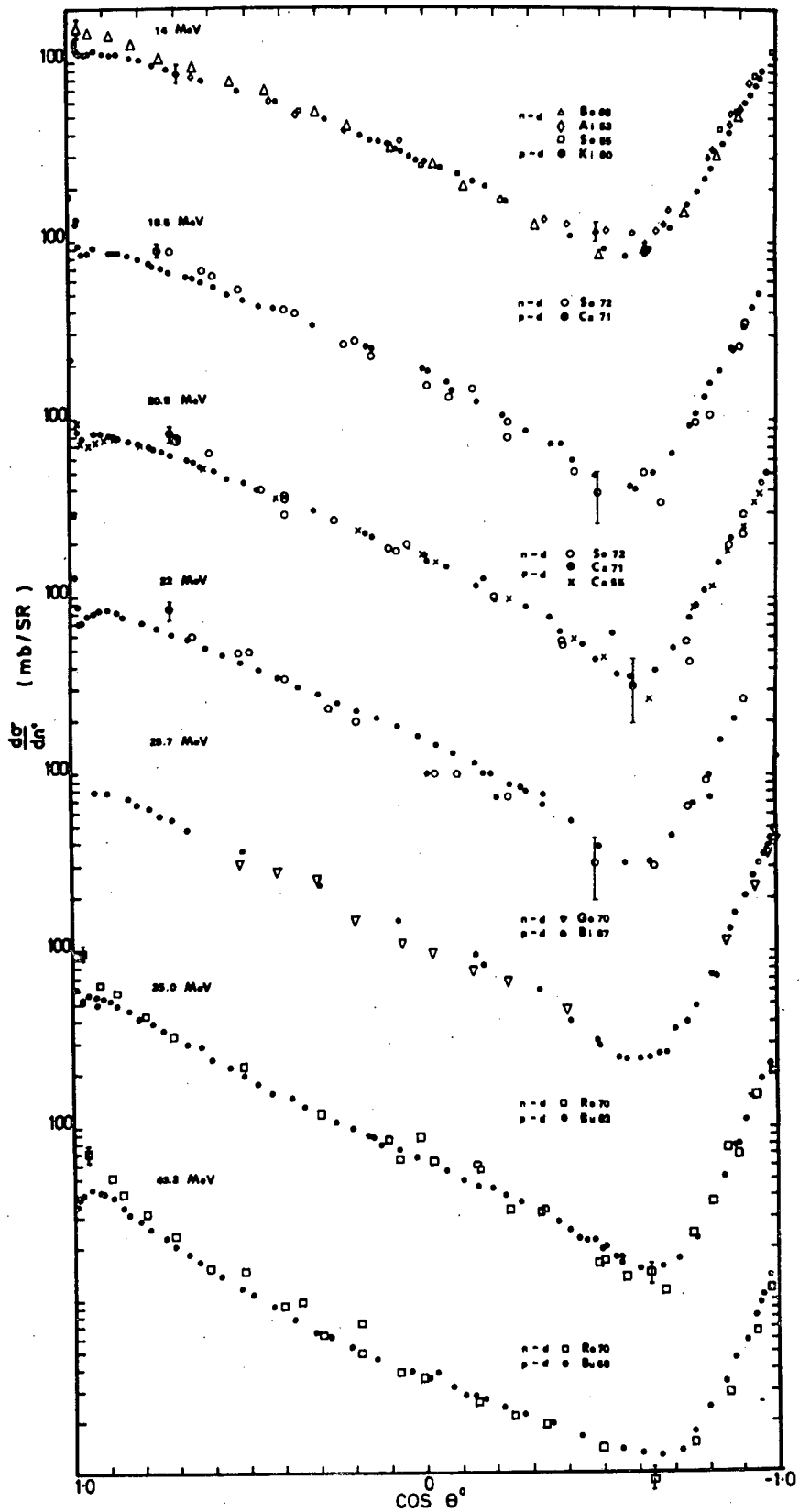

Fig. 1.2. N-d differential cross sections for incident energy E_N ranging between 14 and 50 MeV. The cross sections for the incident energies are shown on the left. e.g. n-d cross sections at 23 MeV have been multiplied by 23/22.

at some specific angle. An even less complete one, is the total yield as a function of angle. Both the above-mentioned incomplete experiments have been performed for the n-d interaction. To our knowledge, there exists no published record of total yield as a function of energy of emission.

1.4 Motivation

It is clear from the preceding section that the total n-d breakup cross section is sensitive to the details of the nuclear force.

This observation is only academic, however, in the absence of the means to include the nuclear interaction realistically in the theory. These means are now in sight, as has been demonstrated by calculations with local S-wave potentials and separable potentials including higher partial waves in the nuclear interaction (Do73) (Kl72).

The experimental data is rather ambiguous. We have a trend (see fig. 1.1) suggested by "indirect" measurements which, in the region of 20 MeV, is considerably higher than that suggested by direct p-d measurements (Ca72) and three indirect n-d measurements (Se72).

The upper trend depends on the assumption that p-d and n-d distributions are the same, except for Coulomb effects. The lower one, on the other hand, depends on the rather less-sound assumption that the total p-d breakup cross section is equal to the n-d one. However, there are measurements of the total p-d cross section, that indicate it is lower than the n-d one (Se70). These are admittedly at higher energies (the lowest is at 90 MeV), but it nevertheless casts doubt

on whether a total p-d breakup cross section can be equated to the n-d one.

In view of these ambiguities, together with the fact that calculations do not include Coulomb effects, there seems to be a need for the direct measurement of the n-d total breakup cross section in the 20 MeV region.

In measuring the total breakup cross section, breakup proton energy distributions were measured and integrated. The advantages of performing complete experiments to isolate specific reaction mechanisms have been mentioned in the previous section. We have, by contrast, the advantages offered by a measurement of the total cross section, which requires the theory to give a correct average of these effects and which, in this case, shows sensitivity to the nuclear forces employed.

Intermediate between these are the energy distributions of emitted protons. These are not altogether featureless and may afford another means for testing the theory.

CHAPTER 2

THEORETICAL EVOLUTION

This chapter contains a broad outline of the theory pertinent to n-d scattering and breakup. The theoretical work on this subject falls into two categories which, according to common usage, are termed "exact" and "approximate" treatments.

The "exact" treatments owe their nomenclature to the Faddeev formalism (Fa61-63) which is exact in principle, while methods used prior to the development of this formalism (e.g. Born Approximation) are referred to by the term approximate.

Most of the theoretical work on the subject was stimulated by the advent of an exact formalism, for which there are several formulations. Although detailed mathematical techniques employed in performing calculations with these formalisms are extremely complex, the underlying ideas are straightforward. One of the short derivations of the Faddeev equations are, therefore, included after pointing out the formal problems which they solve. No pretension is made to mathematical rigour, as this is outside the scope of this work. Following this description of the formalism, an account is given of its application to n-d scattering and breakup, up to the present date. In doing so, little attention has been paid to the results of individual calculations, general developments have been emphasized. It is hoped, in this manner to provide the broader framework in which any study of n-d interaction must be seen.

Although most of the topical work on this subject is

done in the "exact"formalism, some earlier work in Born and impulse approximation is relevant, as well as being useful in describing the more prominent characteristics of the n-d interaction. For these reasons, a brief summary of this formalism has been included.

Finally, some simple models which are specifically useful in understanding prominent features of deuteron breakup spectra, are summarised.

Some concepts relevant to two-body scattering theory are given in Appendix A.

2.1 Formal difficulties

The important aspects of the problem are emphasized by considering the system of three indistinguishable, spinless particles. In this case, the Schrödinger equation for the system can be written

$$(E-H)\psi = o \qquad (2.1)$$

where $H = H_o + V$

$$H_o = \sum_{i=1}^{3} H_{oi} = \sum -\frac{\hbar^2}{2m_i} \nabla^2$$

$$V = V_{12} + V_{23} + V_{31}$$

V_{ij} is a function of $r_{ij} = r_i - r_j$, being the interaction between particles i and j

The first of the difficulties associated with a solution of this equation is due to the number of variables involved. This suggested the application of variational methods which have been successful in dealing with the atomic many-body

problem. However, this technique is far more difficult to apply in nuclear physics because of the complexity and uncertainty of the nuclear force. It is suited to the bound-state problem where it has been applied to calculating bound-state parameters such as the Triton binding energy, e.g. (He72), (De71). These methods are not generally suited to continuum states encountered in scattering problems. In this case (2.1) is generally recast as an integral equation. One writes

$$G_o = (E - H_o)^{-1} \tag{2.2}$$

G_o is known as the free particles Greens' function. As for the two-particle case (see Appendix B), one can recast the Schrödinger equation into a form which contains the transition operators explicitly, viz. the Lipmann-Schwinger equation.

$$T = V + VG_oT \tag{2.3}$$

where T is known as the transition operator whose matrix elements are the scattering amplitudes. Equation (2.3) is an operator equation which is given meaning by inserting complete sets of states of the free particles Greens' function.

$$\langle \underset{\sim}{k}_1'\underset{\sim}{k}_2'\underset{\sim}{k}_3' | T | \underset{\sim}{k}_1\underset{\sim}{k}_2\underset{\sim}{k}_3 \rangle = \langle \underset{\sim}{k}_1'\underset{\sim}{k}_2'\underset{\sim}{k}_3' | V | \underset{\sim}{k}_1\underset{\sim}{k}_2\underset{\sim}{k}_3 \rangle + \langle \underset{\sim}{k}_1'\underset{\sim}{k}_2'\underset{\sim}{k}_3' | K | \underset{\sim}{k}_1''\underset{\sim}{k}_2''\underset{\sim}{k}_3'' \rangle \langle \underset{\sim}{k}_1''\underset{\sim}{k}_2''\underset{\sim}{k}_3'' | T | \underset{\sim}{k}_1\underset{\sim}{k}_2\underset{\sim}{k}_3 \rangle \tag{2.4}$$

where

$$\langle \underset{\sim}{k}_1'\underset{\sim}{k}_2'\underset{\sim}{k}_3' | K | \underset{\sim}{k}_1''\underset{\sim}{k}_2''\underset{\sim}{k}_3'' \rangle = \langle \underset{\sim}{k}_1'\underset{\sim}{k}_2'\underset{\sim}{k}_3' | V | \underset{\sim}{k}_1'''\underset{\sim}{k}_2'''\underset{\sim}{k}_3''' \rangle \langle \underset{\sim}{k}_1'''\underset{\sim}{k}_2'''\underset{\sim}{k}_3''' | G_o | \underset{\sim}{k}_1''\underset{\sim}{k}_2''\underset{\sim}{k}_3'' \rangle \tag{2.5}$$

and, putting $V = V_{12} + V_{23} + V_{31}$, and integrating over the k's

$$\langle \underset{\sim}{k}_1' \underset{\sim}{k}_2' \underset{\sim}{k}_3' | K | \underset{\sim}{k}_1'' \underset{\sim}{k}_2'' \underset{\sim}{k}_3'' \rangle = \frac{(2\pi)^3}{\left(E - \frac{h^2}{2m} \sum k''\right)} [\delta^3(\underset{\sim}{k}_1' - \underset{\sim}{k}_1'') \langle \underset{\sim}{k}_2' \underset{\sim}{k}_3' | V_{23} | \underset{\sim}{k}_2'' \underset{\sim}{k}_3'' \rangle$$

$$+ \delta^3(\underset{\sim}{k}_2' - \underset{\sim}{k}_2'') \langle \underset{\sim}{k}_1'' \underset{\sim}{k}_3' | V_{13} | \underset{\sim}{k}_1'' \underset{\sim}{k}_3'' \rangle$$

$$+ \delta^3(\underset{\sim}{k}_3' - \underset{\sim}{k}_3'') \langle \underset{\sim}{k}_1' \underset{\sim}{k}_2' | V_{12} | k_1'' k_2'' \rangle] \qquad (2.6)$$

K is known as the "kernel" of the integral equation represented by (2.3). A necessary condition for equation (2.3) to be amenable to standard techniques of solution, is that the kernel be square integrable or compact (see Appendix A).

We immediately encounter the second problem which is fundamental to the integral formulation of the three-body problem. In the Lipmann-Schwinger equation, it appears as the delta function in the kernel (Fa61). The delta function appears because, for any one interaction V_{ij} (i,j = 1 to 3), one of the particles is unaffected. This prevents the kernel from being square integrable since its norm contains an integration over the square of the delta function, which is infinite. Consequently, the Lipmann-Schwinger equation cannot be solved for the scattering amplitudes by the standard numerical methods.

This fact can be expressed in a number of ways.

Considering the perturbation expansion (see Appendix A) one says, in the terminology of perturbation theory, that the expansion contains disconnected diagrams representing an infinite number of interactions of two particles while the third remains free.

Equivalently, one can say of the formal theory, that the homogeneous equation has non-zero solutions for a continuum

of energies when there are two-particle bound-states while the third remains free. As a consequence of this, the integral equation for the wavefunction does not have a unique solution (Fi67).

All this amounts to the fact that the Lipmann-Schwinger equation is ill-suited to the treatment of the three-body system.

2.2 Exact Solution

The first formulation of the problem admitting of an exact solution is due to Faddeev (Fa61-63). Later Lovelace (Lo64), beginning with the formalism for rearrangement collisions developed by Ekstein (Ek56) arrived at an equivalent formulation which incorporates explicitly the transition amplitudes.

Apart from considerations of mathematical rigour, the Faddeev formulation is essentially simple. The main features of the method can be summarised briefly and plausibly.

Essentially, Faddeev's procedure consists of inserting the solutions to the two-body subsystems directly into the 3-body Lipmann-Schwinger equation and rearranging the operators.

One starts from the 3-body Lipmann-Schwinger equation

$$T = V + VG_oT \tag{2.3}$$

where V and G_o are defined in equations (2.1). Recalling the definition of V, we write

$$T = (V_{12} + V_{23} + V_{31}) + (V_{12} + V_{23} + V_{31})G_oT \tag{2.7}$$

putting $V_1 = V_{23}, V_2 = V_{13}, V_3 = V_{12}$, the notation simplifies to

$$T = \sum V_i + \sum V_i G_o T \qquad (i = 1 \text{ to } 3) \qquad (2.8)$$

We then define

$$T^{(i)} = V_i + V_i G_o T \qquad (2.9)$$

Obviously

$$T = \sum_i T^{(i)} \qquad (2.10)$$

so that

$$T^{(i)} = V_i + V_i G_o (T^{(1)} + T^{(2)} + T^{(3)}) \qquad (2.11)$$

at this stage we introduce the two-particle transition matrix

$$T_{23} = V_{23} + V_{23} G_o T \qquad (2.12)$$

or, in the notation defined above, putting $T_1 = T_{23}$, $T_2 = T_{13}$ and $T_3 = T_{12}$

$$T_i = V_i + V_i G_o T_i \qquad (2.13)$$

T_i differs from the usual definition of the two-body transition matrix (see Appendix A) in that G_o is the free Green's function for 3 particles. This merely affects the energy of the system as can be seen by writing

$$G_o = (E_i - H_i)^{-1} \qquad (2.14)$$

where $H_i = H_{oj} + H_{ok} \qquad (j,k \neq i)$

and $E_i = E - \frac{\hbar^2 k_i^2}{2m}$

where k_i is the wave number of particle i so that

$$\frac{\hbar^2}{2m}\ (k_1^2 + k_2^2 + k_3^2) = E \qquad (2.15)$$

Since

$$0 \leq \frac{h^2 k_i^2}{2m} \leq E$$

we see that elements of the two-particle transition matrix defined in (2.13) will usually be off the energy shell at both ends (see Appendix A).

This form of the two-particle T-matrix is inserted into (2.11) as follows:

Writing (2.11) as

$$(1 - V_i G_o) T^{(i)} = V_i + V_i G_o\ (T^{(j)} + T^{(k)}) \qquad (2.16)$$

and dividing through by the operator $(1 - V_i G_o)$, we obtain

$$T^{(i)} = \frac{V_i}{(1 - V_i G_o)} + \frac{V_i}{(1 - V_i G_o)}\ G_o\ (T^{(j)} + T^{(k)}) \qquad (2.17)$$

Recognizing $\dfrac{V_i}{(1 - V_i G_o)}$ as the formal solution of equation (2.13) for the two-particle T-matrix, one obtains

$$T^{(i)} = T_i + T_i G_o (T^{(j)} + T^{(k)}) \qquad (2.18)$$

for i,j,k = 1,2,3, i j k, so that

$$\begin{aligned} T^{(1)} &= T_1 + T_1 G_o (T^{(2)} + T^{(3)}) \\ T^{(2)} &= T_2 + T_2 G_o (T^{(3)} + T^{(1)}) \\ T^{(3)} &= T_3 + T_3 G_o (T^{(1)} + T^{(2)}) \end{aligned} \qquad (2.19)$$

The set of coupled equations (2.19) are the Faddeev equations. They are conveniently written in matrix form

$$\begin{pmatrix} T^{(1)} \\ T^{(2)} \\ T^{(3)} \end{pmatrix} = \begin{pmatrix} T_1 \\ T_2 \\ T_3 \end{pmatrix} + \begin{pmatrix} 0 & T_1 & T_2 \\ T_2 & 0 & T_2 \\ T_3 & T_3 & 0 \end{pmatrix} G_0 \begin{pmatrix} T_1 \\ T_2 \\ T_3 \end{pmatrix} \tag{2.20}$$

or simply

$$\underset{\sim}{T}^{(i)} = \underset{\sim}{T}_i + K_F G_0 \underset{\sim}{T}^{(i)} \tag{2.21}$$

Sufficient conditions for these equations to be soluble is that the kernel K_F be square integrable, i.e.

$$|K_F^2| = T_R|KK^\dagger| < \infty \tag{2.22}$$

This has been demonstrated to be the case (Fa63a), (Lo64), (We64). We recall (Section 2.1) that solution of the 3-body Lipmann-Schwinger equation is prevented by the square of a delta-function in the norm of the kernel. It was remarked that this corresponds to an infinte series of two-particle interactions for which the third particle does not interact. One can easily see, by iterating the set of Faddeev equations, that only terms like

$$T_i G_0 T_K \quad (i \neq k) \tag{2.23}$$

occur, and that these will never give the square of a delta function (Du68).

We note that the Faddeev equations do not depend explicitly on the nucleon-nucleon potentials. It is however necessary to know the T-matrix off the energy shell at both ends. On the other hand, by specifying a potential one also specifies the off-shell T-matrix.

It is hoped that the inclusion of phase-equivalent interactions in the Faddeev formalism will help to resolve the ambiguities.

Conversely, the Faddeev formalism enables one, in principle, to obtain exact solutions to the three-body problem in terms of the two-nucleon scattering amplitudes. Assuming that these can be specified exactly both on and off the energy shell, any remaining discrepancy would give indication of three-body forces.

The Faddeev equations are not directly related to the scattering amplitudes. Starting from Ekstein's (Ek56) equations for exchange scattering, Lovelace (Lo64) developed another formulation for the Faddeev equations

$$U_{\alpha\beta} = V_{\delta\beta} + V_{\alpha\beta} + \sum_{\gamma=1}^{3} (1 - \delta_{\alpha\gamma}) T_\alpha G_o U_{\gamma\beta} \qquad (2.24)$$

where $U_{\alpha\beta}$ is the transition operator from channel α to β channel

$$\delta_{\alpha\gamma} = 0 \quad \text{for } \gamma \neq \alpha$$
$$= 1 \quad \text{for } \gamma = \alpha$$

This is also a system of three coupled equations incorporating the two-particle T-matrix T_γ. They can be written in terms of the Faddeev kernel

$$U_{\alpha\beta} = V_{\delta\beta} + V_{\alpha\beta} + K_{F\alpha\gamma} G_o U_{\gamma\beta} \qquad (2.25)$$

Although the formalism admits of exact solution for arbitrarily specified two-body T-matrices, in fact, the complexity of the numerical calculation has restricted their use to idealised interactions. This is essentially because the first fundamental difficulty, viz. the multiplicity of variables, remains.

In the case of the two-body Lipmann-Schwinger equation, the integrals are reduced to a tractable form by making a partial-wave expansion (see Appendix A). This reduces the number of variables over which the integration must be performed to one.

As written in the preceding section, the Faddeev equations involve integration over six variables, after factorising out the centre-of-mass motion. In this form, the solution is impossible for current computational techniques.

As a first step towards reducing this multiplicity, one must perform an angular momentum reduction of the problem analoguous to the partial wave expansion for the two-body case (see Appendix A). Various means for doing so exist. These have been reviewed by (El73), who separates them into two categories - symmetrical and unsymmetrical. The symmetrical method (Om64) consists in choosing, for the six independent variables, the three relative separations (r_{12},r_{13},r_{23}) and the three Euler angles $(\alpha\beta\gamma)$ defining the orientation in space of the triangle formed by these separations. Functions $D^{L}_{MK}(\alpha,\beta,\gamma)$ now define the angular dependence. These are analogous to the $Y_{LM}(\theta,\phi)$ functions in the two-particle case. The problem is now reduced to an integration over three variables. This approach was subsequently simplified to a set of coupled integral equations in two variables (Os66).

The unsymmetric method (Ah65) consists essentially of expanding the three-nucleon states into simultaneous eigenstates of L, L_z, ℓ^2, ℓ_z where L is the relative angular momentum of a pair of particles and ℓ the angular momentum of the third, relative to the centre-of-mass of the first two.

Various generalizations to the case for particles having intrinsic spin have been formulated (El69), (Ha70), (Gr70). Other methods based on separable models also exist (Lo64), (Aa64), (Aa65).

In all the reduction methods described above, except the last, angular momentum reduction results in coupled integral equations for two independent variables. These still constitute a formidable problem.

In order to reduce the problem to a tractable form, one can make approximations which make the term "exact", which is applied to them, somewhat ambiguous (Mi69). This term should therefore be understood to draw a distinction between conventional variational approximations, which start with realistic potentials and derive approximate solutions and methods which use an exact formalism with unrealistic potentials. The approximation first to be applied to the potentials, or equivalently to the scattering amplitudes, is generally known as the "separable approximation" and it permits the problem to be reduced to an equivalent two-body problem consisting of integral equations in one independent variable.

2.3 Separable Interactions

An "exact" formulation of the three-body problem using separable interactions was arrived at independently of Faddeev by Mitra (Mi62), Sitenko and Karchenko (Si63) and Amado (Am63). Concise reviews have been given by Mitra (Mi69) and Duck (Du68).

A separable potential belongs to the broader category

of non-local potentials. For a non-local interaction, the Schrödinger equation for two particles is

$$(E - H_o)\psi(r) = \int V(r,r')\psi(\underset{\sim}{r}')d\underset{\sim}{r}' \tag{2.26}$$

when the potential is also separable

$$V(r,r') = -v(r)\lambda v(r') \tag{2.27}$$

where λ is known as the strength parameter.
These potentials were first proposed by Wigner (Bl52). The simplification which they introduce to the two-nucleon system, was pointed out by Yamaguchi (Ya54). This is seen on transferring to momentum space.

$$\left(E - \frac{\hbar^2}{2m}k^2\right)\psi(\underset{\sim}{k}) = -v(k)\lambda N \tag{2.28}$$

where

$$N = \int d^3\underset{\sim}{k}'\, v(k')\psi(k') \tag{2.29}$$

and $v(k)$ is the transform of $v(r)$, or the potential form factor. For a bound state with energy $-E_B$, we obtain

$$\psi(\underset{\sim}{k}) = \frac{v(k)\lambda N}{\left(E_B + \frac{\hbar k^2}{2m}\right)}$$

multiplying (2.28) by $v(k)$ and integrating over k, we obtain

$$N = \Delta N \tag{2.30}$$

where

$$\Delta = \int d^3\underset{\sim}{k}\, \frac{\lambda v^2(k)}{\left(E_B + \frac{\hbar k^2}{2m}\right)}$$

(2.30) is an equation for E_B. The problem is therefore

reduced to an algebraic relation in momentum space. One can proceed in a similar manner with continuum wave functions and obtain two-body transition matrix elements having the form

$$\langle k'|T|k\rangle = -v(k')\Omega V(k) \tag{2.31}$$

where Ω is a function of k and the form factors which contain bound state poles (Du68).

Generally speaking, therefore, the separable approximation has the virtue of reducing the number of integrals by one. For the two-nucleon case, integral equations are reduced to algebraic ones, whereas for the three-nucleon case, integral equations in two variables are reduced to the equivalent two-nucleon integrals over one variable and consequently rendered tractable.

The properties of separable potentials can be interpreted in physical terms (Mi69). The first property is characteristic of non-local potentials. The non-local potential allows instantaneous change in the relative coordinate ($r \neq r'$)

$$\langle r|V|\underset{\sim}{r}'\rangle = \lambda v(r)v(r') \tag{2.32}$$

while for a local potential this is not permitted

$$\langle \underset{\sim}{r}|V|r'\rangle = \delta(x-x')V(r) \tag{2.33}$$

The second difference is that whereas a local potential incorporates all harmonics, the separable one described above is an S-wave potential. This can easily be seen from (2.26). It is apparent that all angular dependence disappears in the integral. This can be remedied by increasing the "rank" of

the potentials, i.e. by adding separable terms which contain higher harmonics.

The use of such interactions, although convenient, needs justification. Formal justification for the use of separable potentials in the vicinity of bound-states or resonances, is given by Lovelace (Lo64). He has shown that when the scattering amplitude is dominated by a bound-state pole or resonance, the T-matrix reduces to a quasi-separable form and that in suitable circumstances, the non-separable part can be neglected. This can be seen (Mi69) from the operator identity (see Appendix A)

$$T = V + VGV \tag{2.34}$$

where T is the transition matrix and G the full two-particle Green's function.

$$G = (E - H)^{-1} \tag{2.35}$$

$$H = H_o + V$$

G's spectral resolution can be written

$$G = |\psi_B\rangle (E-E_B)^{-1} \langle\psi_B| + \int d\underset{\sim}{k} |\underset{\sim}{k}\rangle \left(E - \frac{h^2}{2m} k^2\right)^{-1} \langle k| \tag{2.36}$$

In the vicinity of a bound-state pole, the second term in (2.36) becomes negligible and when the first term is inserted into (2.34), a separable form for the T-matrix resembling (2.31) is obtained.

However, this condition is not satisfied by some interactions. In particular, the tensor force and the p-wave interaction.

The most important criterion, and one which has been used to overrule the above conditions, is that the potential should fit the two-body scattering data. This has been done with some precision (Ya54), (Ta65) and (Na64). An exception is the separable Yamaguchi S-D tensor force (Ya54a).

The method of constructing a separable interaction which has the bound-state pole structure was further developed by Fuda (Fu69) and has come to be known as the Unitary Pole Approximation (UPA). It consists of starting with a two-nucleon bound-state wave function as determined by some sophisticated potential which one seeks to approximate, and deriving the corresponding separable interaction. This method has had significant success with soft core potentials of the Reid (Re68) type. Apart from reproducing the on-shell elements of the Reid T-matrix, it also has a very similar off-shell structure (Ha70). However, it is not so successful with other potentials. This has been explained by Harms (Ha70) in terms of separable "Unitary Pole Expansions" (UPE) of the T-matrix. Such an expansion is discovered to be extremely rapidly converging for potentials incorporating a soft core, so that its first term, the bound-state pole, can be expected to give a good approximation.

Separable expansions have been shown to be generally possible if the kernels are compact (We63) (see Appendix A). It is therefore possible in such cases to approximate a T-matrix with arbitrary accuracy by a separable expansion. However, the number of terms that can be included in such an expansion is limited by practical considerations (Sl72a).

A realistic description of the S-wave forces already requires a minimum of four terms. In the $^3S_1$ state, one

requires a central and tensor component (Ya54a), while in the ^1S_o state, a realistic interaction should include a repulsive core (Na64), (Ta65). This already introduces four separable terms. For each term, one has to solve a set of coupled differential equations in one variable. The computing time generally increases as the cube of the number of equations (Sl72a), so that one is forced to omit all but the most important terms. It is only recently that continuum state calculations have been able to include tensor forces and soft cores (Sl72).

Generally, early calculations were typified by S-wave separable interactions.

2.4 Application to n-d Scattering and Breakup

The first exact calculations for the three-nucleon system were performed with separable interactions. Two "exact" solutions to the problem were formulated independently of Faddeev's treatment and were shown (Ro64) to be equivalent to it in the separable approximation. However, the Faddeev formalism is more general, as it does not depend intrinsically on the separable assumption.

The first of these is due to Mitra (Mi62), (Mi63) and Sitenko and Karchenko (Si63). This formalism emphasizes the Schrödinger equation rather than the scattering amplitudes and was used principally in bound-state calculations (Bh65a), (Si65), (Mi66), (Sc67).

The second was developed by Amado (Am63). This formalism was developed specifically with the n-d scattering in mind. It has the Born exchange term as a first approximation and

takes the n-p interaction into account exactly as a reduced interaction having the deuteron bound-state pole. This is just a separable potential. The theory is developed in a field theoretical formalism where the deuteron is treated as an elementary or quasi-particle.

Both these early theories were used with S-wave separable potentials. For the special bound-state case ($J = \frac{1}{2}$, $\pi = +$), special separable forms of the $^3S_1 - {}^3D_1$ tensor force, as well as short range repulsion, were taken into account (Si65) (Mi66), (Sc67) in calculating the triton binding energy and low energy scattering parameters. Such potentials were developed by Yamaguchi and Yamaguchi (Ya54a), Tabakin (Ta64), (Ta65) and (Ta68) and others (Na64).

The inclusion of additional separable terms is more difficult in continuum state calculations, however, partly because of the large number of partial waves which must be treated. Amado (Am63) used purely central S-wave interactions and accounted for the D-state admixture of the deuteron bound-state by means of a deuteron wave-function re-normalization constant, which is interpreted as the probability of the deuteron being in a state other than the S-state.

Calculations using this model were made for both n-d scattering (Aa65) and breakup (Aa66). Such calculations were also performed using the Faddeev-Lovelace formalism in the separable approximation (Ph66), (Ph66a). In this case, the effects of the tensor force were accounted for by a phenomenological three-body force (Ph66).

Further calculations with the S-wave central model were performed for both elastic-scattering (Sl71) and breakup

(Ca71), (Ca70) and (Eb72). The breakup calculations are still restricted to the S-wave separable potentials. These are usually of the Yamaguchi type (Ya54), (Ya54a), but form factors developed by Tabakin (Ta68) were also used (Ca71). These calculations are relatively successful in reproducing the main features of the breakup spectra, but fail to reproduce the absolute cross-sections.

The calculations described above are incapable of predicting any vector polarizations because the forces they employ are central. A first step towards improving the interactions used was the incorporation of a tensor force.

Separable forms of the $^3S_1$ - $^3D_1$ tensor force which give the correct deuteron D-state admixture had been developed (Ya54a), (Ta64), (Ta65), (Na64) and used in early calculations for the idealised case of $J = \frac{1}{2}$, $\pi = +$ bound-states (Mi62), (Bh63), (Bh64).

A formalism for including them in continuum state calculations was proposed by Sloan (Sl69) and subsequently employed with Yamaguchi potential form factors (Sl72), (Av71), (Do72), (Do72a). These succeeded in reproducing quadratic tensor polarizations but with the exception of one case (Av71), which was subsequently shown to contain an error (Do72a), they failed to account for the vector polarization.

Recently (Sl72b), the effect of the tensor force was investigated further by performing calculations with both Yamaguchi and Hülthen form factors, as well as with a form factor taken from a UPA approximation to the Reid (Re68) soft core potential. The effect of varying the percentage D-state of the deuteron P_D was also investigated.

The general conclusion drawn was that polarizations are remarkably insensitive to variations in both the form factors and P_D.

Although the inclusion of tensor forces in the separable model improved the model to the extent of reproducing the qualitative features of second-rank tensor polarizations of the deuteron, they failed completely to give the nucleon and deuteron vector polarizations. This is not surprising since the non-central spin-orbit force is omitted. It has in fact been pointed out (Pi72) that the above forces produce no polarization at all in two-body scattering.

The inclusion of higher partial waves in the N-N interaction was clearly indicated and the first attempt to include them was made (Kr70), (Kr70a), (Aa72), (Pi72) using the Unitary First Order Approximation method (Sl68), (Sl69a). This model is a simple modification of the impulse-pickup approximation. The submatrix of the scattering matrix which excludes the breakup channel satisfies a unitary constraint (Sl68). Single-term separable potentials were used to represent the interaction in the S, P and D waves. The non-central part of the interaction was taken into account by including a tensor force and by allowing split P and D waves. Although first attempts (Kr70), (Kr 70a) with this model seemed successful in reproducing vector polarizations, they were subsequently shown to be wrong (Aa72a) and later calculations (Pi72b), (Aa72a) fail completely to reproduce vector polarizations. They do, however, show that the effect of P-waves is considerable, and stimulated efforts to include them in a reliable form.

It has been shown (We63) that a well-behaved T-matrix can be expanded in a series of separable terms which is generally infinite. This suggested the approximation of realistic potentials by the inclusion of more separable terms. Recently, a substantial amount of work has been done on T-matrix expansions (Fu69), (Os69), (Ha70a) and several formalisms incorporating the Faddeev equations in multiseparable expansions have been developed (Sl69), (Sl72), (St70), (Ha70), (Al67). However, as we observed above, the rate at which computing time increases with the number of terms is prohibitive and restricts one to the inclusion of only a few terms, but it has also been observed that the U.P.A. approximation is surprisingly good. This suggests (We63) that higher terms might be treated by perturbation methods.

Such perturbation methods have been developed (Al67), (Ko72), (Sl72). P-waves and D-waves in the N-N interaction have been introduced as first order perturbations (Pi72), (Pi73) in calculations for n-d scattering.

All attempts to improve the N-N interaction which we have so far described have retained the simplifying assumption of separability. Although, as we have remarked, this approximation is able to reproduce the N-N phase shifts accurately up to 100 MeV, and in spite of the success of UPA in reproducing even the off-shell behaviour of the Reid potentials (Sa73), it is nevertheless an idealisation. The application of the Faddeev formalism to more conventional local potentials was clearly desirable. However, this is a problem of forbidding complexity.

Recently, the problem was solved both for the bound state (Ma69) and for the continuum state (Tj70a).

The scattering problem was solved by applying Pade techniques to the Faddeev multiple scattering theory which is generally divergent (Sl69). Using this technique calculations were performed for both n-d scattering (Kl71)(Kl72a)(Kl73) and breakup (Kl72) with potentials incorporating soft cores of the Yukwa and Reid type. The use of local potentials had the effect of improving the elastic angular distributions at smaller angles and of raising the total breakup cross-section. The results were shown to be sensitive to the form of the potentials used.

An alternative approach to introducing local potentials has been proposed (Sa73). It consists in starting with a suitable separable expansion and solving the separable pole terms by a matrix inversion and the higher ones by iteration. It is expected to be a practical method, however, only if the number of terms is small (Kl71).

For the sake of completeness, we mention that an alternative exact solution of the 3-body problem may be obtained using dispersion relations (Av69). This formalism is, in principle, tractable with all kinds of N-N interactions, but it extremely elaborate. Such N/D calculations have been performed for n-d (Av69)(Eb69) and p-d (Eb69) elastic scattering. These were performed with single and double nucleon exchange which, for convenience, were calculated using a simple separable interaction similar to the ones used by calculations in the Faddeev formalism. No attempt was made to include tensor force or short-range repulsion, but for the p-d distributions, Coulomb effects were taken into account, with consequent good agreement with experiment at small forward angles. N-d phase shifts below 25 MeV were found to compare

well with contemporary phase analyses.

It was pointed out, however, that in the approximation in which the N/D calculations were performed, they constitute an approximation to the Faddeev formalism in the separable approximation.

2.5 Approximation Methods

2.5. (1) Born and Impulse Approximations

There have been several efforts to describe n-d elastic and inelastic scattering in terms of Born and impulse approximation e.g. (Ch50)(Gl51). One seeks to evaluate the matrix element

$$\langle \phi_f | V_{fi} | \psi_i \rangle \tag{2.37}$$

where ψ_i is the initial-state wave function in the presence of the interaction V_{fi} and ϕ_f is the asymptotic final-state wave function. V_{fi} is taken to be the sum of interactions between the incident nucleon 1 and the target nucleons 2 and 3. The problem is that of specifying ψ_i .

In Plane Wave Born approximation, ψ_i is taken to be a product of the unperturbed plane-waves describing the incoming nucleon and the deuteron wave function. In the C.M. of the total system (see Appendix B)[†]

[†]The subscript f and i refer to the final and initial state respectively. Where they are omitted, the final-state is implied. The superscript ℓ refers to the laboratory frame. When omitted the total centre-of-mass frame is implied.

$$\psi = \exp(-i\underset{\sim}{k}_i \cdot \underset{\sim}{q})\phi_D(r)\chi_i \qquad (2.38)$$

where χ_i is the channel spin function

$$\underset{\sim}{k}_i = \frac{2}{3}\underset{\sim}{k}_o$$

$$\underset{\sim}{r} = r_{2-3}$$

$$\underset{\sim}{q} = r_{1-23}$$

(the coordinate system is described in Appendix B)

For elastic scattering, ϕ_f describes the scattered nucleon and deuteron in the exit channel.

$$\phi_f = \exp(i\,\underset{\sim}{k}_f \cdot \underset{\sim}{q})\phi_D(r)\chi_i \qquad (2.39)$$

where $k_f = k_{1-23}$

while for inelastic scattering, ϕ_f is usually taken to be a product of wave functions describing:

(1) Three free non-interacting nucleons

$$\phi_f = \exp(\underset{\sim}{k}_f \cdot \underset{\sim}{q}) \exp\, i(\underset{\sim}{k}'_f \underset{\sim}{r}) \qquad (2.40)$$

where $\underset{\sim}{k}'_f = \underset{\sim}{k}_{2-3}$ is the internal wave number in the C.M. system of particles 2 and 3 in the final state.

(2) One free nucleon and two nucleons interacting in the final state

$$\phi_f = \exp\, i(\underset{\sim}{k}_f \cdot \underset{\sim}{q})\phi'_f(k'_f, r) \qquad (2.41)$$

where ϕ'_f is a scattering wave function in the C.M. system of nucleons 2 and 3.

N-d scattering leading to various final states can be

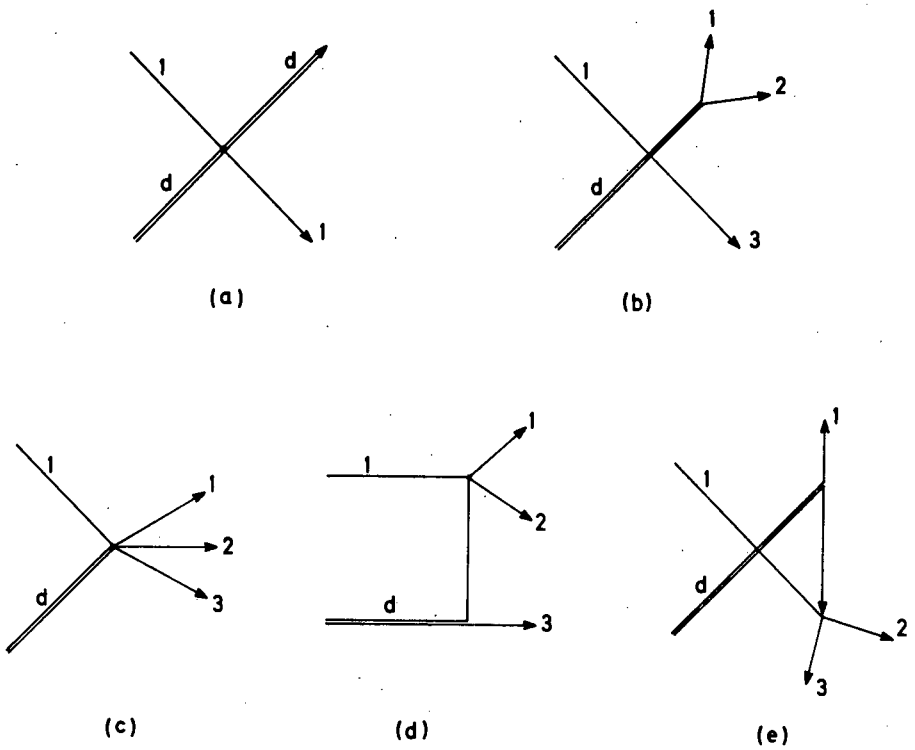

Fig. (2.1) n-d scattering to various final states

(a) Elastic scattering
(b) Inelastic scattering with nucleons 1 and 2 interacting in the final state
(c) Simultaneous breakup
(d) Quasi-free scattering
(e) Rescattering of nucleon 2 from nucleon 3 after decay of the final state (1,2) resonance.

represented diagrammatically as in Fig.(2.1). The approximation can be improved by taking into account re-scattering events. Such re-scattering is represented diagrammatically by the triangle-graph Fig.(2.1e).

The Born approximation for elastic n-d scattering leads to a combination of three integrals, each having a physical interpretation (Ve57).

$$J_1(\theta) \propto \int \exp\, i(\underset{\sim}{k}_f \cdot \underset{\sim}{q})\, \phi_D^*(r) V_{12}\, \exp -i(\underset{\sim}{k}_i \cdot \underset{\sim}{q})\, \phi_D(r)\, d\underset{\sim}{r} d\underset{\sim}{q}$$

$$J_2(\theta) \propto \int \exp\, i(\underset{\sim}{k}_f \cdot \underset{\sim}{q})\, \phi_D^*(r) V_{12}(12) [\exp -i(\underset{\sim}{k}_i \cdot \underset{\sim}{q})\, \phi_D(r)]\, d\underset{\sim}{r} d\underset{\sim}{q}$$

$$J_3(\theta) \propto \int \exp\, i(\underset{\sim}{k}_f \cdot \underset{\sim}{q})\, \phi_D^*(r) V_{12}(13) [\exp -i(\underset{\sim}{k}_i \cdot \underset{\sim}{q})\, \phi_D(r)]\, d\underset{\sim}{r} d\underset{\sim}{q}$$

(2.42)

where (12) and (13) are permutation operators exchanging the coordinates of nucleons (1 and 3) and (2 and 3) respectively.

J_1 represents potential scattering in which the incident nucleon scatters off one of the target nucleons. J_2 and J_3 are consequences of the Pauli principle and exchange forces. J_2 represents a process in which the incident nucleon exchanges place with, or "knocks out" the target nucleon, while J_3 represents the pickup of a target nucleon by the incident one to form a new deuteron.

J_1 and J_2 are expected to be peaked in the forward direction, while J_3 is expected to be peaked in the backward direction.

$V_{1\cdot2}$ is the central part of the interaction between nucleons 1 and 2. In the case of spin and isospin-dependent forces, there are 8 such interactions corresponding to two spin states (triplet and singlet) in each of four isospin states (three T = 1 states and one T = 0 state).

This Born approximation model has been used in several instances (Ch53)(Va67)(Pu68) to compute phase shifts for angular momentum $\ell \geq 1$ which were then used as starting values for phase shift analyses. It has been observed (Ch53) (Am63) that the model yields surprisingly good results in view of the crudity of the assumptions. This is so because

the elastic scattering is dominated by the quartet S-state phase where the dominant terms are exchange ones, so that it is to a large degree independent of short range interactions. In fact, Amado, in constructing his exact theory uses the exchange term as the driving one. This insensitivity to the details of the nuclear force was noted in these early Born approximations (Ch53).

In the case of inelastic scattering, the final-state wave function can be approximated by a product of functions describing one free particle and two particles interacting in the final state. The wave function, $\phi_f'(r)$, describing the two nucleons in a continuum state is obtained by solving for the two-nucleon scattering wave function in some more-or-less simplified potential. Frank and Gammel used zero-range potentials (Fr54). Ilakovac et al. (Il61) used square wave potentials, while Koehler and Mann (Ko64) introduced realistic potentials of the Yukawa type.

The breakup cross-section can in this manner be expressed as a sum of integrals similar to J_1, J_2, J_3 for the elastic case, but describing transitions to continuum state functions.

In the case of central forces, when spin is conserved, the total transition amplitude may be divided into three incoherent terms. When the nucleons interacting in the final state are in a triplet (s = 1) state, the total spin can be $S = \frac{3}{2}$ (quartet state) or $S = \frac{1}{2}$ (singlet state) whereas when $s = 0$, the total spin can only be $S = 1$ (doublet state). Accordingly, the total transition rate can be written

$$T = \frac{2}{3} T(S=\tfrac{3}{2},s=1) + \frac{1}{3} T(S=\tfrac{1}{2},s=1) + \frac{1}{3} T(S=\tfrac{1}{2},s=0) \qquad (2.43)$$

A different approach to the problem is adopted in the impulse approximation formalism (Ch50)(Cr63)(Cr63a). This consists essentially in replacing the real transition matrix with a sum of individual free-nucleon T-matrices. Hence

$$\langle\phi_f|T|\phi_i\rangle \simeq \langle\phi_f|t_1+t_2|\phi_i\rangle \qquad (2.44)$$

where t_1 and t_2 are the free-nucleon transition operators.

This is equivalent to replacing the initial plane-wave function in the PWBA formalism with a function having the momentum distribution of the deuteron. In this manner, quantitative results may be obtained at high energies (> 200 MeV), where the Impulse approximation is valid (Ch52).

2.5. (2) Reaction Mechanisms

There are kinematic conditions in which the transition amplitude is characterised by two-particle interactions which are of two kinds

(1) the final-state interaction (FSI) - Fig.2.1(b)

(2) the quasi-free interaction (QFS) - Fig.2.1(d)

These two reaction mechanisms produce the most pronounced enhancements of phase space.

The condition for QF scattering is that one of the target nucleons should remain unaffected. Therefore, if nucleon 1 scatters off nucleon 2, leaving nucleon 3 unaffected

$$\underset{\sim}{k}_{3f} = \underset{\sim}{k}_{3i} = \underset{\sim}{k}_3$$

Furthermore, since the deuteron is at rest in the laboratory

$$\underset{\sim}{k}_{3i} = - \underset{\sim}{k}_{2i} \tag{2.45}$$

The transition amplitude for quasi-free scattering of nucleon 1 of 1 nucleon 2 in impulse approximation is therefore

$$T_{if} = \langle \underset{\sim}{k}_{1f} \underset{\sim}{k}_{2f} \underset{\sim}{k}_{3i} | t_{12} | \underset{\sim}{k}_{1i} \phi_D \rangle \tag{2.46}$$

The resulting transition amplitude is a product of the momentum-space deuteron bound-state function and a two-nucleon transition amplitude which is off the energy shell (Ku61)

$$\text{i.e.} \quad T_{if} \alpha \phi_D \langle \underset{\sim}{k}_{2f} \underset{\sim}{k}_{1f} | t | \underset{\sim}{k}_{2i} \underset{\sim}{k}_{1i} \rangle \tag{2.47}$$

That the matrix element is off the energy shell can be easily seen as follows

$$\Delta E = E_f - E_i = \frac{\hbar^2}{2m} (k_{2f}^2 + k_{1f}^2 - k_{2i}^2 - k_{1i}^2) \tag{2.48}$$

using identities (2.45)

$$\text{i.e.} \quad k_{2i}^2 = k_{3f}^2$$

and remembering that

$$\frac{h^2}{2m} (k_{1f}^2 + k_{2f}^2 + k_{3f}^2) = E = \frac{\hbar^2 k^2_i}{2m} - E_B \tag{2.49}$$

where E_B is the deuteron binding energy, one obtains

$$\Delta E = \frac{\hbar^2 k^2_3}{2m} + E_B = 2E_3 + E_B \tag{2.50}$$

The usual approximation made is to replace the off-shell transition amplitude with an on-shell one. This model is known as the spectator model (SM). Kuckes, Wilson and Cooper (Ku61) used a Hulthen deuteron wave function (Hu57)

to obtain†

$$\frac{d^2\sigma}{dE_1^{\ell} d\Omega_1^{\ell} d\Omega_2^{\ell}} = \left(\frac{d\sigma}{d\Omega}\right)^{cm}_{free} \frac{4\sqrt{2}}{\pi^2} \left(E_o\right)^{-\frac{1}{2}} \frac{(E_\beta E_B)^{\frac{1}{2}}(E_B^{\frac{1}{2}} + E_\beta^{\frac{1}{2}})}{(E_B+2E_3^{\ell})\ (E+2E_3^{\ell})} \frac{h^6\rho}{m^3} \tag{2.51}$$

where ρ is the phase-space factor (See Appendix A)

E_B = 2.226 MeV is the deuteron binding energy

E_β = 59.8 MeV

$\left(\frac{d\sigma}{d\Omega}\right)^{cm}_{free}$ is the differential cross-section (in the centre-of mass of the interacting nucleons) at a relative energy and angle given by

$$E_{1-2f} = \frac{\hbar^2 k^2_{1-2f}}{2\mu_{2-3}}$$

and

$$\cos\theta_{12} = \frac{\underset{\sim}{k}_{1-2i} \cdot \underset{\sim}{k}_{1-2f}}{|\underset{\sim}{k}_{1-2i} \cdot \underset{\sim}{k}_{1-2f}|} \tag{2.52}$$

The reason why quasi-free scattering produces an enhancement is due to the influence of the bound-state pole. It can be seen from expression (2.51) that there is a second-order pole in the unphysical region of $E_3^{\ell} = -\frac{E_B}{2}$. Because of the small binding energy of the deuteron, this pole is not far removed from the physical region and therefore causes an enhancement of the transition amplitude as E_B tends to zero.

---

†This expression was taken from (Ar70), as the original expression given in (Ku61) is wrong.

It is known to distort phase-space even at low incident energies ($E_n \sim 14$ MeV) where the impulse approximation is not a good one (Ar70).

Expression (2.51) is for the absolute cross-section. It can predict reliable cross-sections only at high (> 200 MeV) energies. At low ($\sim$ 14 MeV), the cross-section predicted is usually a factor of $\sim$10 larger than the observed one. At these energies therefore, it can be relied on only to give a qualitative description of the quasi-free mechanism.

The FSI mechanism was described in general terms by Watson and Migdal (Wa52)(Mi55). A similar formulation was given by Phillips (Ph60).

Watson shows that when suitable conditions are fulfilled, the total interaction may be divided into a localized primary interaction and a final-state one between two out-going nucleons and that, in this case, the transition amplitude is enhanced by the final-state interaction. These conditions are

(1) that the primary interaction be a short range one which is localized in a certain volume τ.
(2) that the internal energy of the nucleons interacting in the final-state be low.
(3) that the final-state interaction be strong and attractive.

When these conditions are fulfilled, the final-state interaction cross-section may be thought to be larger than the cross-sectional area of the primary interaction. By considering the inverse reaction, one can see qualitatively (Wa52) that incoming interacting nucleons are drawn together by their strong attractive interaction so as to enhance their probability

of entering into the primary-interaction volume.

When the above conditions are fulfilled, the transition amplitude may be expressed as a product of two terms

$$T = \frac{\sin \delta}{k'} f(\theta) \tag{2.53}$$

where δ is the phase of the particles interacting in the final state, k' is the relative momentum and $f(\theta)$ is a factor varying slowly with k'. When k' is small, the phase may be described by Bethe effective range theory

i.e. $$k' \cot \delta = -\frac{1}{a} + \frac{1}{2} r_o k'^2 \tag{2.54}$$

where r_o is the effective range

and a is the N-N scattering length.

Assuming only one final-state interaction between nucleons 2 and 3, the differential cross-section can be written

$$\frac{d\sigma}{dE_1 \, d\Omega_1 \, d\Omega_2} \propto |T^2| \rho \left| \frac{\sin^2 \delta}{k'^2} \right| |f(\theta)| \rho \tag{2.55}$$

where ρ is the phase-space factor (see Appendix B). Substituting the effective range approximation for the phase shift into (2.55) and neglecting a term $\frac{1}{4} r_o^2 k'^4$, one obtains (Ph62)

$$\frac{d\sigma}{dE_1 \, d\Omega_1 \, d\Omega_2} \propto \frac{|f(\theta)|^2}{k'^2 + \left(-\frac{1}{a} + \frac{1}{2} r_o^2 k'^2 \right)} \rho \tag{2.56}$$

$$\frac{|f(\theta)|^2}{\left(1 - \frac{r_o}{a}\right) (k'^2 + \alpha^2)} \rho$$

where

$$\alpha^2 = \frac{1}{a^2 \left(1 - \frac{r_o}{a}\right)}$$

The above expression (2.56) is sharply peaked at maximum E corresponding to a zero relative momentum P . This can easily be seen by neglecting the effective range contribution i.e.

$$k' \cot \delta \simeq - \frac{1}{a} \tag{2.57}$$

Substituting this expression into (2.55), one obtains

$$\frac{d\sigma}{dE_1 d\Omega_1 d\Omega_2} = \frac{|f(\theta)|^2}{k'^2 + \frac{1}{a^2}} \tag{2.58}$$

This expression has a pole at $k'^2 = - \frac{1}{a^2}$. If a is large, this pole is close to the physical region and consequently enhances the cross section. In practice, this expression can be used to describe the shape of the energy distribution only in a restricted energy range around zero internal momentum k'. As the internal energy increases, the influence of the FSI becomes progressively less dominant.

Since the mechanisms described above produce the most significant enhancements of phase space, distributions may be simulated by a combination of amplitudes corresponding to (FSI), (SM) mechanisms and a featureless term describing the contribution of other processes.

One writes

$$T = \sum A_i T_{FSI} + \sum B_i T_{SM} + C \tag{2.59}$$

then, neglecting interference terms, we write

$$\frac{d^3\sigma}{dE_1 d\Omega_1 d\Omega_2} \propto \left(\sum A_i^2 T_{FSI}^2 + \sum B_i^2 T_{SM}^2 + C^2 \right) \rho \tag{2.60}$$

where ρ is the phase-space factor.

The factors A_i , B_i and C are treated as adjustable factors which can be normalised to the observed cross section in the region of phase space which is dominated by the corresponding mechanism. The SM model does give quantitative results, but as remarked before, they are not reliable in the low-energy region. At low energies, the SM model should be used only to give qualitative descriptions as we have described above.

CHAPTER 3

PREVIOUS MEASUREMENTS AND CALCULATIONS

3.1 Measurements

There are two ways of obtaining total breakup cross sections. The first, which we term "direct",consists of detecting the breakup products. The second, which we term "indirect", consists in subtracting the integrated elastic differential cross sections from the total n-d cross section. This is possible because the breakup reaction is the only significant inelastic process at energies greater than 100 eV, (below which the cross section for radiative capture becomes significant) and less than the threshold for pion production at 270 MeV.

The uncertainties in the indirect method are determined by the uncertainties in the total and the elastic cross sections. The total n-d elastic cross section is known accurately (Se72) (Se70) (Ho68) (Cl72) (Br72a) in the region of interest the uncertainties being typically about 2%. However, the integrated elastic angular distribution is subject to larger errors, both systematic and statistical, especially in the case of n-d elastic scattering. For energies in the region of 20 MeV therefore, where the elastic cross section accounts for two-thirds of the total cross section, the possible error in the inelastic cross section obtained by subtracting the integrated elastic one, is large, being typically twice (on a percentage basis) the error on the elastic cross section.

Both direct and indirect measurements have been tabulated

in Table 3.1, together with references, and are displayed in fig. I.1.

The early indirect measurements were obtained from the evaluations of Horsley (Ho68). These authors used both p-d and n-d elastic angular distributions for energies less than 20 MeV to obtain evaluated curves for the n-d differential cross sections in that energy range. They corrected for the Coulomb effects in elastic p-d distributions by extrapolating past the Coulomb interference at small forward angles. In performing the extrapolation, these authors were guided by two criteria:

(a) changes in the slope of the distributions should be minimized

(b) the zero-degree cross section should be greater than Wick's limit (Wi43).

This latter criterion follows from the Optical Theorem.

Implicit in this procedure are the assumptions that the Coulomb penetration factor is negligible and that possible asymmetries in the nuclear force do not effect the phases significantly. The first assumption has been shown to be valid above 15 MeV (Va67). Justification for the second has been suggested in Chapter 1. In fact, the agreement between measured p-d and n-d angular distributions is, except for small forward angles, generally observed to be very good even at 14 MeV (See fig. I.2). The agreement is especially good over the back-angle exchange peak (Ho68). At energies below 9 MeV, there is a tendency for p-d differential cross sections to be slightly lower than corresponding p-d ones (Se72), as is expected.

Table 3.1

Indirect measurements of N-D breakup cross section

E_N MeV	Reaction	σ_T (mb)	σ_e (mb)	σ_B (mb)	Reference
14.10	n-d	803	638	164	Al53,Se55
14.10	p-d	803	638	164	Ki60
14.30	n-d	800	659	143	Be68
14.90	p-d	764	582	182	Ca71
15.50	p-d	753	550	198	Ca71
16.20	p-d	721	541	180	Ca71
16.90	p-d	698	502	196	Ca71
17.10	p-d	692	524	169	Ca71
17.70	p-d	674	479	195	Ca71
18.50	p-d	650	442	208	Ca71
18.55	n-d	649	486	163	Se72
19.00	p-d	635	426	209	Ca71
19.92	p-d	610	409	210	Ca71
20.50	n-d	595	447	148	Se72
20.57	p-d	595	389	206	Ca55
23.00	n-d	527	404	123	Se72
22.00	p-d	549	367	182	Bu68
25.70	p-d	486	323	160	Bi68
28.00	n-d	428	300	128	Go70
31.00	p-d	385	250	127	Ki64
35.00	p-d	332	191	141	Bu68
36.00	n-d	325	205	120	Ro70
46.30	n-d	243	145	98	Ro70
46.30	p-d	243	125	118	Bu68

The criteria used by Horsley have been used here to extend the evaluations to data that appeared after Horsley's publication. The difference between the integrals over these evaluated angular distributions and the total n-d cross section, are tabulated in Table 3.1 and plotted in fig. I.1. No attempt was made to estimate the uncertainty in these values. Only data above 14 MeV and below 50 MeV were considered. An idea of the magnitude of these uncertainties is given by Seagrave's indirect measurements which were obtained with his n-d elastic angular distributions at 18.55, 20.50 and 23 MeV, and published (Se72)(Se70) with estimates of uncertainty. It is not necessary to comment on individual measurements of elastic angular distributions since this has been done in several review articles (Se72)(Se70)(Ho68).

Direct measurements are sparse. All measurements of the total n-d breakup cross section are confined to energies below 14.1 MeV. Recently, the inelastic p-d breakup cross section has been measured (Ca72) at energies ranging between 23 and 50 MeV. We are not aware of any direct measurements in the energy region between 14.1 and 23 MeV.

Direct measurements of the total n-d cross sections were made with large liquid Cadmium- and Gadolinium-loaded scintillators (Ca61)(As58)(Ho69) having neutron detection efficiencies in excess of 90% and designed to determine neutron multiplicities. These data were also evaluated by Horsley (Ho68) and the conclusion was reached that Holmberg's data (Ho69), which extend from 4.0 to 6.5 MeV, are too low to be consistent with a smooth dependence, taking into account Catron's (Ca61)(As58) data at higher energies.

A value was obtained at 14.5 MeV (Se72) by measuring and

integrating the total proton energy distribution. This method is similar to the one used in this work. The value obtained is lower than a previous measurement at 14.1 MeV (Ca61).

Other values could be obtained from the measurements of the differential cross section for proton emission (Al53) (Se55) (Sh68). Unfortunately, these are rather incomplete, being restricted to the forward hemisphere and to proton energies in excess of $\sim$3 MeV. This latter restriction makes them useful only if the proton energy spectra were measured in obtaining the differential angular distributions. In this case, extrapolations could be made to zero proton energy. Only the data of Seagrave (Se55) at 14.1 MeV, permitted this to be done over a wide angular range (0-80^{o}lab), but no attempt was made to extrapolate to back angles.

Similar measurements were made of neutron energy spectra from p-d breakup at 6.5 MeV (Cr59) and 9.0 MeV (Ni61). These were rather more extensive, and values of 65 $\pm$ 10 mb and 110 $\pm$ 6 mb respectively, were obtained, in good agreement with n-d data at these energies.

The recent p-d measurements above 23 MeV were made using a modified transmission method in which transmitted protons, as well as elastically scattered ones, were used to veto events. A wide-angle detector close to the target, is able to detect a large fraction of elastically scattered protons because elastically scattered protons proceed in a forward direction only, and the solid angle ratio is small at large recoil angles. However, the solid angle increases with decreasing energy, so that at lower energies covered by these measurements, elastic corrections are not negligible (Ca72).

3.2 Calculations and Phase Analyses

There exists a large body of early theoretical work on n-d scattering (Ma58)(Ve57). Most of this work is of a very approximate nature and results are not relevant, except in an historical context. An exception is the work of Christian and Gammel (Ch53) and Frank and Gammel (Fr54), who used Born approximation to calculate elastic (Ch53) and breakup (Fr54) cross sections. These authors used the Born approximation (See Chapter 2) as formulated by Gluckstern and Bethe (Gl51) with central spin-dependent potentials. To calculate breakup cross sections, they used a scattering wave function which took account only of a n-p final state interaction and, obtaining an integral similar to that for elastic scattering (Ch53), they replaced it with experimental elastic angular distributions.

This kind of impulse approximation was used to calculate energy distributions of the breakup products, which were integrated to obtain differential total breakup cross sections below 14 MeV. The results were compared with measurements of differential cross sections from n-d (Al53) and p-d (Fr54) breakup. The comparison was found to be satisfactory. Comparison with later measurements of the total breakup cross section (Ca61)(Ho69) was also found to be reasonable, although calculated values tended to be too small at higher energies. This was attributed to the failure to include the n-n final-state interaction in the final-state wave function.

In a theory which satisfies unitarity, the total breakup is more easily obtained from the imaginary part of the inelastic scattering amplitudes. This cannot be done in Born approxi-

mation since the phase shifts obtained in this manner, are real. However, these have been useful as starting values for phase analyses. This was the procedure adopted by Christian and Gammel (Ch53), but in their phase analyses inelasticities were not taken into account.

Considerably later, Van Oers and Brockman (Va67) used the same method to obtain starting points of their phase analyses of p-d data between 1 and 40 MeV. These authors considered only central forces, as did Christian and Gammel, but they allowed for inelasticities. The real parts of the phase shifts for partial waves with angular momentum $\ell \geq 1$ (up to $\ell = 11$) were calculated in Born Approximation. These were then used as starting values for an analysis of p-d elastic differential cross sections, in which S, P and D phase parameters were allowed to vary.

The total breakup cross section was used to set an additional constraint on the analysis, through the expression for the breakup cross section σ_B in terms of the inelastic parameters ${}^{2s+1}Y_\ell$

$$\frac{k_o^2}{\pi}\,\sigma_B = \frac{2}{3}\sum_\ell (2\ell+1)[1-({}^4Y_\ell)^2] + \frac{1}{3}\sum (2\ell+1)[1-({}^2Y_\ell)^2]$$

where the inelastic parameters were defined as

$${}^{2s+1}Y_\ell = \exp(-2\,{}^{2s+1}\varepsilon_\ell)$$

for complete phases $({}^{2s+1}\delta_\ell + i\,{}^{2s+1}\varepsilon_\ell)$

Both direct and indirect measurements of the total breakup cross section were used. The indirect ones were obtained from elastic p-d angular distributions, and comprise some of the values plotted in fig. I.1. These authors found it

difficult to determine inelastic parameters and, in order to prevent unrealistic solutions, they constrained the ^2S and ^4S inelastic parameters, as well as the ^2D and ^4D ones, to be equal. This analysis was subsequently extended (Va67a) to include n-d data, but the inelastic parameters were held equal to those obtained previously.

Phase analyses with split phases were also attempted to allow for the effect of non-central forces (Ar67)(Br71). The first comprehensive "exact" calculations of n-d scattering and breakup were published by Aaron, Amado and Yam (Aa65). These were performed using the model developed by Amado (Am63). S-wave spin-dependent, separable potentials were used and no account was taken of non-central forces. The D-wave admixture of the deuteron which follows from the $^3S_1$ - $^3D_1$ tensor force was obtained by introducing a phenomenological renormalization factor which expressed the probability of the deuteron being in a D-state. Apart from the triton binding energy and the zero-energy n-d scattering parameters, angular distributions, total cross sections and phase shifts were calculated at 5 energies between 2 and 14 MeV. Agreement with measured angular distributions is fair, and with the total breakup cross section, good in the energy range considered. The phases were found by Van Oers and Brockman (Va67) to be in good agreement with their phase analysis.

About the same time, another "exact" calculation was performed by Phillips (Ph66), using the formalism of Lovelace (Lo64). Separable potentials similar to Amado's were used, but the effects of the tensor force were simulated by means of a separable phenomenological three-body force. The n-d elastic angular distributions and total cross sections were

calculated for energies below 20 MeV. The agreement with experiment is not as good as for Amado's calculations. In particular, the total breakup cross section is considerably lower than experiment. Later, both authors extended these calculations to calculate energy spectra of breakup products (Aa66)(Ph66a). It has been suggested (Am69) that the calculations of Aaron, Amado and Yam are more reliable than those of Phillips because of the superiority of the contour deformation method used by these authors to deal with singularities in the kernels of the integral equations.

Calculations using Amado's model were later revised and extended to higher energies by Sloan (Sl71), with only minor differences in computational method. Besides complex phase shifts, elastic angular distributions and the total breakup cross section were calculated for energies below 40 MeV. The calculated total breakup cross section, together with the results of other calculations described below, is shown in fig. 1.1.

Calculations were also performed using dispersion theory (Av69). These calculations obtained S, P and D complex phase shifts, as well as differential cross sections below 30 MeV. The calculations were performed with separable interactions for convenience, and it has been observed (Sl71) that they constitute an approximation to the exact calculations using Amado's model (Sl71). A notable simplifying procedure in these calculations was the use of the experimental doublet inelastic parameters of Van Oers and Brockman (Va67) to calculate the doublet elastic phases.

A comparion of results (Se72) reveals that while the overall agreement between experiment and theory is good for

the real quartet phases, this is not the case for the doublet ones, while in the case of the inelastic phase parameters, it is as bad as it could be. This disagreement is reflected in the disagreement between Sloan's calculation of the total breakup cross section and the experimental values obtained by Van Oers and Brockman.

The successive inclusion of $^3S_1$ - $^3D_1$ tensor forces and higher partial waves has been described in Chapter 2. Several calculations were performed of elastic angular distributions and polarization observables. The polarization observables were found to be most sensitive to the details of the nuclear force and successively indicated the need to include $^3S_1$ - $^3D_1$ tensor forces and higher partial waves.

Most recently, S, P and D-wave separable forces have been included (Pi72), by means of a perturbation method (Sl72), in extensive calculations of elastic angular distributions and polarization observables between 2 and 77 MeV. Later, these authors also included the $^3S_1$ - $^3D_1$ tensor force (Pi72c)(Pi73). Separable tensor and P-wave forces were included exactly in calculations at 14.1 and 22.7 MeV (Do73). Both these calculations showed marked improvements in both the calculated polarizations and the elastic angular distributions. Total breakup cross sections were also calculated (Do73a) and are plotted in fig. 1.1.

A breakthrough in another direction was made by the inclusion of local potentials (Tj70a) in the Faddeev formalism. Calculations using S-wave local potentials incorporating hard cores (Ma69)(Re68) were performed for n-d elastic scattering (Kl71)(Kl72a)(Kl73), as well as breakup (Kl72)(Kl73). The total breakup cross section predicted by these calculations

with two types of Yukawa potentials are shown in fig. 1.1. To test the effect of varying the form of the potential, the nature of the core, as well as the low-energy scattering parameters, were varied in the singlet state for calculations at 14.4 MeV (Kl73). Phase parameters were also calculated at this energy. Although generally substantiating the results of Sloan (Sl71) in preference to the phase analyses (Va67) there is some discrepancy between the two calculations in the lower partial waves.

The breakup cross section was found to be sensitive to changes in the potentials in general. It is seen to be particularly dependent on whether potentials are local or separable (see fig. 1.1).

CHAPTER 4

THE EXPERIMENT

4.1 Outline

A schematic representation of the experiment is given in fig. 4.1. Monoenergetic neutrons were obtained from the $T(d,n)^4He$ and $D(d,n)^3He$ reactions using a pulsed deuteron beam from a 5.5 MV pulsed Van de Graaff accelerator. The neutron energy was varied by changing the selected angle of emission with respect to the beam axis. Incident gammas and lower energy neutrons were separated out in a time-of-flight system.

Deuterated scintillators, optically coupled to photomultipliers, were used both as deuterium targets and detectors of charged recoil particles and reaction products. The energy of charged particles was deduced from the integrated scintillation output or pulse height L. A pulse-shape-discrimination (PSD) circuit incorporated in the detector assembly was used to obtain a pulse (S) characteristic of the scintillation decay time and hence the nature of the ionising particle. When analysed in coincidence in a 64 × 64 two-parameter analyser, various ionising particles are observed to lie on separate, well-defined ridges (see fig. 4.6). In particular, the breakup protons are clearly separated from the recoil deuterons over a wide range of L (and hence proton and deuteron energy). The projections of these ridges (see fig. 4.12) on the L-axis represent the energy distributions of the corresponding particles, modified by the non-linear pulse-height response and finite resolution of the detector.

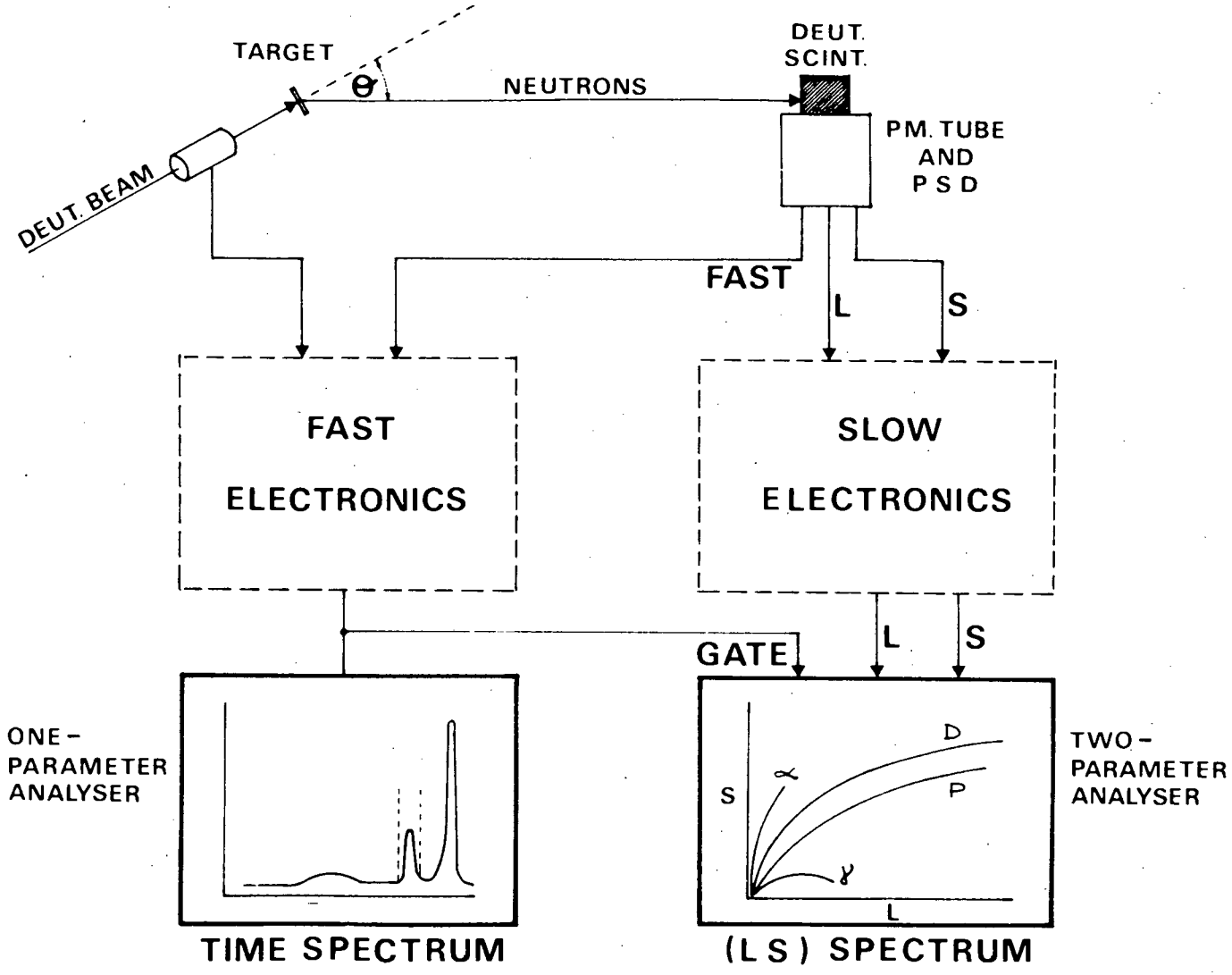

Fig. 4.1. Schematic representation of the experiment. The "fast" electronics are used to obtain a time-of-flight spectrum of the neutrons incident on the deuterated scintillator. The "slow" electronics enable the pulses L and S to be analysed coincidentally in a two-parameter analyser. These events are usually coincidence gated by events falling on a window set on the primary neutron peak in the time-of-flight spectrum.

The response of deuterated benzene scintillators was obtained directly by using an incident neutron spectrum containing a wide range of energies and analysing pulse-height L and the neutron time-of-flight τ in the two-parameter analyser. For any incident neutron energy, the maximum deuteron recoil energy is known. Since the recoil deuteron energy distribution peaks sharply at maximum energy, the corresponding pulse-height is a well-defined function of incident neutron energy.

4.2 Neutron Production

Monoenergetic neutrons were obtained from the $T(d,n)^4He$ and the $D(d,n)^3He$ reactions. Deuterons were produced by the 5.5 MV Van de Graaff accelerator of the Southern Universities Nuclear Institute (S.U.N.I.). The accelerator is capable of beam currents up to 5 μA. The beam energy is monitored by a nuclear magnetic resonance (NMR) probe inserted in the field of the accelerator analysing magnet. The NMR probe was calibrated periodically by observing the threshold (1.881 MeV) of the $^7Li(p,n)^7Be$ reaction. The accelerator is pulsed with a frequency of 2 MHz and is equipped with a Klystron bunching system which delivers pulses of $\sim$2 ns duration for a deuteron beam.

Both solid and gaseous tritium and deuterium targets were used. The solid targets were tritiated and deuterated titanium deposited on gold foil (obtained from UKAEA-Amersham). The gaseous targets were locally produced cylindrical cells with nickel and Havar windows for deuterium and tritium respectively. To prevent thermal outgassing of the solid

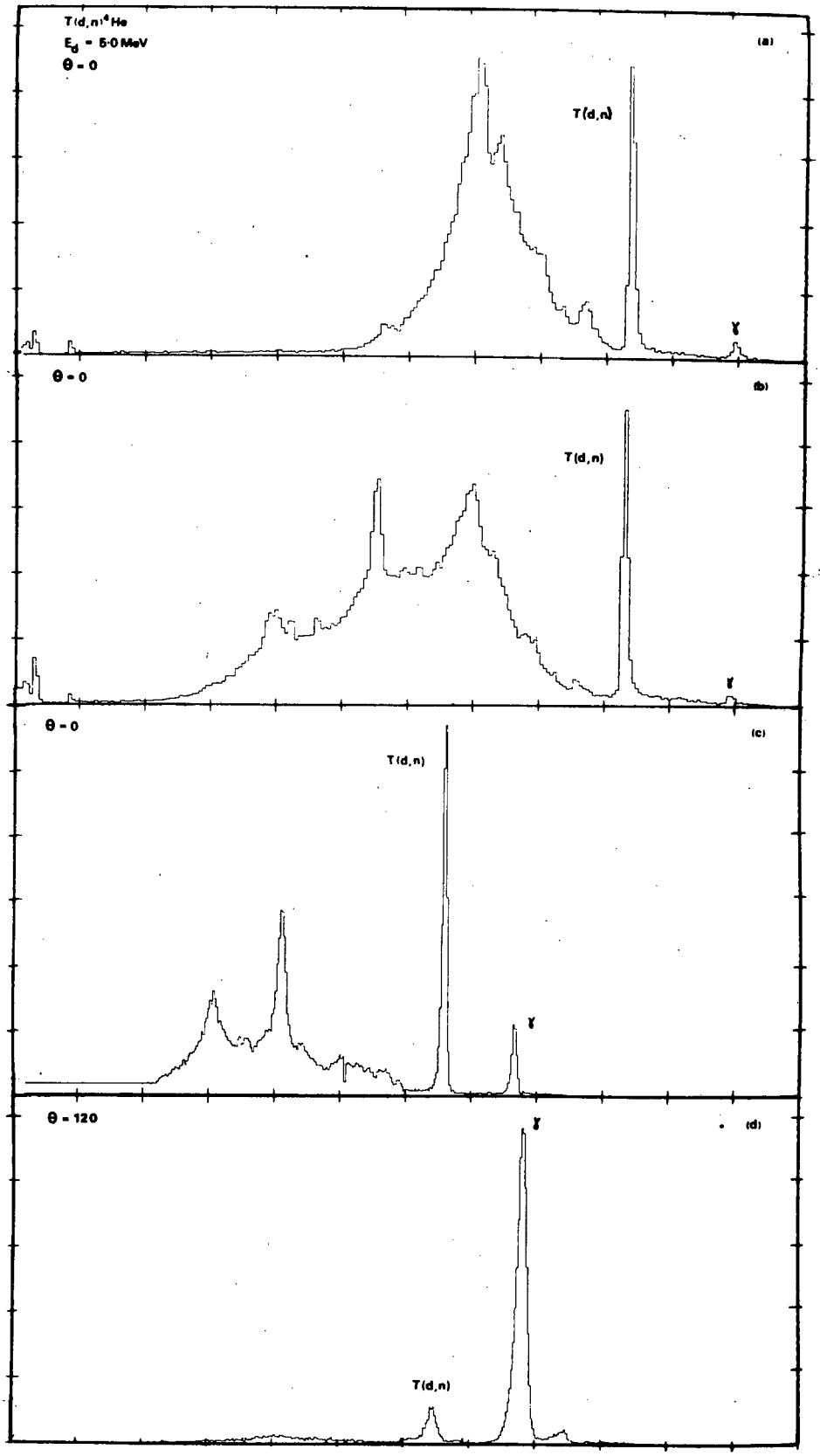

Fig. 4.2. Time-of-flight spectra for the $T(d,n)^4He$ reaction at 5.0 MeV obtained with a solid target for

(a) bad beam optics
(b) bad beam optics and shielding
(c) good beam optics and no shielding
(d) 120 neutron angle of emission.

The low-energy neutrons in (c) and (d) are due principally to deuterium breakup on tritium and on heavier target constituents. PSD was applied to (a), (b) and (c) to discriminate against gamma

targets, cooling was effected by a liquid nitrogen cold trap coupled to the target by means of a copper cold finger. The gas targets were cooled by a pressurized jet of air directed at the cell.

The neutrons were analysed in a time-of-flight system. Flight paths ranged between 1 and 6 metres. Time-of-flight spectra recorded with different targets are displayed in figs. 4.2 and 4.3. The spectra are seen to contain a low energy component from deuteron breakup. The two distinct groups are attributed to the breakup on tritium and on heavier target constituents.

The effects of shielding and deterioration of beam optics on the background were investigated (fig. 2.2). The level of the background was seen to be very dependent on beam optics. This can be seen by contrasting the various spectra displayed in fig. 4.2 some of which were obtained with a badly focussed beam.

The effect of shielding the detector with a mixture of Li_2CO_3 and paraffin wax was also tested. The result was an increase in the background level at all energies (see fig. 4.2) and a particularly marked increase at low energies. Open geometry was consequently used for the experiment.

Gamma discrimination (see fig. 4.2) showed that most of the background under the primary neutron peak was due to room-scattered gammas. At forward angles, the background level is seen to be negligibly small. The peak to background ratio decreases as one moves to backward angles because the differential cross section for the T(d,n)^{4}He reaction decreases rapidly with increasing angle of emission (Go63). Nevertheless it is good even at 120^0(see fig.4.2). More can be learnt about the nature

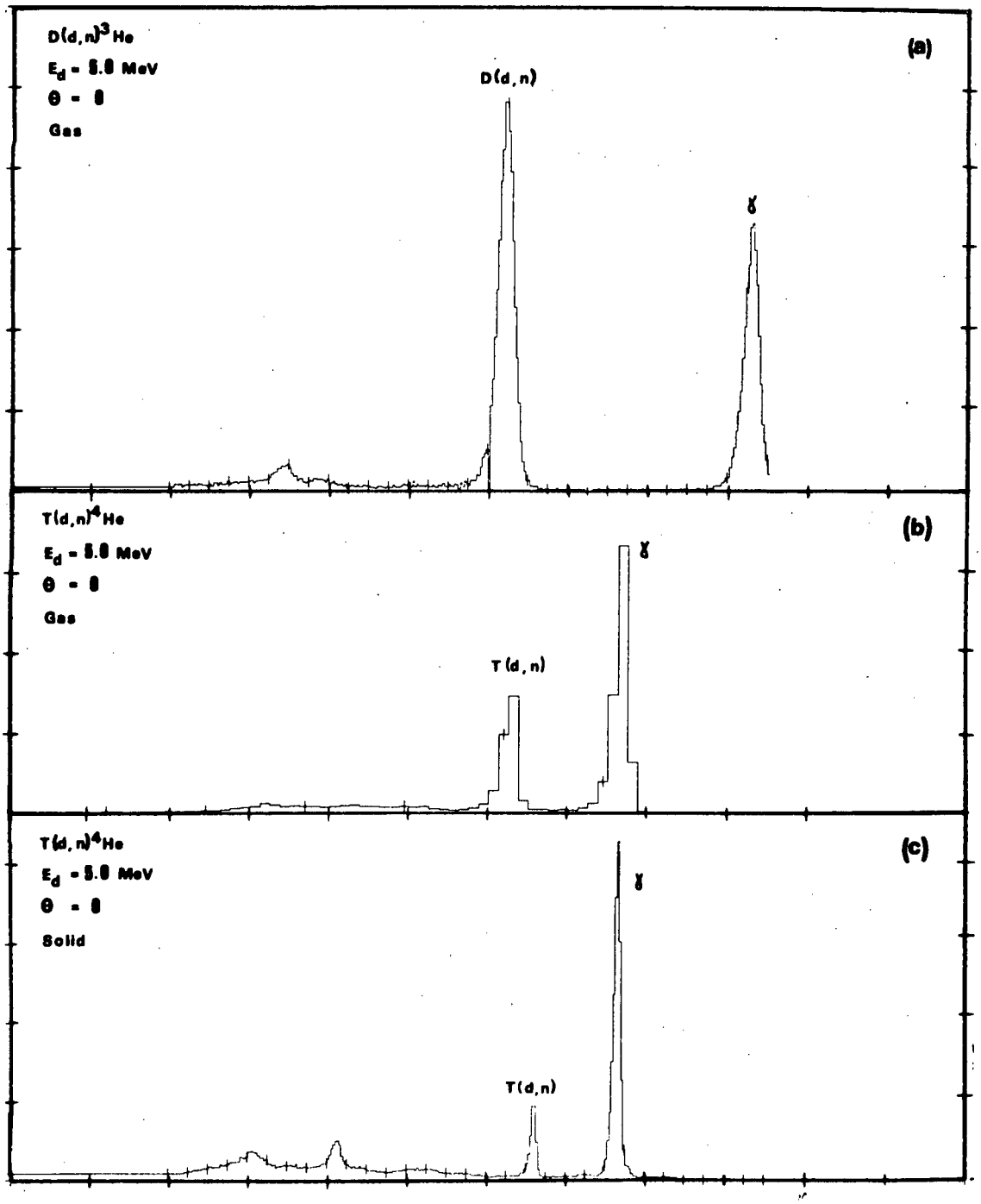

Fig. 4.3. Time-of-flight spectra for the D(d,n)^{3}He and T(d,n)^{4}He reactions at 5.0 MeV using different targets.

(a) D(d,n)^{3}He with a gas target
(b) T(d,n)^{4}He with a gas target
(c) T(d,n)^{4}He with a solid target

All spectra were recorded at 0^o neutron angle of emission and PSD was not applied to discriminate against γ.

of this background from the two-parameter analyses of pulse-height and time-of-flight (L-τ spectra - see section 4.5.). Such an analysis, performed at an emission angle of 120°, is shown in fig. 4.13. From the pulse-heights in the region of the neutron peak, it was concluded that, if any significant neutron background was present, the background comprised only low-energy (< 1 MeV) neutrons. Consequently, it would not effect the experiment since the energy cutoff of our analysis (see chapter 5) was usually > 2 MeV.

4.3 Deuterated Scintillators

Deuterated scintillators were used both as deuterium targets and as detectors of recoil deuterons and protons from n-d breakup. They are commonly used as target-detectors to reduce background levels when a scattered or breakup neutron is counted in a second detector. However, they have seldom been used as spectrometers (Be68)(Ve63)(Bl64) and, to our knowledge, the pulse-shape discrimination (PSD) capabilities of one (deuterated benzene) have been expolited fully in only one instance (Gr71).

However, it has been observed more than once (Cz70)(Sm68)(Bo72) that NE230 has excellent PSD characteristics, better in fact than NE213 (Cz70).

Deuterated benzene (NE230) was obtained in bulk from Nuclear Enterprises Ltd. and was sealed in cylindrical glass capsules at the University of Cape Town. See fig. 4.4
In order to ensure optimum PSD performance, care was taken to free the scintillator of dissolved oxygen. This was done by either or both of two methods.

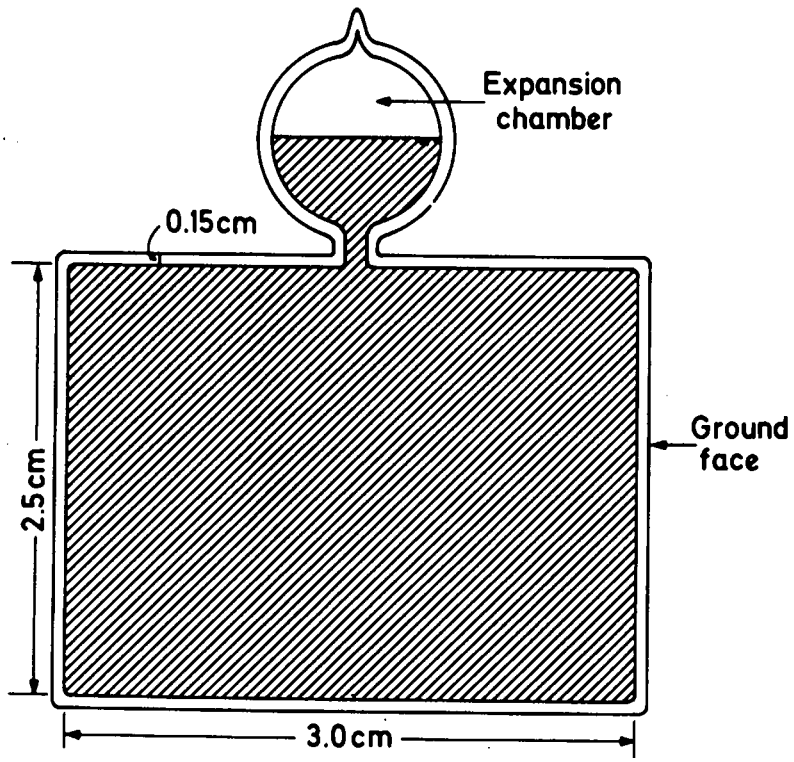

Fig. 4.4 Cross section of a cylindrical capsule used to contain deuterated benzene.

One method consists of displacing dissolved oxygen by bubbling nitrogen through the scintillator contained in the capsule. The capsule is then kept under nitrogen atmosphere and cooled to liquid nitrogen temperatures where it can be sealed by fusing without fear of igniting the benzene gas. Immediately prior to fusing, the expansion chamber (see fig. 4.4) is evacuated. When it is returned to normal temperatures the sealed capsule contains only a small partial pressure of nitrogen (due to the nitrogen which was in solution when the scintillator was frozen). The scintillator can therefore expand and contract under normal temperature variations without building up high pressures in the capsule.

Dissolved oxygen can also be expelled by two or more cycles of freezing, evacuation and thawing. As a result of

this procedure, the residual partial pressures of nitrogen and oxygen in the capsule are essentially zero.

In order to study the dependence of rescattering and edge effects on the volume of the scintillator, capsules of three different dimensions were made. The capsules were cylinders of 3 cm diameter and their heights were 1.5 cm, 2.5 cm and 4 cm.

4.4 Detection and Particle Discrimination

The deuterated scintillators were optically coupled to 56 AVP photomultipliers. A voltage divider chain similar to one used by Hyman et al. (Hy64) was selected (see fig.4.5). This distribution was developed (Hy64) to preserve linearity over a wide dynamic range and was therefore suitable for our purposes. The design of further circuitry associated with the voltage distribution chain, was determined by the need to preserve stability over a wide dynamic range, while at the same time, being able to cope with high count rates. To preserve stability the last ten dynodes were shunted capacitatively to earth. It was considered preferable to shunt each dynode to earth individually rather than to use interdynode shunts since, with the latter alternative, large pulses near the anode are more likely to effect voltages at the upper end of the chain. Circuit components were chosen to preserve voltage stability to better than 1% for peak currents of 10 ma. at dynode 13. The resulting maximum RC time constant is 40 μsec. A constant cathode-first dynode voltage was maintained by means of zener diodes. Inductive effects were reduced by keeping the shunt-capacitor leads

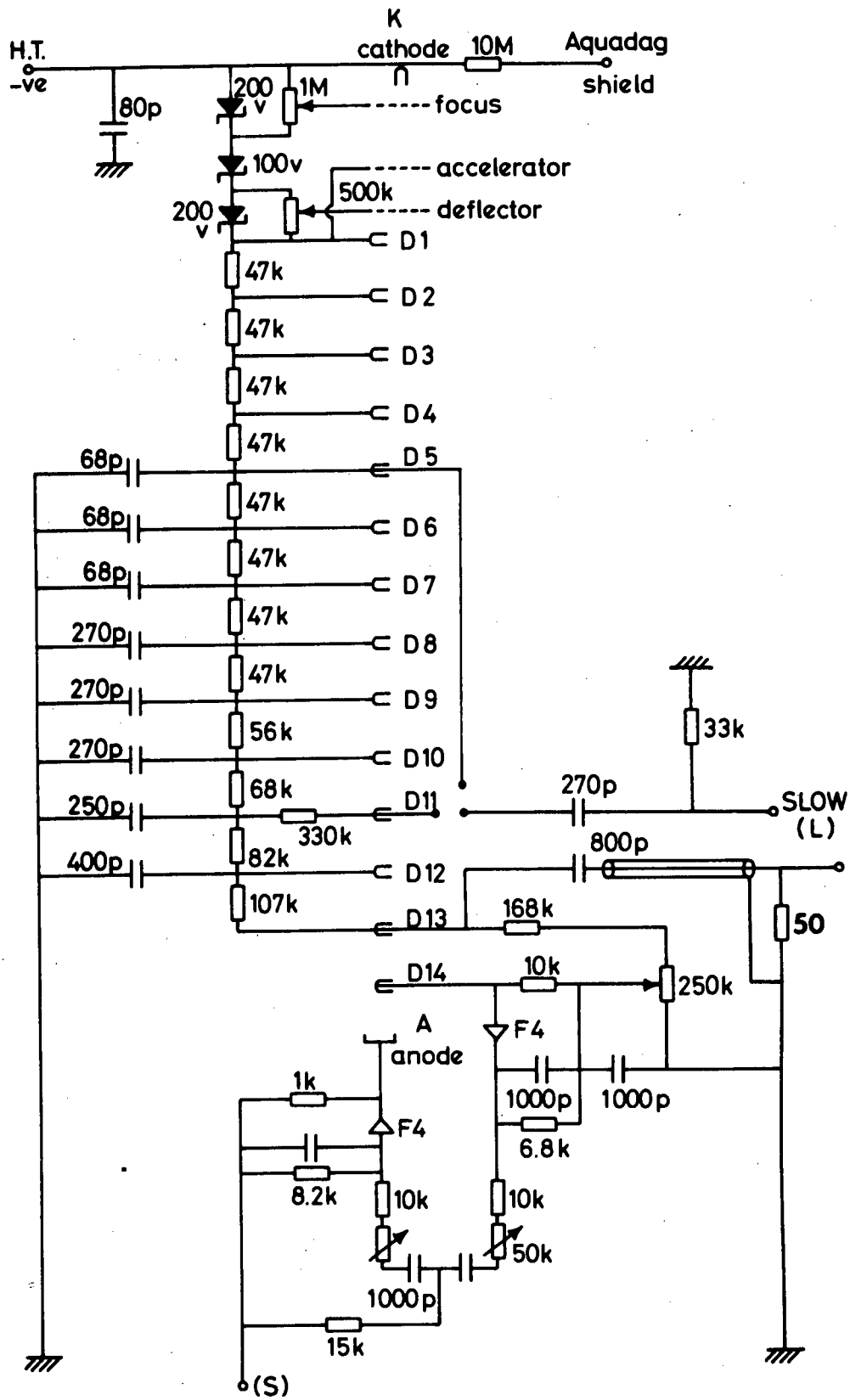

Fig. 4.5. Dynode chain potential divider and pulse shape discrimination circuits.

short in general and by shielding longer leads with coaxial cables. Detailed accounts of the design of photomultiplier circuitry are given by (Hy64)(Be63)(Be64)(RCA70)(PHI70).

A pulse-shape discrimination circuit (Br59) was coupled to the photomultiplier base of the detector (see fig. 4.5). This circuit produces an output pulse (S) which is a function of the decay times ("shape") of the light emission, and consequently of the nature of the particle.

After amplification, this and the linear pulse (L) (taken from dynode 11) were fed into the ADC's of a two-parameter analyser (see section 4.5). The L-S spectrum resulting from such an analysis is shown in fig. 4.6 and fig. 4.7. The events corresponding to different ionising particles are seen to lie on well-defined ridges in the L-S plane. Ridges corresponding to carbon (C) and deuterium (D) ions, alphas (α) from carbon breakup, protons (P) from deuterium breakup, and electrons (e) produced principally by Compton scattering, are identified. The ridges are well-separated at high energies, but the separation diminishes with decreasing energy. This is due to the statistical nature of the light production and amplification process. As the number of photons in the scintillation decreases, the fractional variance of the mean number increases. With the aid of computer techniques described in section 4.5, the proton energy at which protons could be separated from deuterons was extended down to 3 MeV. Below this energy the multiplicity of peaks which merged did not permit reliable separation of the proton contribution.

A figure of merit for the degree of separation is given by

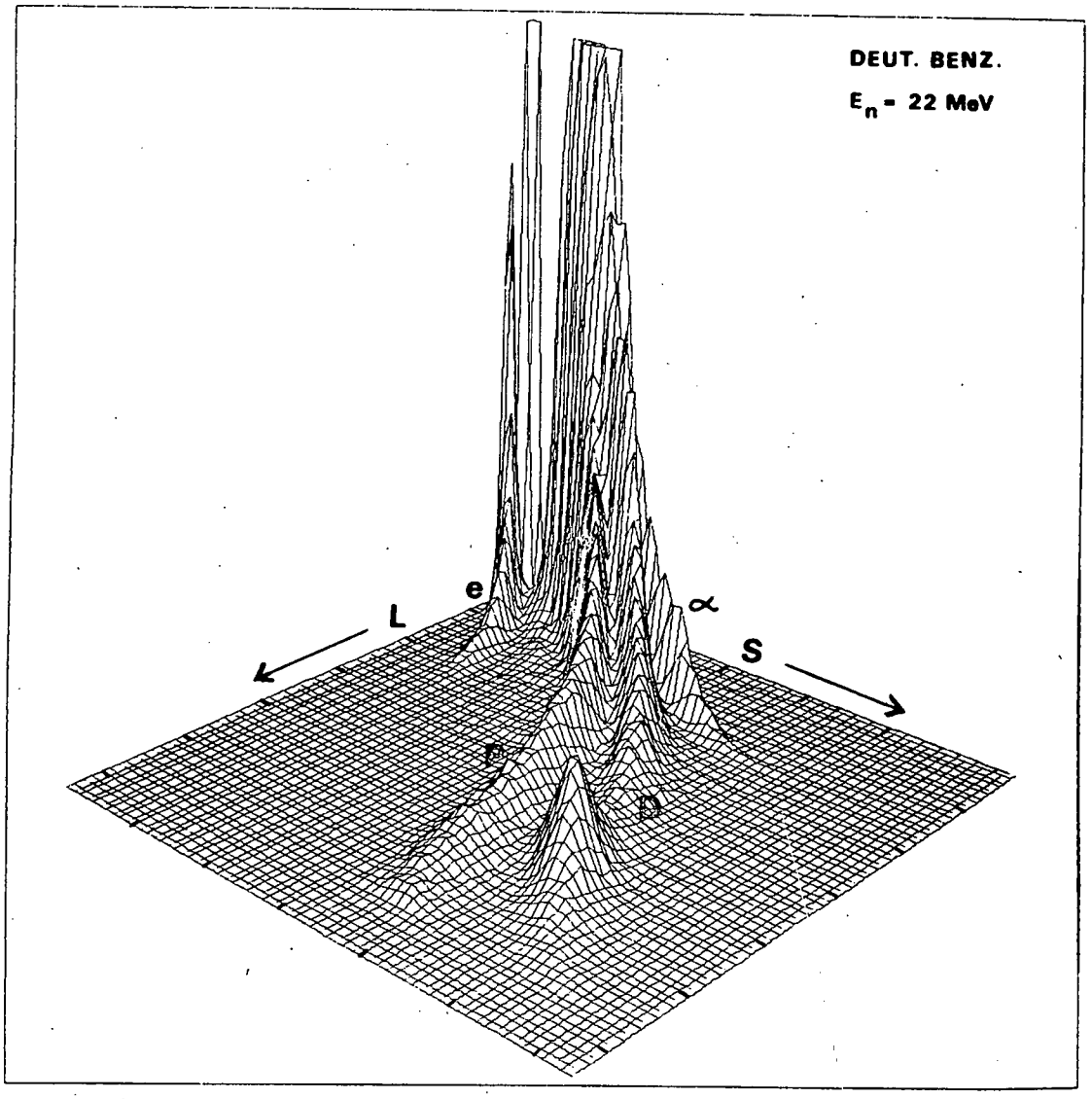

Fig. 4.6. An isometric representation of an (LS) spectrum obtained for 22 MeV neutrons incident on deuterated benzene. Letters e, P and D and α indicate that the corresponding ridges are due to Compton electrons, protons, deuterons and alphas respectively.

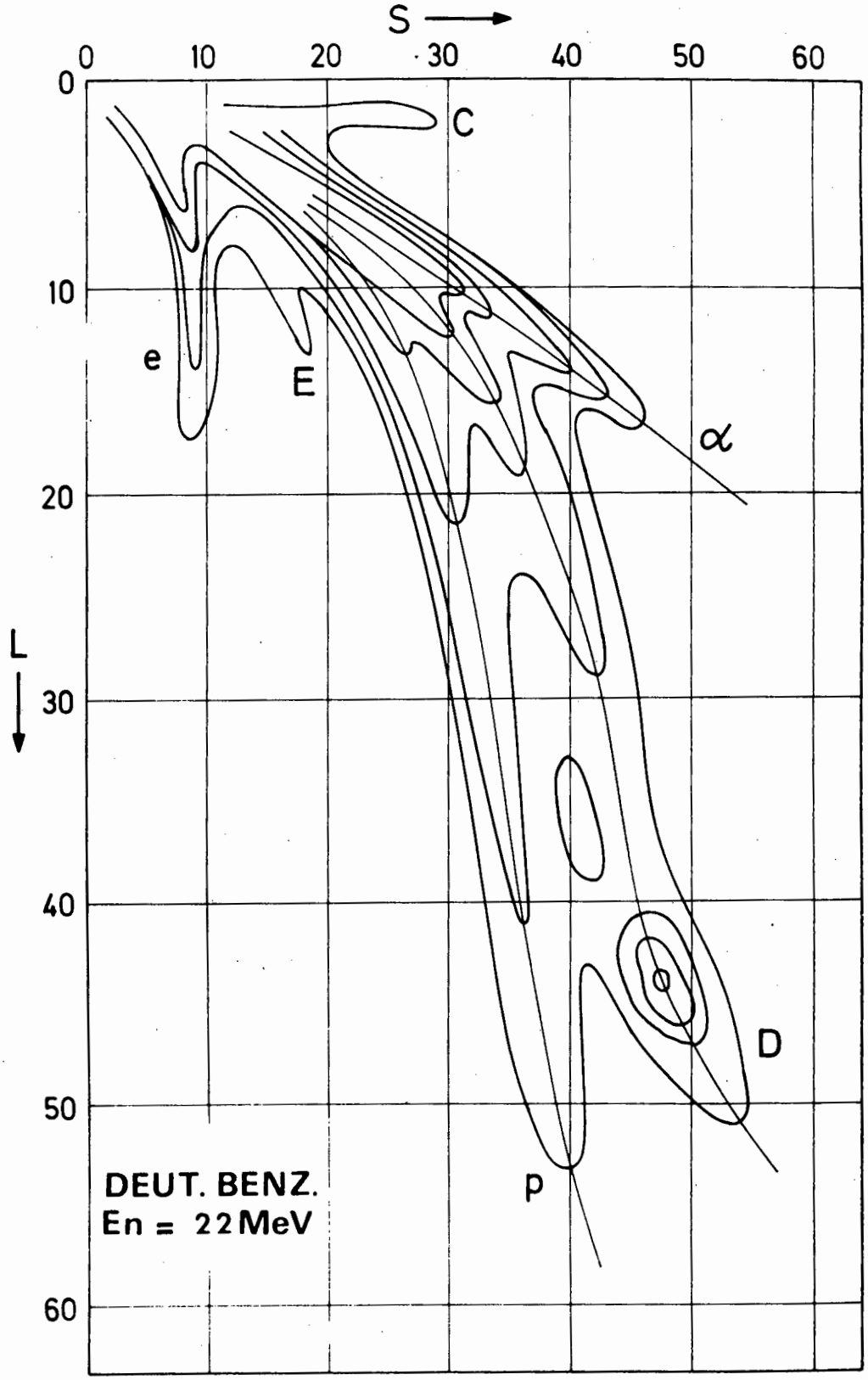

Fig. 4.7 Contour Representation of an (LS) spectrum obtained for 22 MeV neutrons incident in deuterated benzene The letters e, E, P, D, α and C indicate that the corresponding ridges are due to Compton electrons, escapes, protons, deuterons and alphas respectively.

$$M = \frac{S_D(L) - S_P(L)}{\Delta_D - \Delta_P}$$

where Δ_D and Δ_P are the half-widths of the peaks obtained when a section of the ridges is taken at pulse-height L (see fig. 4.11). For L-values corresponding to deuterons recoiling with an energy of 19.7 MeV (corresponding to 22 MeV incident neutrons) M was generally $\sim$2 for deuterated benzene (NE 230). The PSD qualities of NE 230 (and NE 231) were generally found to be superior to those of NE 213. This is in agreement with previous observations (Cz70).

Several other pulse-shape discrimination circuits have been designed (Ow58)(De62)(Fo62)(Ga62)(Al61). The one which is most often used is the zero cross-over technique first proposed by Alexander and Goulding (Al61). The possibility of using this technique was investigated, but it was found possible to discriminate only between electrons and the heavier ionising particles (see fig. 4.8).

4.5 Data Accumulation and Reduction

A block diagram of the electronic configuration is given in fig. 4.9. Apart from minor variations, this configuration was retained throughout the various experimental runs.

Background is reduced by time-of-flight analysis. A window was set on the primary neutron peak and this was used to gate the accumulation of events in the (L,S) spectra. Optimum timing resolution ($\sim$2n.sec = beam pulse-width) was obtained with "Constant Fraction" (CFD) timing discriminators

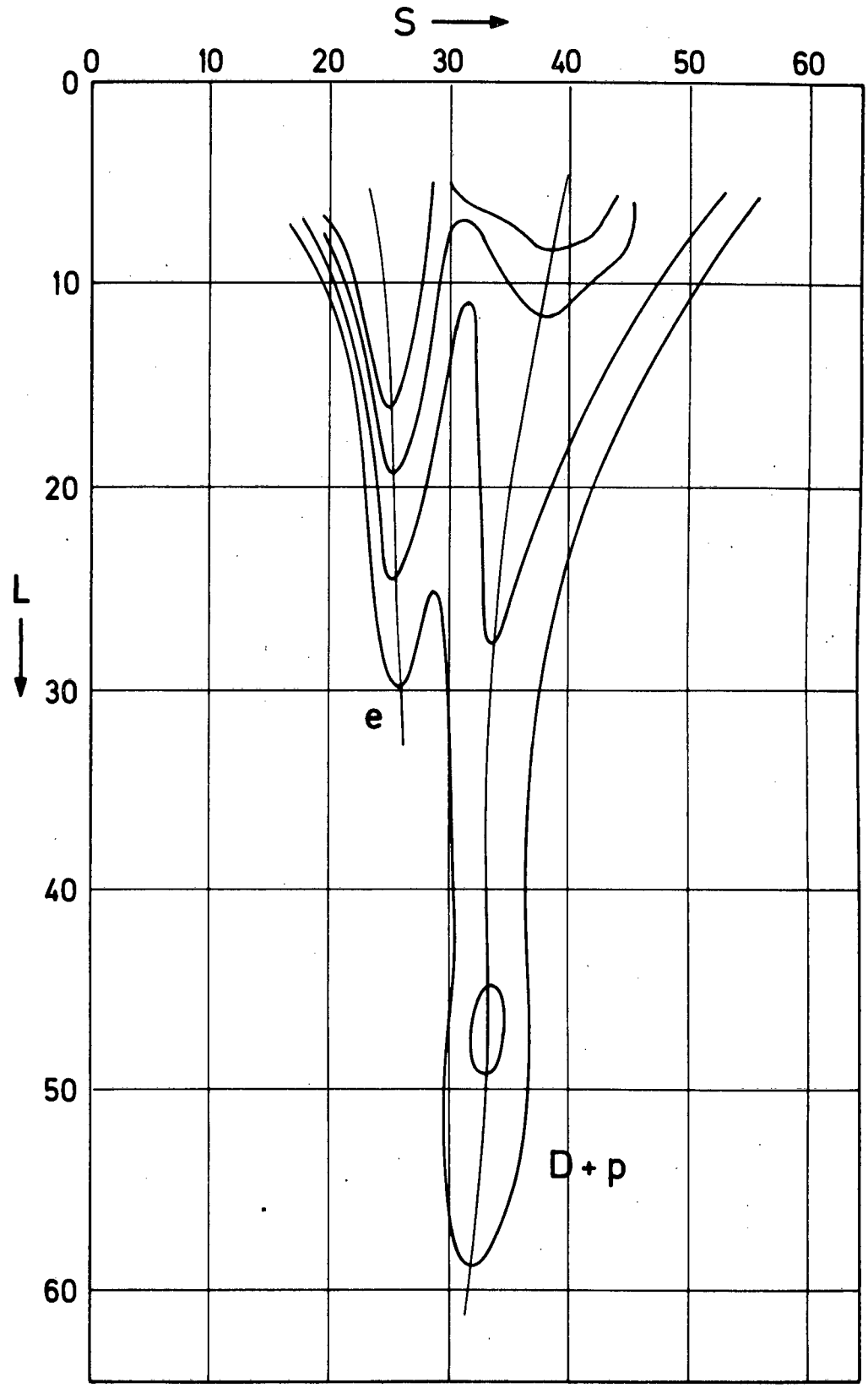

Fig. 4.8. Contour representation of an (LS) spectrum obtained with a cross-over pulse shape discrimination technique. The letters e, D, p indicate that the corresponding ridges are due to Compton electrons, deuterons and protons. The deuteron and proton ridges are not separated.

(ORTEC 463). This permitted 22 MeV neutrons to be resolved from the γ-flash at flight-paths as short as 0.5 m. Adequate count-rates were obtained at 1 m. The time-of-flight spectrum was monitored continuously to keep a check on deterioration of beam optics and electronic stability.

Because of the high γ-flux, it was feared that pile-up might distort the pulse-height spectra. However, upon incorporating pile-up rejection, no significant difference was observed.

The data were accumulated during several independent runs. Measurements were repeated at some energies to verify that they were consistent, and with scintillators of three different sizes (see section 4.3) to test methods of correction for edge effects and rescattering. In each set of measurements, the linearity of the amplifier and the zero of the true pulse-height distribution amplifier on the L-side was checked by making additional runs with the amplifier gain reduced by a known factor.

For some (LS) spectra, corresponding (Lτ) spectra were obtained by replacing S-pulses into the two-parameter analyser, with the output (τ) of the TAC. The time-of-flight gate was rendered inoperative for these runs.

For this purpose, the low energy neutrons due to deuteron breakup were useful in providing a limited range of incident neutron energies. A wider range could be obtained by moderating the neutron spectrum. This was done by placing iron and paraffin wax between the neutron source and the detector. However, with this method, the amount of scatterer that one may use is limited to dimensions which are small compared with the flight path. Consequently, long runs were needed to accumulate sufficient statistics. For this purpose, a neutron

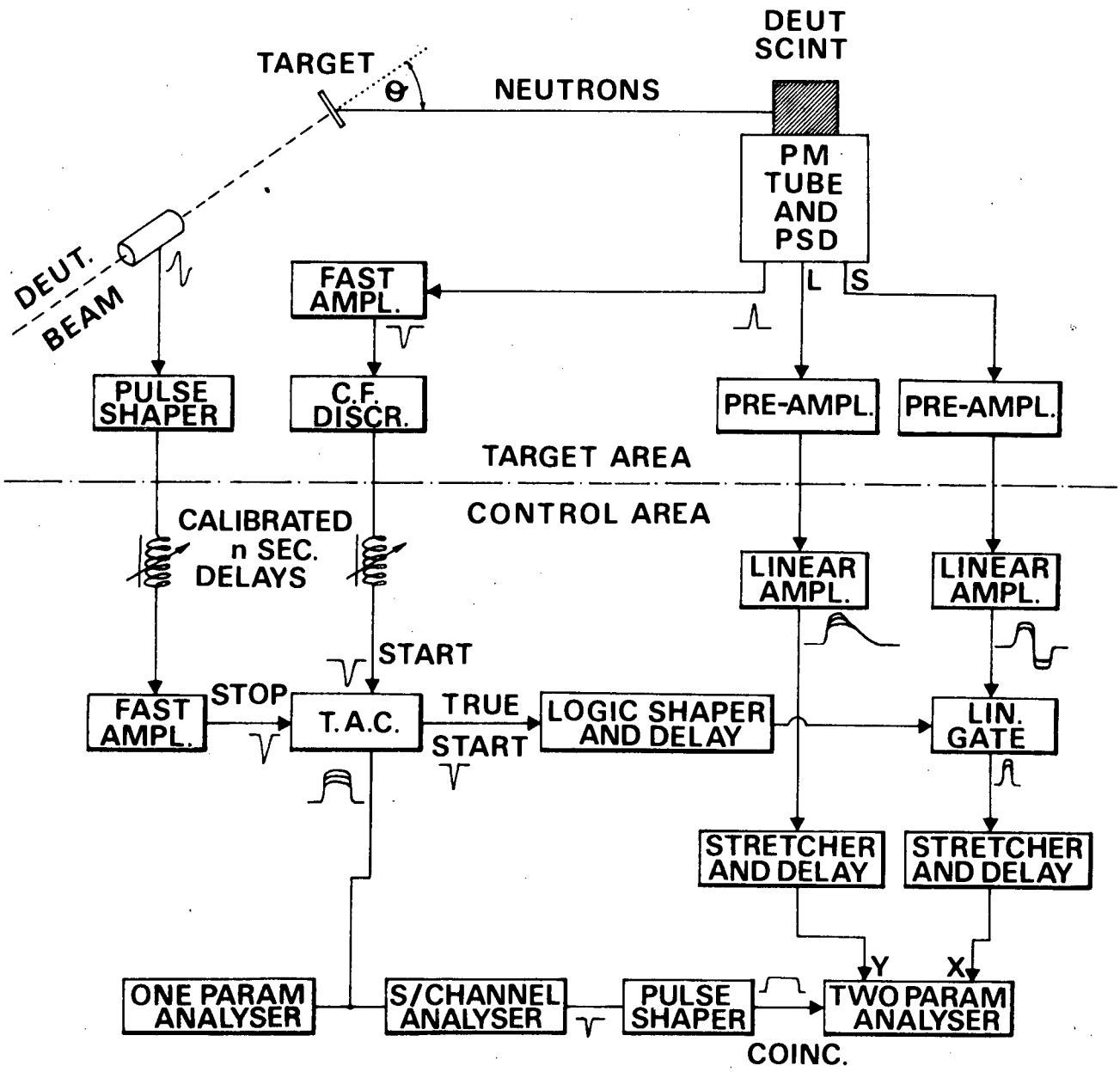

Fig. 4.9. A block diagram of the electronic configuration. The fast electronics on the left-hand side are used to obtain a time-of-flight spectrum of incident neutrons whereas the slow electrons on the right-hand side are used to analyse the L and S pulses coincidentally and obtain an (LS) spectrum. This spectrum may be gated by a window which is set on the neutron. The function of various parts of the circuit is represented schematically in Fig. 4.1. The right-hand side of this configuration corresponds to the slow electronics on Fig. 4.1 and the left-hand side to the fast electronics.

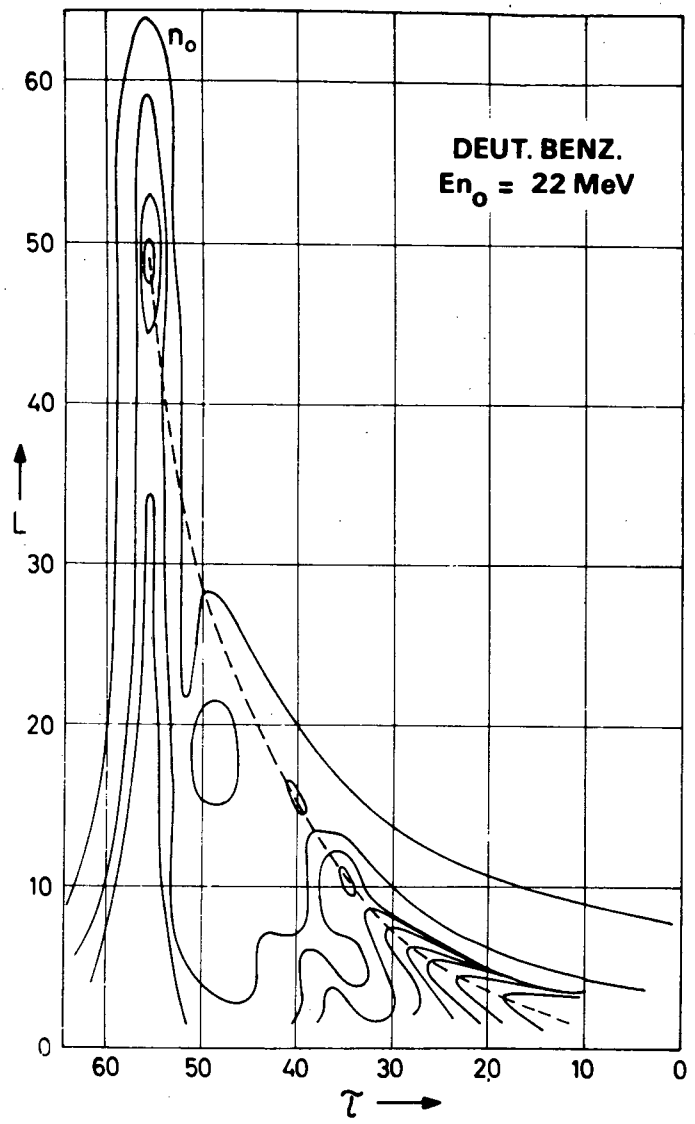

Fig. 4.10(a). Contour representations of (Lτ) spectra obtained with a wide spectrum of incident neutron energies. The dotted line indicates the position of the forward recoil peak.

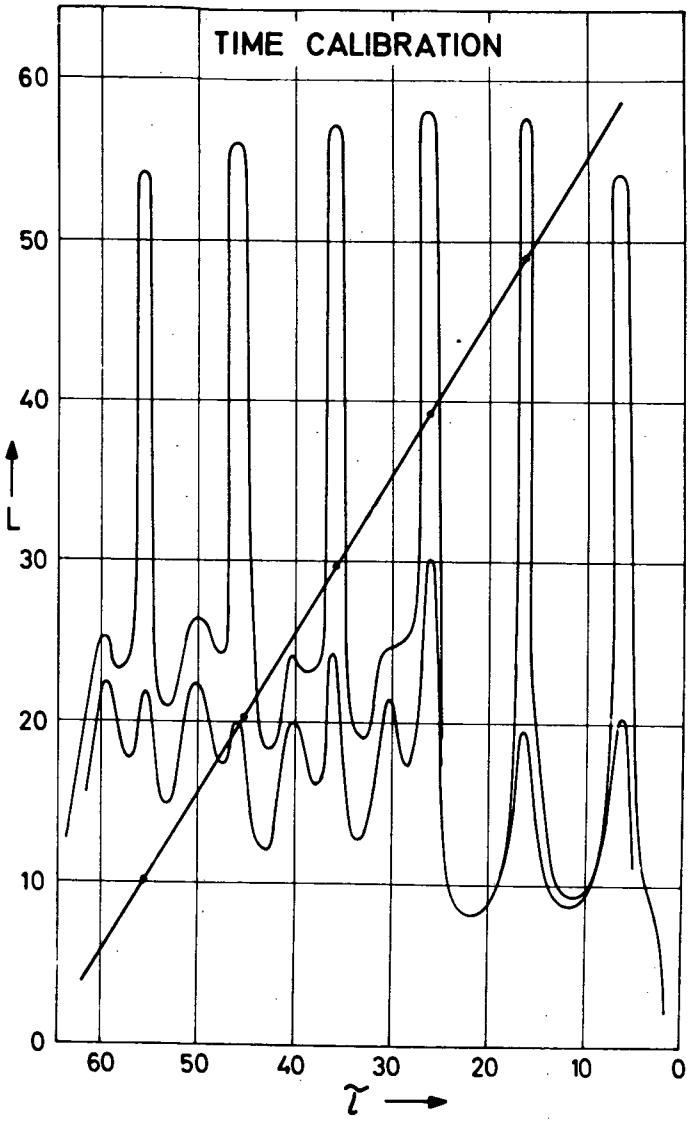

Fig. 4.10(b). The time calibration (channel vs delay in n sec) which is used to obtain the time scale of (a).

source like the $^{7}Li(d,n)^{8}Be$ reaction, which yields a wider range of neutron energies, would be more suitable.

The data was usually accumulated in 64 × 64 matrices by the two-parameter analysers. For some runs, an analyser connected on-line to a PDP 15 computer was used to obtain a larger dispersion. This system enabled the array dimensions to be expanded to 8192 × 8192.

All data was stored on magnetic tape in blocks of 64 × 64 and processed by an off-line computer. Contour, as well as isometric plots were obtained for both (LS) and (Lτ) spectra. Typical plots of (LS) spectra obtained at 22 MeV are shown in figs 4.6 and 4.7. Plots of (Lτ) spectra are shown in figs. 4.10 and 4.13. In fig. 4.10 the (Lτ) spectrum is accompanied by a time calibration. The high energy neutron peak is a good reference peak for this purpose.

Fig. 4.11 shows S-distributions taken at two L-values. It is observed that breakup protons and recoil deuterons lie on well-separated ridges at higher energies, but that these ridges merge at lower ones. In order to separate the protons from the deuterons at energies where the edges overlap, a computer program was used which fits a Gaussian distribution to the peak corresponding to each of the charged particles. It is seen from fits at energies where the peaks are well separated, that the Gaussian distribution fits the observed distributions well.

The integral of the data under the peak is obtained for each ridge at all L-values where the peaks can be resolved. This amounts to "projecting" each ridge onto the L-axis. Typical projections or pulse-height distributions for the breakup proton and recoil deuteron distributions at an incident

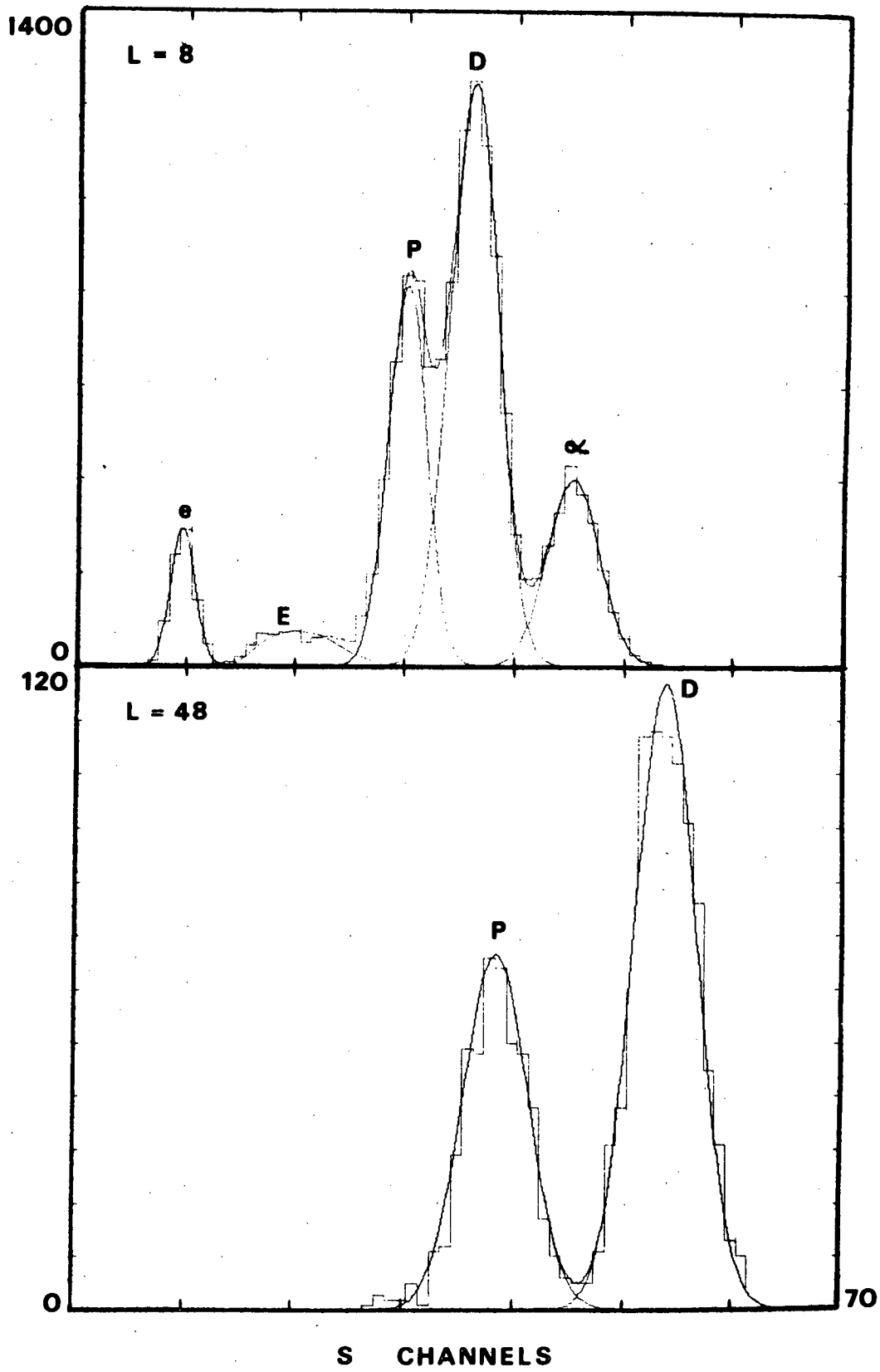

Fig. 4.11. A cross section of the (LS) spectra for two values of L. The upper cross section is taken where the ridges corresponding to various particles are not well separated. This is contrasted with the bottom one (L = 48) where they are. The solid lines represent the gaussian functions which are fitted to the peaks in order to obtain the integral

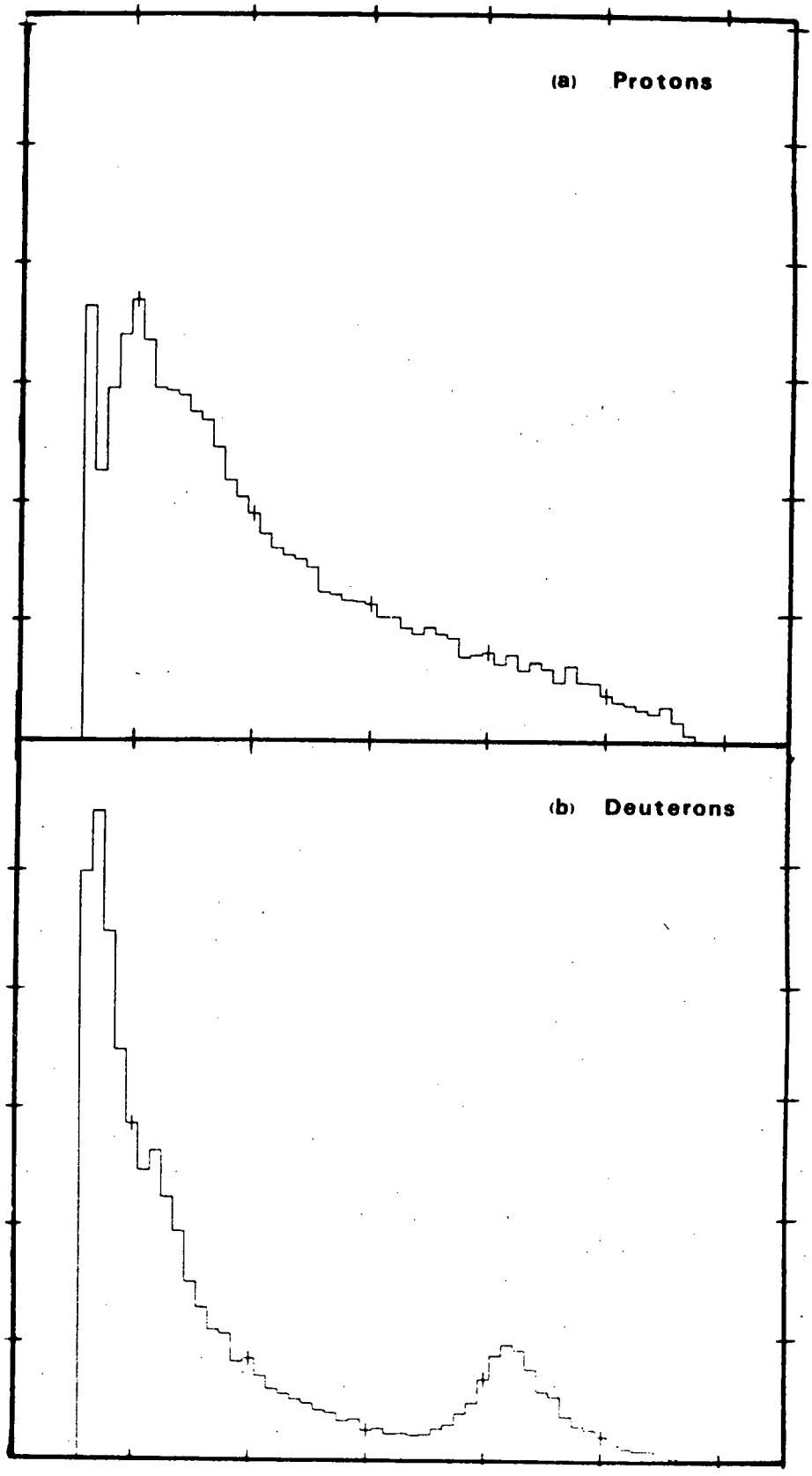

Fig. 4.12. The projections of the ridges corresponding to (a) protons (P) and (b) deuterons (D) in the (LS) spectra. These pulse height distributions correspond to the energy distributions of breakup protons and recoil deuterons modified by the nonlinear pulse-height response and finite resolution of the detector.

neutron energy of 22 MeV are shown in fig. 4.12. In this manner, the pulse-height distributions could be obtained down to proton energies ranging between 3 and 4 MeV.

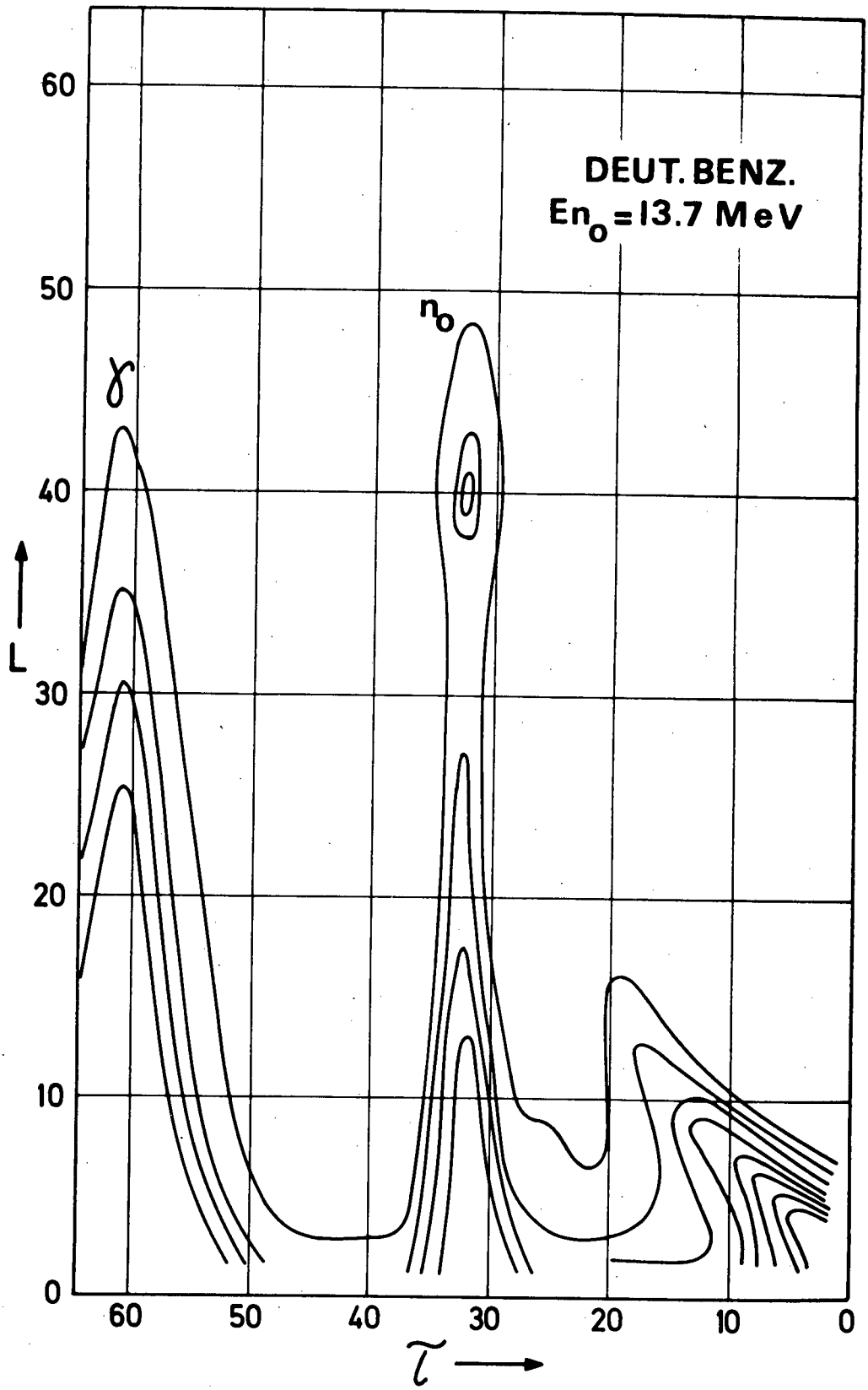

Fig. 4.13. A contour representation of an (Lτ) spectrum obtained at 120°(lab.) with a range of incident neutron energies. The low L-values between the γ and no peaks indicate that the background present is due to low-energy radiation.

CHAPTER 5

ANALYSIS

5.1 Outline

The measurements and data reduction described in the previous chapter have resulted in L-S spectra from which pulse-height distributions for both recoil deuterons and breakup protons (see fig. 4.12) were obtained. Further analysis is needed in order to obtain the total breakup cross section.

This may be done as follows (Method A):

(1) the measured proton pulse-height distribution is integrated upward from a lower limit (the "cutoff") below which it can not be reliably determined;

(2) the integral is corrected for the counts lost below the cutoff.

Then, since the deuteron energy distributions are measured simultaneously, the total breakup cross section σ_B may be obtained from the (corrected) proton integral (I_p) by comparing the measured recoil deuteron energy distributions with N-d differential cross sections at the same energy. Thus

$$\sigma_B = I_p \times \frac{\sigma_{peak}}{I_{peak}} \qquad (5.1)$$

where I_{peak} is obtained by integrating the measured distributions, upward from the well-defined minimum, over the forward recoil peak, and σ_{peak} is the corresponding integral obtained from N-d differential elastic cross section data.

Alternatively (Method B) one may use the differential

elastic cross section data to obtain the total deuteron integral I_D from the measured part of the distribution. Then, since the total cross section (σ_T) comprises virtually only the breakup (σ_B) and elastic (σ_e) cross sections, the breakup cross section may be obtained as follows

$$\frac{I_P + I_D}{I_P} = \frac{\sigma_T}{\sigma_B}$$

or

$$1 + \frac{I_D}{I_P} = \frac{\sigma_T}{\sigma_B} \qquad (5.2)$$

It is not necessary to know either the number of target nucleons or that of incident neutrons so that uncertainties associated with the determination of these quantities are absent. However, to correct for the counts lost below the cutoff, it is necessary to make more or less justified assumptions regarding the shape of the energy distributions at low energies. On the grounds of their resemblance over the range where measurements were made, it was assumed that the proton energy distribution below cutoff was that predicted by the phase space distribution.

To obtain the energy corresponding to the cutoff, it is necessary to determine the pulse-height versus energy relation. The response functions can be obtained from measurements of the limiting (maximum) pulse heights in the deuteron spectra observed for different incident neutron energies. A knowledge of the pulse height resolution of the detector and its effect on the energy distributions is required for the response calibration.

This was obtained by modifying parametrized forms of the deuteron energy distribution with detector response and an assumed resolution function, and matching these modified distributions with the measured ones. As a result of this procedure, the resolution width is obtained and the relative shift in the forward recoil peak (due to the finite resolution) as a function of the maximum deuteron recoil energy (or incident neutron energy) is predicted. With this information the variation of the forward deuteron recoil peak with τ in the $(L\tau)$ spectra can be used to determine the relative pulse height response of the detector.

Experimentally, the cutoffs are determined by the ability to resolve reliably between breakup protons and recoil deuterons. This usually corresponds to an energy $\gtrsim$ 3 MeV, while at higher incident energies the cutoffs were chosen above the maximum energies of protons from $^{12}C(n,np)^{11}B$. Consequently, the results rest rather heavily on the distributions assumed to correct for the counts lost below the cutoff.

In principle, this uncertainty may be reduced by a third method (C) (see Chapter 6,sect.5).This consists essentially of reducing the cutoff energy by taking into account the counts which are due to neutron-induced carbon reactions, against which it is impossible to discriminate at lower pulse-heights. However, it can only reliably be applied where the cross sections for these processes are known.

It has been assumed above that the measured distributions had been corrected for edge effects and multiple scattering. These effects have been considered (see section 5.7) and the necessary corrections applied.

5.2 The effects of detector resolution

The energy distribution of particles detected in a scintillation counter is modified by the finite resolution of the detector and by its non-linear response.

Given an energy distribution I(E), a response function L(E) and a resolution function R(L), the "smeared" pulse-height distribution is given by a Fredholm integral or convolution

$$I'(L) = \int_0^{L_{MAX}} I(E) \frac{dL'}{dE} R(L'-L)\,dL' \qquad (5.3)$$

If the energy distribution I(E) is well established, one can compare the convoluted distribution with experiment to extract information about R and L.

The recoil deuteron distributions are well-determined and were parametrized (Lu70). In addition to this, their shapes are well suited for the purpose, i.e. they are generally characterised by a narrow forward recoil peak and a well-defined minimum. The forward recoil peak, being narrow, is a sensitive function of the resolution, while its shape is relatively insensitive to the dependence of L on E.

This latter conclusion results from inspection of the integrand in (5.3). Since both I(E) and R vary far more rapidly with respect to E than does L, the shape of the peak (though not its absolute position), is determined by them. Thus, to a good approximation, one can study the effects of resolution, namely the relative width of the peak and its relative shift, independently of the response. This is important since, as will be described in the next section,

the variation in the position of the forward recoil peak with incident neutron energy was used to determine the detector response.

Thus, published (Sm68) scintillation response functions for NE230 were used in expression (5.2) to obtain a "smeared" deuteron pulse-height distribution which was matched with the measured one over the region of the forward recoil peak by the method of least squares. In this manner the resolution width and the peak shift were obtained. By assuming a pulse-height dependence of the resolution described below, the smeared spectra were calculated for various incident neutron energies and the peak shift was obtained as a function of incident neutron energy (see fig. 5.3). This curve was used to obtain the "true" position of the forward recoil peak. When used in conjunction with (L_T) spectra, the detector response function could be determined. (See next section)

Once the relative response function had been determined it could be used to obtain the energy pulse-height relation for any distribution. As a first approximation the pronounced minimum in the deuteron pulse-height distributions was taken as a calibration point. The deuteron energy corresponding to this minimum is a well-defined function of incident neutron energy (see fig. 5.8 and section 5.5) and since the distribution is almost symmetric about it, its position is relatively less affected by the finite resolution. However, to obtain an accurate energy calibration, expression (5.2) was used and the calibration L-value was varied to obtain a best fit to the forward recoil peak.

To evaluate expression (5.3) with a general distribution

I(E), the integration is performed numerically on a Univac 1106 computer. Details are given in Appendix E. Here, it will suffice to consider the terms in the integrand of (5.3).

The resolution function R(L) of scintillation detector has been discussed by Birks (Bi64). It is shown that, for a large number of photons and Poisson statistics, the resolution fuction is well approximated by a Gaussian distribution

$$R(L) = \frac{1}{\sqrt{2\pi}\sigma} \exp\{-(L-\ell)^2/2\sigma^2\} \tag{5.4}$$

The full-width η of the distribution at half-maximum, which is commonly referred to as the resolution, is related to σ by

$$\eta = \sqrt{5.56}\,\sigma \tag{5.5}$$

Furthermore, it can be shown (Bi64) that to a good approximation, σ depends linearly on the root of the mean response L i.e.

$$\sigma^2 = sL \tag{5.6}$$

where s is a constant

Implicit in this form and dependence of the resolution function is the assumption that we may neglect the influence of the variance of the mean photon transfer (Bi64). This is not always strictly true in our case, but may be assumed to be so to a good approximation.

The detector response function L(E) will be discussed in the next section, and its approximation by means of a table of values and an interpolation routine in Appendix E. Over

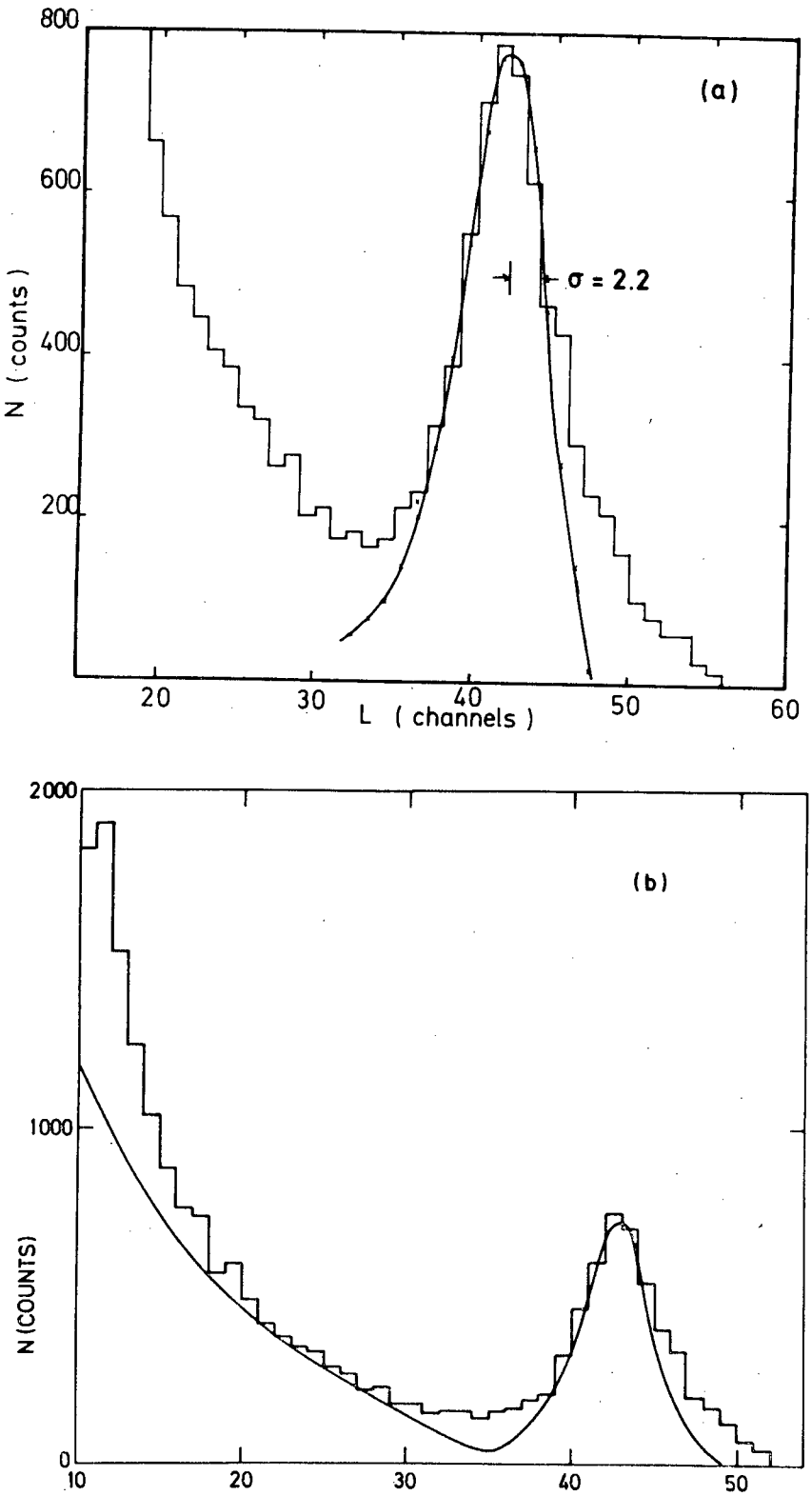

Fig. 5.2. Simulated pulse height spectra using (a) expression 5.8 and (b) Ludin's formula. In each of the cases a best fit to the forward recoil peak was obtained with resolution σ = 2 channels.

a limited energy range however ($\sim$ 5 MeV), $\ell n(L)$ is well approximated by a linear function of $\ell n(E)$ (See fig. 5.6).

$$\ell n(L) - \ell n(L_1) = \gamma\{\ell n(E) - \ell n(E_1)\}$$

or

$$\left(\frac{L}{L_1}\right) = \left(\frac{E}{E_1}\right) \qquad (5.7)$$

The energy distribution of recoil deuterons has been parametrized by Ludin (Lu70), and is discussed in Appendix C and section 5.4. Its form (see expression C.1) suggests what has often been observed of elastic angular distributions, viz. that over the forward recoil peak (and to a lesser extent the backward one), the distribution is very nearly an exponential function of the centre-of-mass cosine $\cos\theta^c$ so that, to a very good approximation, we may write

$$\log\left(\frac{d\sigma}{d\Omega^c}\right) = g\,(\cos\theta^c - \cos\theta^c\,m) + C \qquad (5.8)$$

where g is the slope of the straight line approximating the log of the distribution and is to be determined from the literature (e.g. Ho68) and $\cos\theta^c_m$ is the cosine centre-of-mass angle corresponding to the minimum in the angular distribution (see fig. 5.1).

This latter approximation was used with expression (5.7) for the response, in expression (5.3) to simulate the observed forward recoil peaks. The energy distributions are simply related to the centre-of-mass angular distributions by

$$E_D = \frac{4}{9}\,E_n\,(1 + \cos\theta^c)$$

$$\text{and}\quad \frac{d\Omega^c}{dE_D} = \frac{9}{4}\,E_n \qquad (5.9)$$

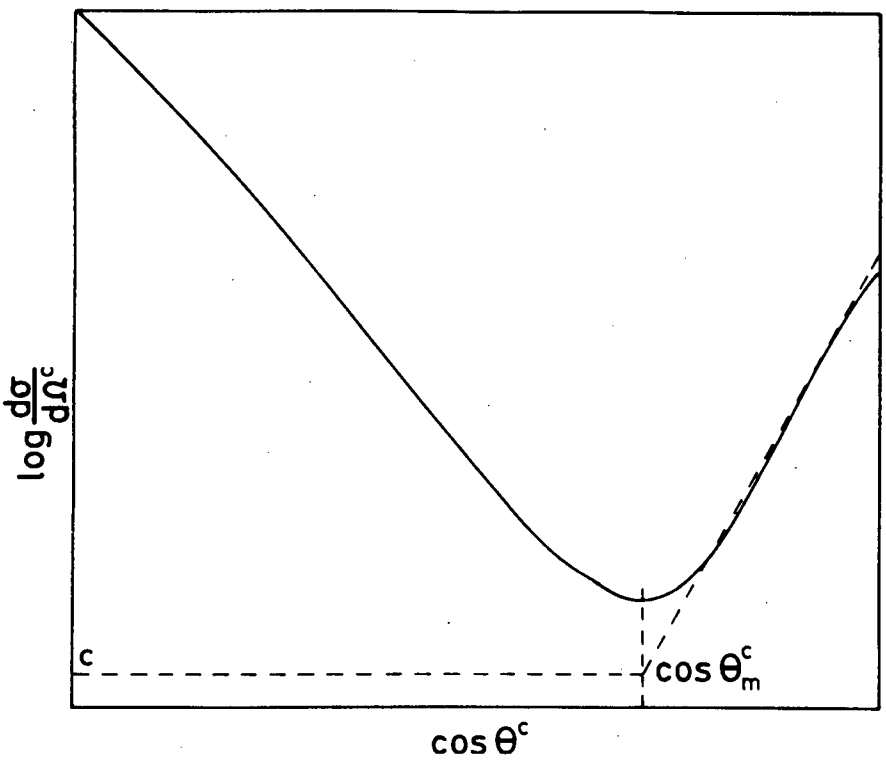

Fig. 5.1 A hypothetical elastic angular distribution illustrating approximation

Both Ludin's parametric form (see Appendix D) of the elastic angular distribution and the empirical form described above, were used to simulate observed energy spectra. Typical results of these simulations are shown in fig. 5.2. Fig. 5.3 shows the dependence of the relative peak shift ΔL on $\sqrt{L}$. This was obtained assuming that the dependence of the resolution in L is given by (5.6).

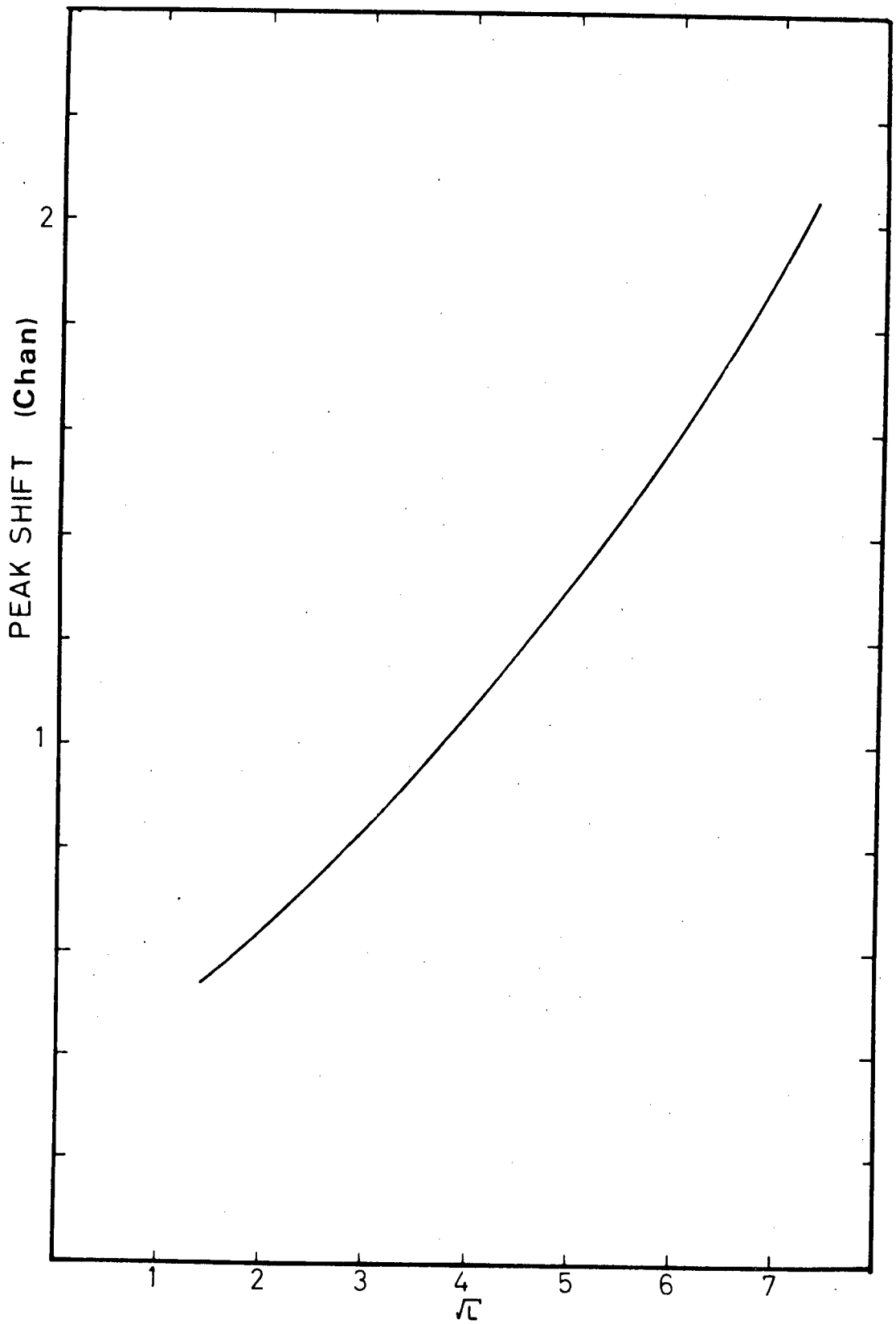

Fig. 5.3 The shift in the forward recoil peak as a function of the pulse-height L (in channels) for a resolution of 2 (channels) at L = 52.

5.3 The Scintillator response function

For each measurement, it is necessary to know the response of the scintillator to deuterons and protons as a function of energy E = ∿0.5 to E = E_o MeV (E_o is the incident energy). The response of NE230 to deuterons has been determined on two separate occasions (Sm68) (Be72). However, these measurements extend only up to 11 MeV. The data of Smith and Polk (Sm68) was subsequently analysed by Craun and Smith (Cr70) in terms of semi-empirical formulae. These formulae are used here, together with the parameters extracted by Craun and Smith, to extend the response curves to higher energies.

These semi-empirical formulae are discussed by Birks (Bi64). The more commonly used of these is that proposed by Birks. Assuming that the ionization density along a particle track is responsible for the quenching of the primary radiation and considering only unimolecular quenching, Birks obtained the following expression

$$\frac{dL}{dE} = \frac{S}{1 + kB(dE/dx)} \qquad (5.10)$$

where $\frac{dL}{dE}$ is the fluorescent light emitted per unit energy

dE/dx is the stopping power or specific energy loss of the scintillator

S is the scintillation efficiency

B(dE/dx) is the ionization density

k is the quenching parameter or relative quenching probability

The other formula used by Craun and Smith was proposed by

Chou (Ch52). It is a simple extension of the Birks formula.

$$\frac{dL}{dx} = \frac{S}{1 + kB(dE/dx) + C(dE/dx)^2} \qquad (5.11)$$

It is difficult to give a theoretical interpretation to C, and it serves principally to improve the fit of theory to experiment. For electrons with energies $\gtrsim$ 125 keV, $\frac{dE}{dx} \simeq o$ and the above expressions reduce to

$$L_e(E) = SE + \ell_o \qquad (5.12)$$

The above expressions are usually used simultaneously to calculate the scintillation amplitudes of both electrons and heavier particles under identical experimental conditions.

In view of its simplicity and the fact that it has only two adjustable parameters, the Birks fit has been remarkably successful in reproducing both the individual and relative responses of a variety of particles in a variety of scintillators. This agreement between theory and experiment can be improved by adding an additional parameter, as did Chou. However, it is dangerous to use parameters determined in one energy range to extrapolate to a wider one. This is particularly so in our case since, as will be seen in section 5.4, we require accurately only the relative response. Extension of Craun and Smith's analysis to a wider energy range could easily involve an alteration of both kB and S, without significantly affecting the fit over the more restricted energy range, but with a serious effect on the ratio of the responses to, say 2 MeV protons and 20 MeV protons.

The possibility should also be considered that the composition of the commercially supplied scintillator could

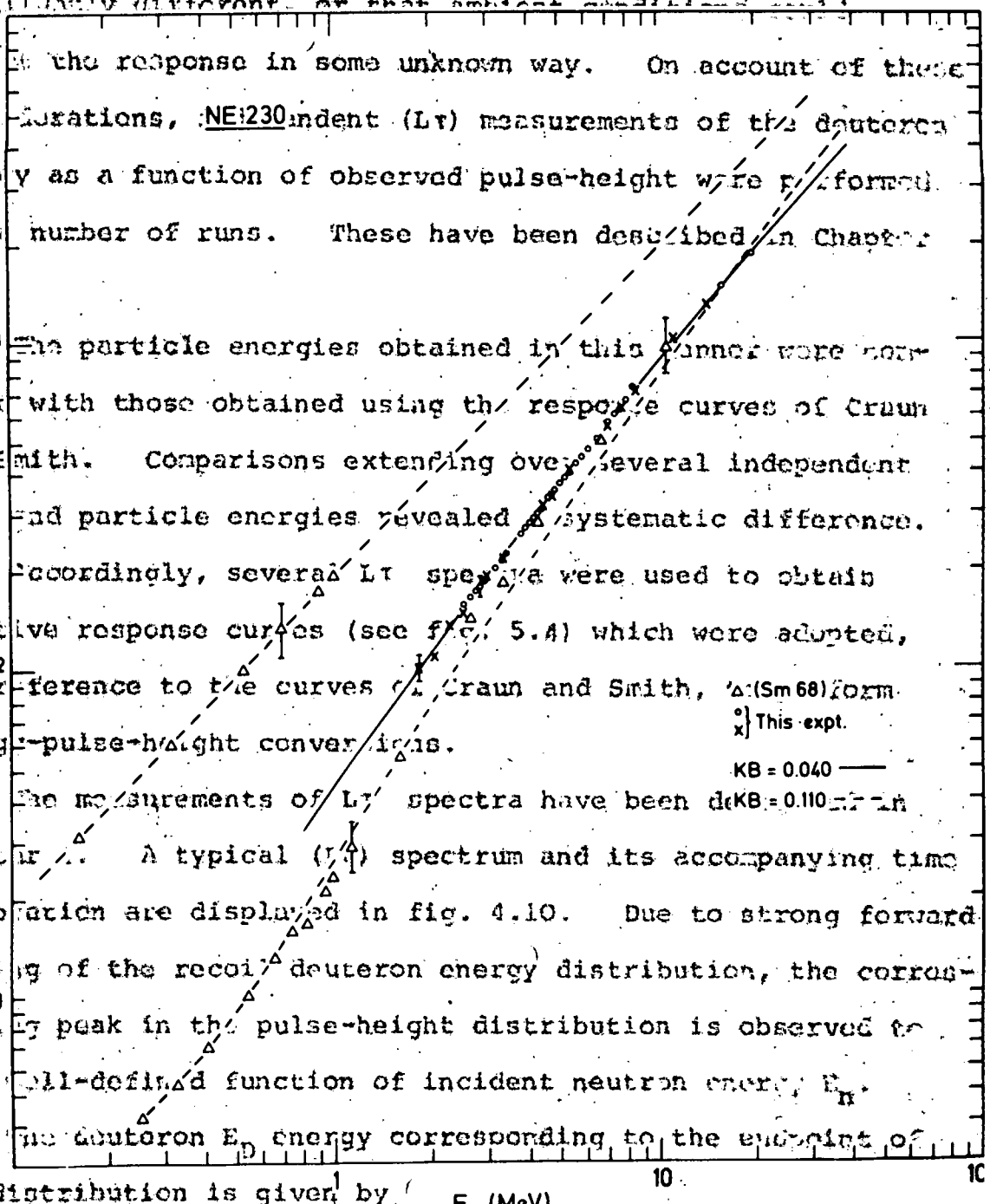

Fig. 5.4 Relative response curves for NE230 deuterated benzene scintillator to deuterons. The measurements from this work were normalised to those of Smith and Polk (Sm68) at 15.7 MeV.

affect the response in some unknown way. On account of these considerations, NE230 dependent (L_T) measurements of the deuteron energy as a function of observed pulse-height were performed for a number of runs. These have been described in Chapter 4.

The particle energies obtained in this manner were compared with those obtained using the response curves of Craun and Smith. Comparisons extending over several independent runs and particle energies revealed a systematic difference. Accordingly, several L_T spectra were used to obtain relative response curves (see fig. 5.4) which were adopted, in preference to the curves of Craun and Smith, for (Sm68) form energy-pulse-height conversions.

The measurements of L_T spectra have been described in Chapter 4. A typical (L_T) spectrum and its accompanying time calibration are displayed in fig. 4.10. Due to strong forward peaking of the recoil deuteron energy distribution, the corresponding peak in the pulse-height distribution is observed to be a well-defined function of incident neutron energy E_n. The deuteron E_p energy corresponding to the endpoint of the distribution is given by

$$E_{max} = \frac{8}{9} E_n \qquad (5.13)$$

To obtain the pulse-height corresponding to this energy, it is necessary to account for the effect of the finite detector resolution on the position of the peak. The study of the effects of resolution on the position of the forward recoil peak has been described in the previous section. The curve shown in fig. 5.4 was used to obtain correct spectrum endpoints

for all E_n and thus the deuteron response.

Three independent(L_T) spectra were combined to obtain the response curve shown in fig. 5.4. Their results are seen to be consistent. Most other L_T spectra did not include a wide range of incident neutron energies and were used only to calibrate their accompanying LS spectra.

The response obtained in this manner was normalised to that of Craun and Smith at 6 MeV deuteron energy. It is seen that the slopes of the curves are significantly different, even over the range 0-10 MeV. A systematic discrepancy of the same kind is also apparent in a later measurement (Be72) for the deuteron energies 1 to 7 MeV although these latter authors considered the overall agreement between their measurements and those of Craun and Smith, good within the limits of uncertainty.

In order to interpolate the measured values of response, the Birks formula was used. A best value of kB was obtained by the method of least squares. Details are given in an Appendix. This procedure does not constitute a complete comparison with Birks theory since, to do this, the electron response must be fitted simultaneously. However, it is not certain over what energy range Birks theory can be reliably applied and, for our purposes, it is more important to obtain a good fit to the relative curve. The purpose of the fit is merely to guide interpolations between measurements.

The measured response is for deuterons but it can also be applied to protons by means of a simple expression relating the responses of the scintillator to protons and deuterons, viz.

$$L_d(2E) = 2L_p(E)$$

or, equivalently

$$E_d(2L) = 2E_p(L) \qquad (5.14)$$

Justification for this relation is given in Appendix D. It has been used extensively to obtain proton energies from deuteron response calibrations.

The response curves for deuterons obtained from Birks' formula, with parameters obtained by Craun and Smith, are included in fig. 5.4. Values of the stopping power given by Craun and Smith up to 14 MeV (deuteron energy) were supplemented with values calculated from the stopping powers of Northcliffe and Schilling (No70a). Uncertainties in kB associated principally with uncertainties in $\frac{dE}{dx}$, were estimated (Cr70) at ± 10%.

5.4 Extrapolation of proton Integral

The first step towards obtaining the total breakup cross section is to correct for the protons lost below the cutoff. The proton energy distributions were compared with distributions obtained using the phase-space model. This model assumes that the transition amplitude is independent of the momentum transfer variables and thus given by the density of final states (see section 6.2). The measured distribution was found to resemble phase-space with the exception of enhancements at high and medium proton energies which are attributed to the n-n and n-p final-state interactions (see Chap.6 fig. 6.3). Assuming that the overall resemblance continues at lower energies where the distributions were not measured,

the phase-space distribution was used to extrapolate the proton integral to zero energy. If the magnitude of the deviations at lower energies is comparable to that due to the n-p FSI, this assumption should not be a bad one. The n-p FSI at medium energies is less pronounced, since owing to kinematics, it is spread over a wider energy region. These questions will be discussed further in section 6.3.

The extrapolation was performed from a suitably determined lower limit, or cutoff. This cutoff was determined as follows:

(a) For incident energies below 20 MeV, the cutoff was chosen where the proton and deuteron distributions could no longer reliably be separated. This was usually at about 4 MeV proton energy. At lower energies, the proton distribution was swamped by the rapidly rising deuteron distribution (See section 4.5).

(b) At incident energies above 17 MeV, one expects contributions from competing reactions (See section 5.6) to the proton distributions at energies above 3 MeV. Above 16 MeV, the $^{12}C(n,p)^{12}B$ reaction is expected to contribute significantly (see fig. 5.8), while at energies above 20 MeV, one could expect contributions from the $^{12}C(n,np)^{11}B$ reaction, for which the cross section is not known. For these energies the cutoff was taken above the maximum energy for protons from the $^{12}C(n,np)^{11}B$ reaction.

The proton integrals were corrected for the contribution from $^{12}C(n,p)^{11}B$ on the grounds of the known cross section for transitions to the lower states. Contributions from transitions to higher excited states were neglected.

Some of the proton induced scintillations from competing reactions will not be included in the proton energy distribution since they are accompanied by heavier charged reaction products. When the energy of these reaction products is sufficiently high, the events will be displaced to higher S-values and will consequently not be included in the proton ridge. This question will be discussed further in connection with multiple scattering (See section 5.9). It was estimated that, when the energy of $^{11}B \gtrsim 2$ MeV, the protons from $^{12}C(n,p)^{11}B$ would not be included in the proton distribution. For example, at 22 MeV incident energy, the maximum energy of ^{11}B is 4.1 MeV. Therefore, only half of the protons from $^{12}C(n,p)^{11}B$ will be included in the proton distribution if one assumes that their distribution is isotropic. However, at 20 MeV they will all be included. Having chosen the cutoff, integrated the proton distribution down to this point, and, at higher incident energies, corrected for the $^{12}C(n,p)^{12}B$ reaction†, a value of the total proton integral is obtained by estimating the number of protons which are lost below the cutoff.

This can be done by normalising a phase space distribution to a region of the measured distribution where the effects of the n-n and n-p FSI are not expected to be significant, that is, where the phase space approximation is expected to

---

†It has been assumed throughout this section, that the measured distributions had been corrected for edge effects and elastic scattering. The correction methods are discussed in section 5.7.

be a good one. This is the case for the energy range $0.4\ E_{max} \lesssim E \lesssim 0.7\ E_{max}$ (where E_{max} is the maximum proton energy) (see section 6.3). A normalisation which averages over statistical effects and which is not sensitive to the exact point in the selected energy region is obtained as follows.

Two energies E and E' are chosen in this energy region and the proton distribution is integrated from maximum proton energy down to each of these energies.

An unnormalised phase space distribution is also integrated down to the same energies and the ratios R and R' of the total phase space integral to each of the partial integrals is obtained. Since the (n-n) FSI enhancement is concentrated at higher proton energies, each of the data integrals I and I' may be written

$$\begin{aligned} I &= \mathcal{I} + \delta \\ I' &= \mathcal{I}' + \delta \end{aligned} \qquad (5.15)$$

where $\mathcal{I}$ and $\mathcal{I}'$ are the corresponding integrals over the normalised phase space distribution and δ is the enhancement attributed to the FSI. To obtain δ and $\mathcal{I}$, one multiplies each of these by the corresponding ratios R and R'. Then

$$RI - R'I' = R(\mathcal{I}+\delta) - R'(\mathcal{I}'+\delta)$$

and, since $R\mathcal{I} = R\mathcal{I}'$

$$\delta = \frac{RI - RI'}{R - R'} \qquad (5.16)$$

This procedure was repeated using different values of δ to check consistency. The result of such a normalisation is shown in Chapter 6, fig.6.4. This procedure will be discussed further in Chapter 6.

5.5 Determination of total Breakup Cross Section

5.5(a) Method A

One way in which the absolute value of the total breakup cross section may be obtained from the (corrected)proton integral is given by expression (5.1)(Method A). One relies on the knowledge of the integral over the forward recoil (or backward scattering) peak in the differential elastic cross section data. This part of the differential elastic cross sections is generally very well determinted. Furthermore, above 14 MeV, no appreciable difference due to coulomb effects, is expected (Va67) between n-d and p-d data, except for coulomb interference at small forward scattering angles This is generally observed to be the case (Ho68) (Se70)(and fig. 1.2) even at energies below 14 MeV (Ho68). Consequently, one may use both p-d and n-d data to obtain the integral σ_{peak} as a function of incident neutron energy.

All the n-d and p-d data in the region 14-22 MeV were evaluated as described in Chapter 3 and the integral $\hat{\sigma}_{peak}$ over the forward recoil peak was obtained. To obtain the best smooth curve for the mean value of σ_{peak} as a function of incident neutron energy, most of the data in the energy ranges 2-14 MeV and 22-50 MeV were also analysed in a similar manner. The results of these evaluations are tabulated in table 5.1 and plotted in fig. 5.5. A curve representing the mean value of the data as a function of incident energy was used to obtain σ_{peak}. The average scatter about this curve is generally $< 5\%$ and it is usually larger for the n-d data since the experimental uncertainties in these data are larger. The p-d data of Cahill (Ca71) are seen to be consistently

Table 5.1

E_N (MeV)	Reaction	cos θ_m	σ_{peak} (mb)	S	Reference
5.50	p-d	-0.35	400.00	3.71	Br60
5.60	n-d	-0.37	414.00	3.73	Bo69
7.01	n-d	-0.44	344.00	3.92	Bo69
7.85	p-d	-0.46	257.00	4.40	Br60
9.04	n-d	-0.52	194.00	4.99	Bo69
9.70	p-d	-0.50	194.00	4.99	Al52
11.50	p-d	-0.54	132.00	5.97	Va66
12.17	p-d	-0.55	125.00	5.79	Br60
13.93	p-d	-0.57	94.70	6.65	Ki60
14.10	n-d	-0.57	94.70	6.65	Al53
14.30	n-d	-0.57	94.70	6.91	Be68
14.90	p-d	-0.55	83.70	6.92	Ca71
15.50	p-d	-0.57	77.10	7.07	Ca71
16.20	p-d	-0.58	75.00	7.19	Ca71
16.90	p-d	-0.59	66.50	7.52	Ca71
17.10	p-d	-0.59	67.70	7.79	Ca71
17.70	p-d	-0.59	65.30	7.30	Ca71
18.50	p-d	-0.59	54.10	8.10	Ca71
18.55	n-d	-0.61	49.80	9.80	Se72
19.00	p-d	-0.60	54.10	7.80	Ca71
19.92	p-d	-0.60	46.20	8.80	Ca71
20.50	n-d	-0.61	40.80	10.20	Se72
20.57	p-d	-0.61	38.50	9.75	Ca55
22.00	p-d	-0.61	38.20	9.66	Bu68
23.00	n-d	-0.61	38.90	10.40	Se72
25.70	p-d	-0.63	32.80	9.80	Bi68
28.00	n-d	(-0.60)	26.50	11.30	Go70
31.00	p-d	-0.63	27.70	9.26	Ki64
35.00	p-d	-0.64	16.78	11.31	Bu68
36.00	n-d	-0.64	15.60	13.10	Ro70
46.30	n-d	-0.65	8.69	16.70	Ro70
46.30	p-d	-0.66	10.08	12.31	Bu68

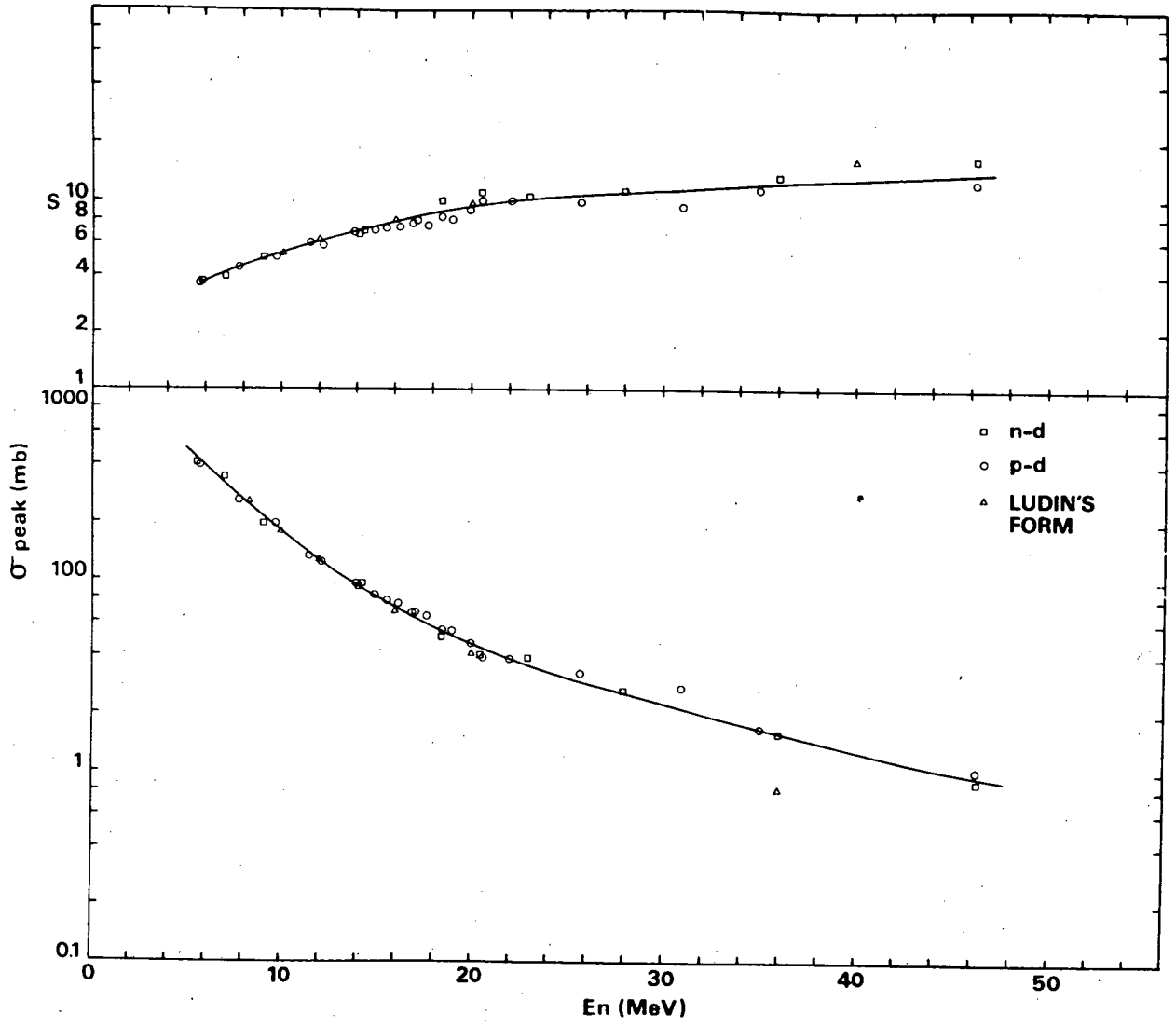

Fig. 5.5. σ_{peak} and S as functions of incident nucleon energy E_N. These values were obtained from evaluation of n-d and p-d differential cross section data. Also plotted at some energies are values obtained using Ludin's formula.

above the curve which was drawn so as to minimise changes in slope. Such a discrepancy between p-d and n-d data is in the opposite sense to that expected from coulomb effects. Furthermore, no consistent evidence of such effects is observed at lower incident energies.

While performing these evaluations, the cosine ($\cos \theta_m$) of the centre-of-mass angle corresponding to the minimum was also tabulated (table 5.1) and plotted (fig. 5.6). The corresponding minimum in the energy distributions was used as a first approximation to obtain energy calibrations for the pulse-height distributions (see section 5.2). It is seen to be a very well-defined function of incident neutron energy.

Values of σ_{peak} and $\cos \theta_m$ obtained with Ludin's parametrization (Lu70) of differential elastic cross sections were also plotted in figs. 5.5 and 5.6. They are seen to agree well with experimental data for energies below 14 MeV. However, they deviate from experiment at higher energies.

5.5(b) Method B

To apply Method B it is necessary to determine the total deuteron integral I_D. Although a large range of recoil deuteron energy was covered by the measurements, it was found preferable, for reasons to be set out below, to use only the forward recoil peak as a measure of the total recoil deuteron integral, I_D. Thus, if the data integral over the forward recoil peak is I_{peak}, then the integral over the total deuteron distribution was taken to be

$$I_D = S\, I_{peak} \qquad (5.17)$$

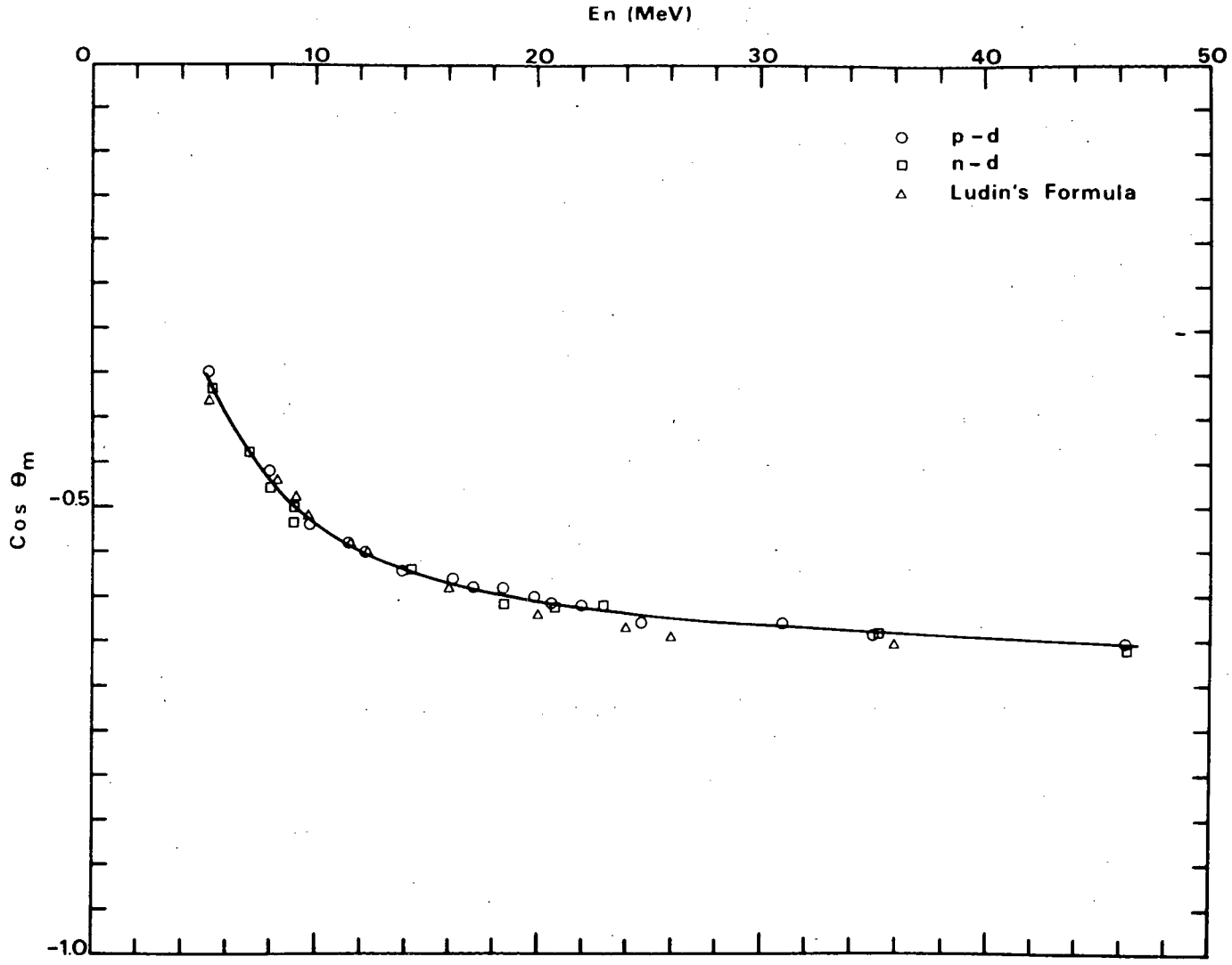

Fig. 5.6. Centre-of-mass cosine ($\cos_m$) corresponding to the minimum in N-d differential cross section data as a function of incident nucleon energy. Also plotted at some energies are values obtained with Ludin's formula.

where S is obtained from differential elastic cross section data (table 5.1 and fig. 5.5), i.e.

$$S = \frac{\int_{\theta_m}^{\pi} \frac{d\sigma}{d\Omega} \sin\theta \, d\theta}{\int_{0}^{\pi} \frac{d\sigma}{d\Omega} \sin\theta \, d\theta} = \frac{\sigma_{peak}}{\sigma_e} \qquad (5.18)$$

where θ_m is the recoil angle corresponding to the minimum in the distribution and σ_e is the total elastic cross section.

It will be recalled from section 5.1, that the breakup cross section σ_B is related to the total proton and deuteron integrals, I_P and I_D, as follows

$$1 + \frac{I_D}{I_P} = \frac{\sigma_T}{\sigma_B}$$

which one can write

$$\sigma_B = \frac{\sigma_T}{1 + (I_D/I_P)} = \frac{\sigma_T}{1 + (S \times I_{peak}/I_P)} \qquad (5.19)$$

Since the denominator of the above expression contains two terms, σ_B obtained by method B is less sensitive to errors in S, I_P and I_{peak} than σ_B by method A is to errors in I_P, I_{peak} and σ_{peak}. However, S is not as well-determined as σ_{peak} (see fig. 5.5) because of the uncertainties in the n-d distributions at small forward angles and because of the uncertainty in correcting the p-d data for coulomb interference. The uncertainty in σ_T is negligibly small (Se70)(Se72).

σ_B was obtained from all measurements using both methods A and B. The degree of consistency between the results is a test of our evaluations of the N-d differential elastic cross sections.

It is worth noting that S is not sensitive to systematic differences in the absolute values of the differential cross sections such as those which might be introduced by coulomb effects. The total data integral I_D could also be obtained by integrating the deuteron distributions down to the cutoff and using the differential cross section data to correct for the deuterons lost below the cutoff. The advantages of using only the forward recoil peak are as follows:

(1) Owing to reaction kinematics and the geometry of the scintillator capsule, the forward recoil peak is easily and accurately corrected for edge effects. (See section 5.7)

(2) Multiple scattering has a negligible effect on the forward recoil peaks. (See section 5.7)

It should also be noted that any uncertainty in determining the lower limit of integration, that is, the position of the minimum has a very small effect on I_{peak}. An uncertainty in determining the energy of the cutoff at lower deuteron energies has a large effect on the corresponding integral because the cross section rises exponentially at lower energies.

5.6 Competing Reactions

By far the major constituents of the scintillators used are carbon and deuterium. Other constituents such as wavelength shifters (Bi64) occur in very small quantities and may be neglected. Therefore, apart from n-d elastic scattering and breakup, the only reactions which (for neutron energies $\lesssim$ 22 MeV) are expected to result in protons or deuterons are those listed in Table 5.2, together with their Q-values and thresholds. Reactions not resulting in the emission of protons or deuterons, e.g. $^{11}C(n,\alpha)^{9}Be$, do not contribute to the proton or deuteron distributions. According to the principle of our particle discrimination method (see sections 4.3 and 5.7), L for these particles bears a different relation to S and they are consequently situated on a different ridge in the L-S plane (see figure 5.9). The ridges merge at lower energies, but the cutoff was usually chosen above this point.

Of the γ-induced reactions in Table 5.2, only the $D(\gamma,p)n$ reaction can contribute. This is so because primary gamma radiation was discriminated against a time-of-flight system (see section 4.2). Consequently, the γ-induced events recorded in the L-S spectra (see fig.5.9) are due almost entirely to electromagnetic de-excitation of excited states in the carbon nucleus. Thus, since the γ-induced reactions are secondary effects and since their cross sections are of the order of microbarns, they may be neglected.

Table 5.2

Competing Reactions

Reaction	Q(g.s) MeV	E_{th}(g.s) MeV
$^{12}C(n,p)^{12}B$	-12.59	13.63
$^{12}C(n,np)^{11}B$	-15.96	17.30
$^{12}C(\gamma,p)^{11}B$	-15.96	15.96
$D(\gamma,p)n$	-2.23	2.23
$^{12}C(n,d)^{11}B$	-13.73	14.9
$D(\gamma,\gamma)D$	-	-

Competing reactions resulting in recoil or breakup deuterons will not be considered in detail since they do not contribute to the forward recoil peak.

Contributions to the proton integral can be expected from $^{12}C(p,n)^{12}B$ and $^{12}C(n,np)^{11}B$. The kinematic loci corresponding to the maximum proton energy from these reactions, as a function of incident neutron energy, are displayed in fig. 5.7.

The cross section for $^{12}C(n,p)^{12}B_{g.s}$ has been measured (Kr59)(Ri68)(Ba70) by analyses of the β-spectrum from $^{12}B_{g.s}$ after activation, and consequently only the cross section for interactions leading to activation of the ground state of ^{12}B is known. Since the first four states are unstable to particle emission and since they may decay to the ground state by gamma emission, some of the cross section measured by activation analyses is due to these. The cross section is displayed in fig. 5.7. However, there are indications that these contributions are small (Ri68). By far the more dependable results are those of Rimmer (Ri68). It is apparent from these measurements, that the contribution from this reaction is most serious at about 18 MeV incident energy. However, preliminary results from a more recent measurement (Ba70) indicate that the cross section may be considerably smaller than indicated by Rimmer's measurement ($\sim$ 5 mb at 18 MeV).

Considerably less is known of the $^{12}C(n,np)^{11}B$ reaction. To our knowledge, the only estimate of its cross section was made in our laboratory (Sh70) ($\sim$ 30 mb at 22 MeV).

It must be remembered when considering contributions from competing reactions, that the particle discrimination

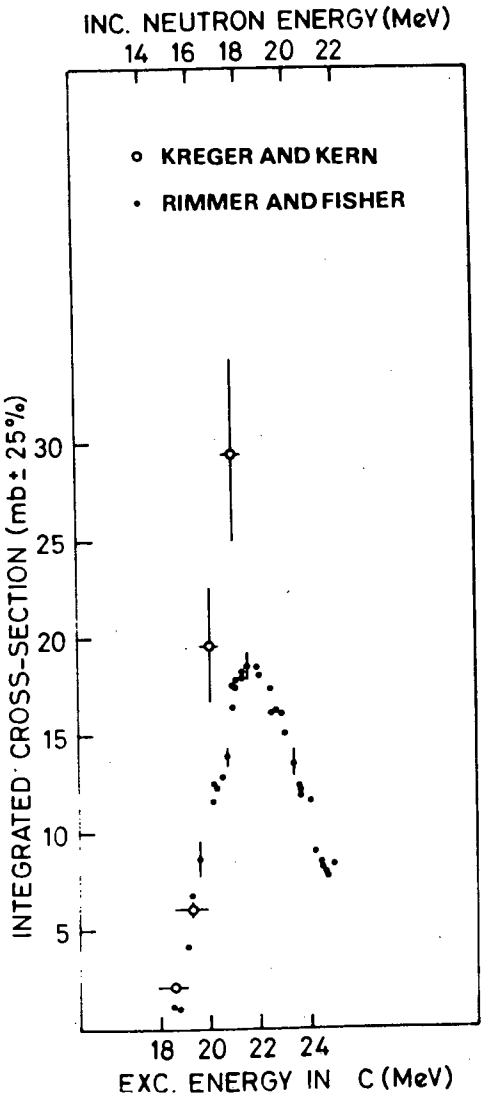

Fig.5.7(a). The cross section for the $^{12}C(n,p)^{12}B$ reaction obtained by activation analysis (Ri68)

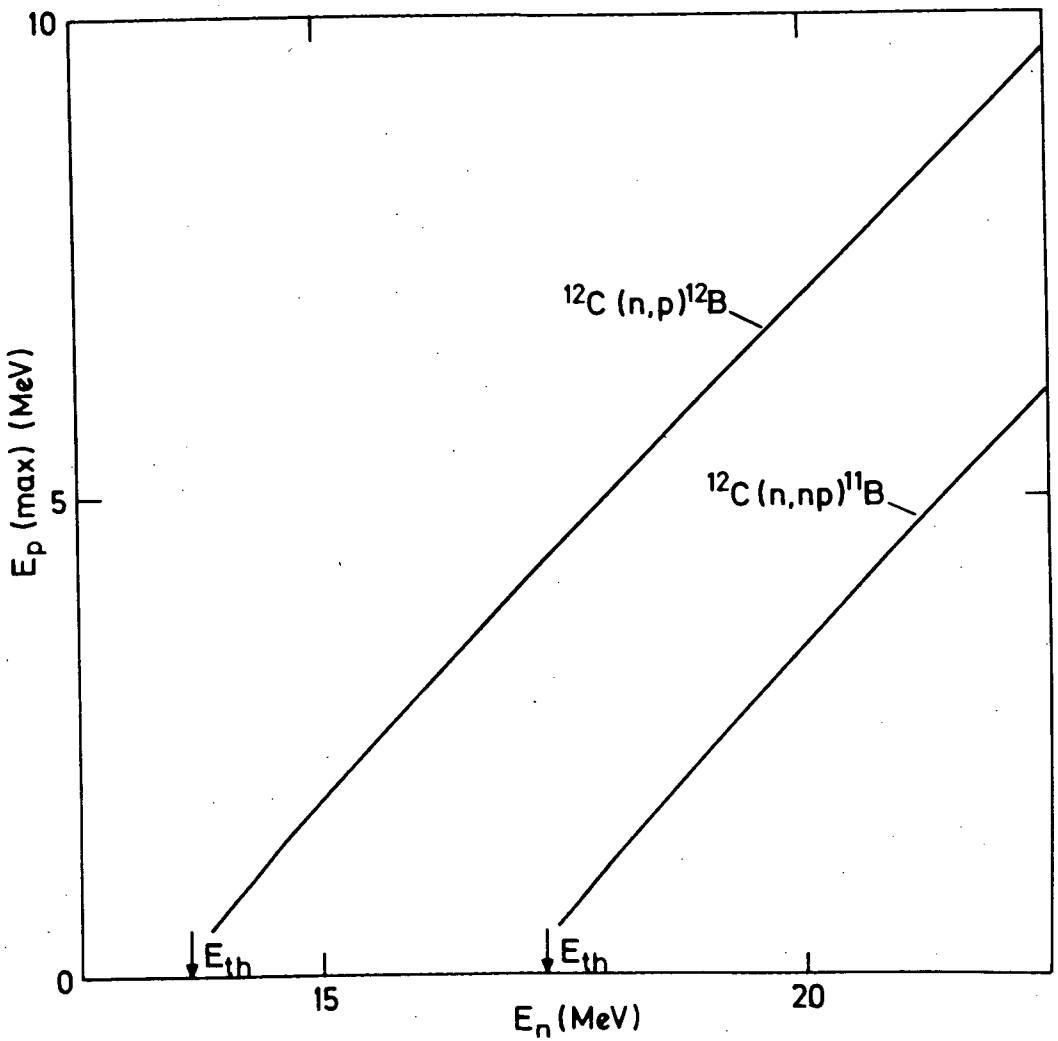

Fig.5.7(b). Maximum proton energy (E_p) as a function of incident neutron energy (E_n) for protons from the $^{12}C(n,p)^{12}B$ and $^{12}C(n,np)^{11}B$ reactions.

system employed in this work provides partial discrimination against these events. Since these reactions result in the production of heavy ions, it is expected that when the energy of the heavy reaction product is sufficiently high, the event will be interpreted as a single heavier particle and displaced to higher S-values in the (LS) spectra. (This effect will be discussed in connection with multiple scattering). If we assume (see next section) that for energies of the heavier reaction product in excess of 2 MeV, the event will not be included in the proton integral, then at incident energies in excess of 20 MeV, the contribution from $^{12}C(n,p)^{12}B$ will be reduced.

5.7 Corrections

Apart from competing reactions which we have considered above, the ideal pulse-height distribution obtained from an L-S spectrum is modified by

(a) edge effects

(b) multiple scattering

(c) recoil protons from n-p scattering

The last of these is due to the impurity hydrogen from which deuterated scintillators are never entirely free. It is easily corrected for, and the manner in which this was done, is described below. More difficult, is the correction for edge effects and especially multiple scattering, both of which effects are significant in our case.

The manner in which these effects modify the distributions is determined in part by the method of particle discrimination. To see this, it is necessary to recall some of the details of

the method.

Particle discrimination in scintillators is based on the following phenomena:

(a) Following the passage of an ionising particle the time-dependence of the light emission in some scintillators is known to comprise both a fast and a slow component.

(b) The ratio of the light in the slow component to that in the fast is dependent on the density of ionisation in the track of the particle, and hence on its nature.

Pulse-shape discrimination circuits provide an output pulse whose amplitude is sensitive to the ratio of fast to slow component.

The initial density of ionisation in the particle track is proportional to the specific energy loss dE/dx. Thus, the heavier the ionising particles, the larger dE/dx, and consequently, the larger the ratio of slow to fast component. This information enables one to estimate the effect of our L-S analysis in multiple scatter and escape events.

Since dE/dx increases rapidly with decreasing particle energy the ionisation density is highest at the end of the particle's trajectory (see fig. 5.8). Consequently, the average ionisation density in the track of a particle escaping before it has deposited all its energy will be considerably reduced. The PSD circuit will consequently interpret the event as being caused by a lighter particle. In our L-S analysis, the event, due to an escaping proton, will be on a locus intermediate between the proton and electron ridges (see figs. 5.8 and 5.9).

On the other hand, when the first scattering is followed by further ones, the energy of the recoil particle will be

(a) A typical elastic differential cross section as a function of laboratory deuteron recoil angle.

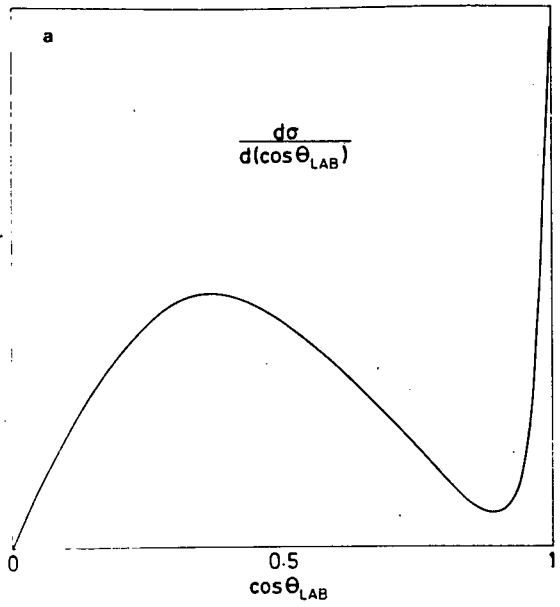

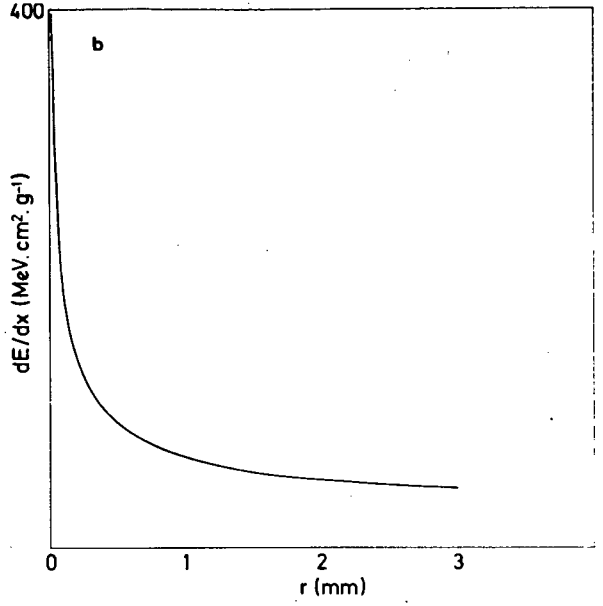

(b) Specific energy loss for deuterons NE230 deuterated benzene scintillator as a function of range of the deuteron.

(c) Schematic diagram illustrating how rescatterings are affected by (LS) analysis

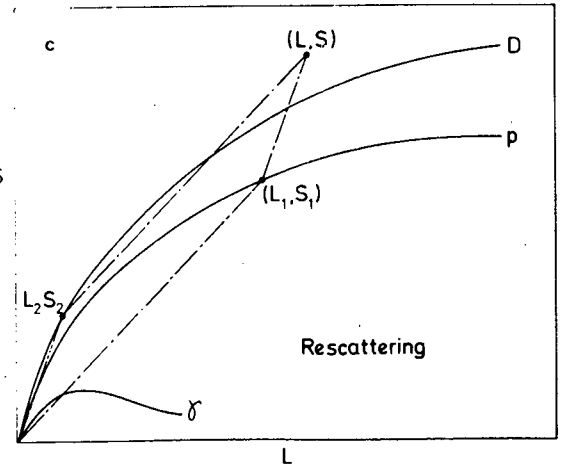

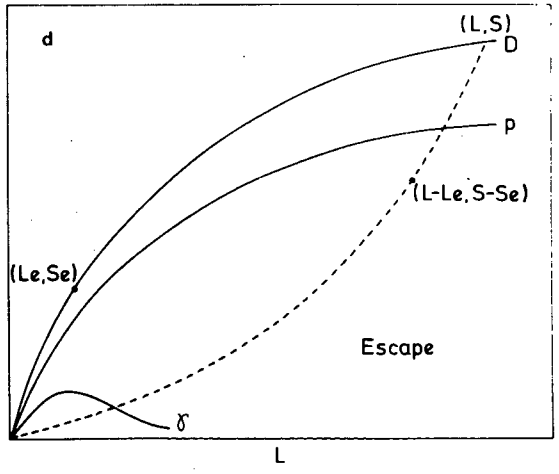

(d) Schematic diagrams illustrating how escapes are affected by (LS) analysis.

Fig. 5.8

degraded with every scattering and the average ionisation density in the corresponding tracks will be higher. Consequently, their combined light output will appear to result from a heavier particle and the events will be displaced to higher S.

The above considerations result in a qualitative understanding of these effects. However, in order to correct for them, we need a quantitative one. Since the escape events appear to lie on a well-defined ridge (see fig. 5.9). one can obtain a quantitative estimate of the total escape from an integral over this ridge. This is clearly not sufficient to determine, as we need to do, the percentage escape as a function of energy for each of the proton and deuteron distributions. To devise a means for doing so, we consider an idealised PSD circuit. It will be useful to establish a terminology with reference to a representation of an L-S spectrum like the one shown in fig. 5.9. An event recorded in an L-S spectrum is said to have coordinates (LS). When unaffected by escape, or multiple scattering, these coordinates define a particle "locus" corresponding to one of the ridges in fig. 4.6. Different ionising particles define different loci.

When a simplifying assumption is made, it is easy to establish criteria for quantitative estimates. This assumption is that the PSD circuit is linear. In fact, it is not[†], but the conclusions drawn with this assumption can be altered to

---

[†]This is mainly due to the non-linear characteristics of the diodes (See fig. 4.5). Space charge saturation in the last dynode-anode region also often plays a part.

consider cases when it does not hold.

An immediate consequence of this assumption is the following: when a number of ionising particles, (L_i,S_i), contribute simultaneously to the L and S amplitude, these amplitudes are the sum of those from each ionising particle considered individually, i.e.

$$\begin{aligned} L &= \Sigma L_i \\ S &= \Sigma S_i \end{aligned} \tag{5.23}$$

Therefore, in this ideal case, the resultant coordinates of a double scattering are those shown in fig. 5.8 .

Another useful conclusion may be arrived at by considering L and S as functions of the ionising particle track-length r. It can be shown that, for a linear circuit, both $\frac{dL}{dr}$ and $\frac{dS}{dr}$ are independent of the total track-length (or initial energy). For a particle having initial energy E, total range R, and coordinates (L,S), one can write

$$\begin{aligned} L &= \int_0^{R-\Delta} \frac{dL}{dr}\, dr + \int_{R-\Delta}^{R} \frac{dL}{dr}\, dr \\ R &= \int_0^{R-\Delta} \frac{dS}{dr}\, dr + \int_{R-\Delta}^{R} \frac{dS}{dr}\, dr \end{aligned} \tag{5.24}$$

The integrands, and therefore the second term in each of the above expressions, are independent of R (or E). Thus

$$\int_{R-\Delta}^{R} \frac{dS}{dr}\, dr = \int_0^{\Delta} \frac{dS}{dr}\, dr \tag{5.25}$$

i.e. regardless of the initial energy E, (L_e,S_e) are ridge coordinates as indicated in fig. 5.10. Consequently, a

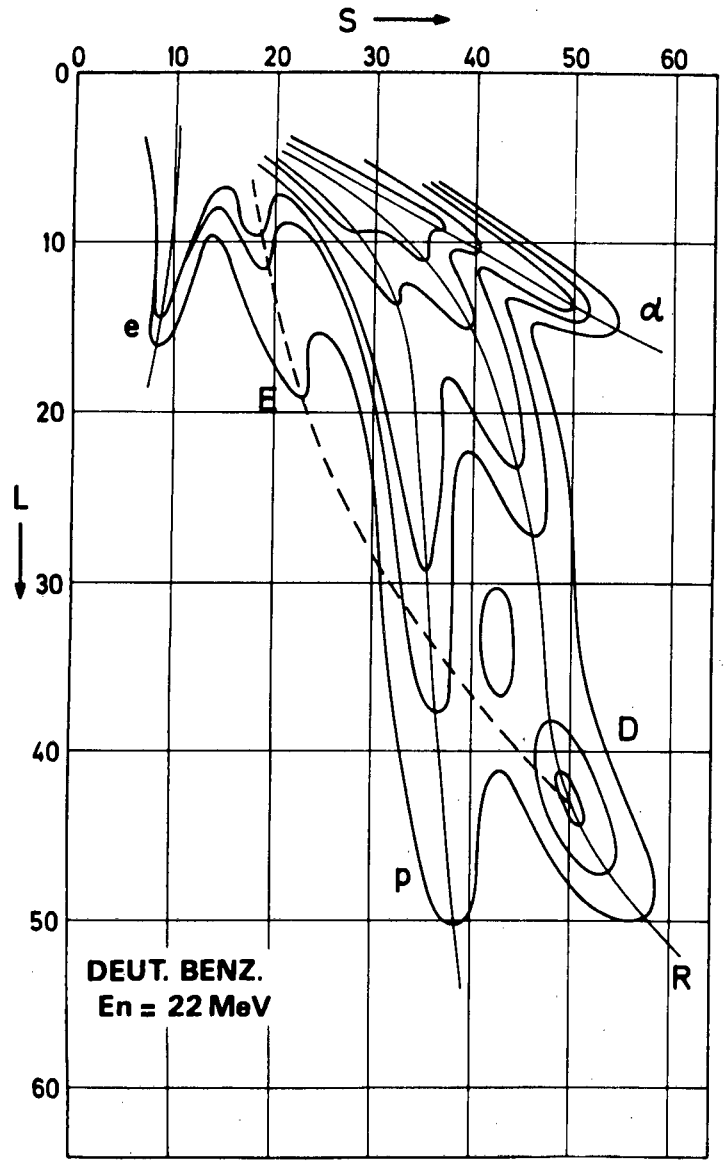

Fig.5.9(a). Contour representation of an (LS) spectrum for 22 MeV neutrons on deuterated benzene. The locus of escape events is indicated by a dashed line. The projection of the D-locus (R) beyond the forward recoil scale is determined to a large extent by rescattering events.

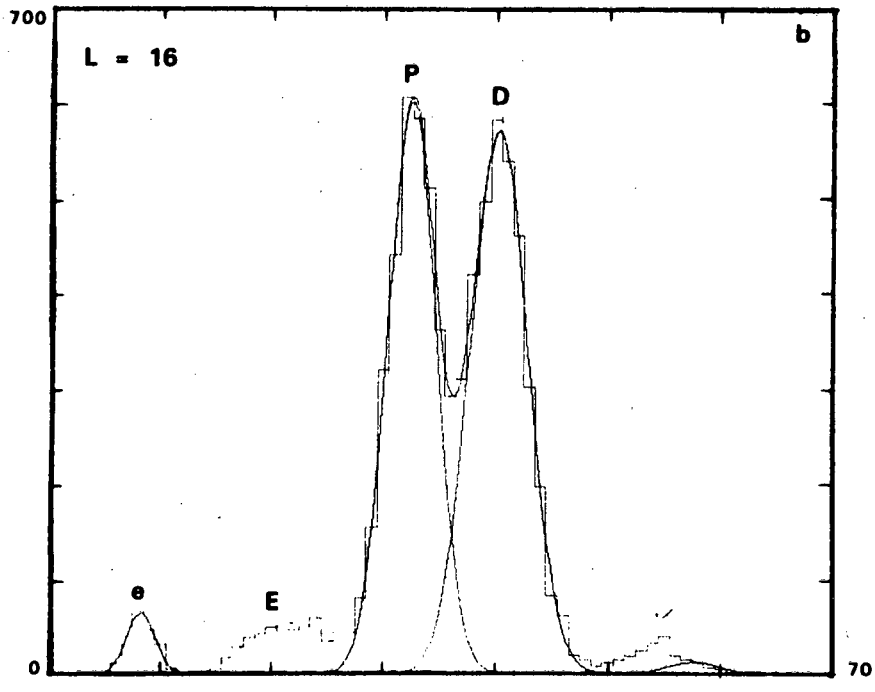

Fig.5.9(b). A cross-section of an (LS) spectrum taken showing the locus (E) of escapes.

particle escaping after travelling a distance $R-\Delta$ will have coordinates $(L-L_e, S-S_e)$ as indicated in fig. 5.8 , and the locus defined by these escapes will be an inverted particle locus with the origin at (L,S). Furthermore, it can easily be seen that the escape events will be evenly distributed along this locus.

This conclusion agrees fairly well with what is observed (see fig. 5.9). Since the elastic energy distribution is strongly peaked at forward recoil angles where escape probability is greatest, the locus corresponding to escapes from this peak is well-defined. However, the slope of dS/dL of the escape locus near its origin (i.e. the forward recoil peak), is not as large as the slope of the corresponding deuteron ridge at zero energy. This may be attributed to non-linearity of the actual PSD circuit which, according to the characteristics of the diodes, is most pronounced at low L-values. The good definition of the escape locus from the forward recoil peak is therefore useful in assessing the effect of non-linearity when estimating the displacement due to rescattering. In this, one is also guided by the upper end of the deuteron distribution. The locus beyond the end-point of the distribution is largely determined by the events displaced from the forward recoil peak by multiple scattering. It therefore defines dS/dL for rescattering in this region. This should be comparable with dS/dL of the escape locus. It is encouraging to note that this appears to be so (see fig. 5. 9).

One last observation will complete the information needed to perform quantitative corrections for escape and

multiple scattering. It can be shown† that, for low energies, it is a good approximation to assume that the S-displacement (though not the L-displacement) is the same for all particles having the same energy E.

Thus, in correcting for multiple scatter and escape of both deuterons and protons, the deuteron escape locus and the multiple scatter locus beyond the end-point of the deuteron spectrum were used to estimate the displacement due to multiple scatter and escape.

For all escape and multiple scattering corrections, ranges were determined from specific energy losses given by Craun and Smith (Cr70) and calculated from the tables of Northcliffe and Schilling (No70). In the range 5-40 MeV, the range of deuterons in deuterated benzene is well approximated by a quadratic

$$r(E) = 0.0057E^2 + 0.0475E - 0.17 \text{ (mm)} \qquad (5.26)$$

Over restricted energy regions ($\lesssim$ 5 MeV) it was often approximated by a linear function for convenience. As for the responses (see section 5.3), the range of the proton is related to the range of the deuteron by

$$r_p(E) = \tfrac{1}{2} r_D(E) \qquad (5.27)$$

---

†This may be deduced from the relatively small dependence of the slow component of scintillation decay on dE/dx (Bi64). It is not a very good approximation in all cases since dE/dx sometimes differs by orders of magnitude from particle to particle at the same energy. However, this is not the case from hydrogen to deuterium.

(a) Edge Effects

(1) Recoil deuterons:

Edge effects for recoil deuterons are relatively easily corrected for analytically because the energy of the recoil deuterons is well-defined and simply related ($E_D = \frac{8}{9} E_n \cos^2 \theta^{\ell}$) to their recoil deuteron angle (θ_{ℓ}) and because their energy distributions are well known and well approximated by low-order functions. (This is particularly true of the forward recoil peak (see fig. 5.8), where the distribution is well approximated by a linear function).

The case is considered for a cylindrical scintillator (see fig. 5.12) where a deuteron (energy E, range r recoils at an angle θ

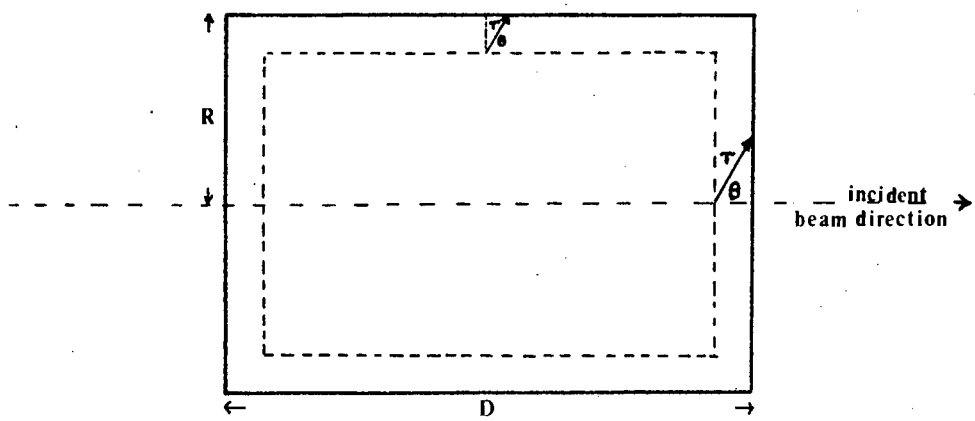

Fig. 5.10. Cross section of a D cylindrical scintillator. r is the range of the deuteron recoiling at angle θ. The shaded area represents that area from which deuterons recoiling at angle θ will escape.

If r is much smaller than the dimensions of the scintillator, the probability of escape from the front face is given by

$$P_{ef}(E) = \frac{r \cos \theta}{D} \qquad (5.28)$$

To obtain the probability of escape from the sides, one must average over θ. One obtains

$$P_{es}(E) = \frac{1}{\pi} r \sin \frac{2}{R} \tag{5.29}$$

Using these expressions, the proportion of deuterons recoiling at angle θ with energy E which escape from, say, the front face, is given by $I_D(E)P_{ef}(E)$ (where $I_D(E)$ is the deuteron energy distribution) and the total number of escapes in an energy region E, including a total (corrected)number of events N, is given by

$$-\Delta_e N = N \frac{\int_E^{E+\Delta E} I_D(E)\, P_{ef}(E)\,dE}{\int_E^{E+\Delta E} I_D(E)\,dE} \tag{5.30}$$

To estimate the fraction of these escape events which are excluded from the deuteron integral, one makes use of the escape locus described above. The escape events are evenly distributed along this locus. If, judging from the slope dS/dL of the escape locus and our method of determining the number of events in the ridge (see section 4.5), one assumes that a deuteron escaping with energy $>\delta$ MeV will be excluded from the distribution, one can conclude that the fractional number of events excluded due to edge effects from an L-channel corresponding to deuteron energy E, is given by

$$(\delta/E)P_{ef}(E) \tag{5.31}$$

In most cases, δ was chosen to be 2 MeV.

Some of the deuteron escape events fall in the proton integral (see fig. 5.9). These are a known fraction of the

deuteron escapes since the locus on which they lie is known.

(2) Breakup Protons:

Correction of the proton energy distribution for edge effects is not as straightforward as for the deuteron distribution. Here, the problem is complicated by two factors:

(a) The angle of emission corresponding to a particular proton energy is not well-defined. This is due to the presence of three particles in the final state of the reaction. For each proton energy, one can at most define a range of emission angles (see Appendix B).

(b) The distribution of the breakup protons with energy and angle of emission is not as well-known as for the recoil deuteron. Although it is well-approximated by phase space, there are enhancements due to final-state interactions (e.g. I161). The enchancement most likely to effect us is that due to the n-n FSI at maximum proton energy where the escape probability is greatest.

Assuming a distribution $I_p(E,\theta)$, the proportion e_{pf} of protons having energy E which escape from, say, the front face of the scintillator is given by

$$e_{pf}(E) = \frac{\int_{\Omega^\ell} I_p(E,\theta) P_{ef}(\theta,E) d\Omega^\ell}{\int_{\Omega^\ell} I_p(E,\theta) d\Omega} \qquad (5.32)$$

where Ω^ℓ is the laboratory angle of emission of the breakup proton. If one approximates $I_p(E,\theta)$ by the phase-space distribution $\rho(E,\theta)$ (see Appendix B), the total number of proton escapes in an energy region ΔE, including a total

(corrected) number of events N, is given by

$$-\Delta_e N = N \frac{\int_{E\Omega} \rho(E,\theta) P_{ef}(\theta,E)\, dEd\Omega}{\int_{\Omega} \rho(E,\theta)\, dEd\Omega} \qquad (5.33)$$

One recalls that the differential cross section for $\frac{d\sigma}{dEd\Omega}$ for protons emitted at forward angles is sharply peaked at maximum proton energy owing to the effects of the n-n FSI (e.g. I161) see fig. 6.4). Ideally, in obtaining $e_{pf}(E)$ one should take this peak into account since it has the effect of concentrating protons at maximum energy. However, this peak is known to decrease rapidly with increasing angle of proton emission so that it has virtually disappeared at 30 degrees (lab) (see fig 6.4). Therefore, it does not persist at lower proton energies. Furthermore, the angular range of proton emission is small at higher proton energies and since $P_e(\theta,E)$ has a $(\cos\theta)$-dependence, it varies little over a small angular range about zero. Consequently, one can approximate expression (5.23) at high proton energies by taking $P_{ef}(\theta,E)$ outside the integral. Then

$$e_{pf}(E) = P_{ef}(\theta,E) \qquad (5.34)$$

i.e. If one normalises the angular integral separately for each energy E, one can neglect the effect of the n-n FSI at high proton energies in correcting for proton integral for escape.

(b) Rescattering Corrections

The coordinates (L,S) resulting from rescattering are determined in combination by all the recoil particles. Consequently, rescattering can have one of two effects on the integral of the energy distributions.

(1) It may result in the loss of events (positive correction). Consider, for example, the case where a neutron, resulting from the breakup of a deuteron, scatters elastically off another deuteron. The event will be displaced to higher S (see fig. 5.8). If the energy of the recoil particle is sufficiently high, it will not be included in the proton integral.

(2) It may contribute spurious events (negative correction). The same example described above may contribute a spurious event to the recoil deuteron integral. This again depends on the energy of the recoil deuteron. Both kinds of corrections were considered. Only double scattering was taken into account. The possible double scatterings are listed in Table 5.3, together with the nature of the correction they require in each of the breakup proton and recoil deuteron integrals.

It is seen that the total recoil deuteron integral must be corrected for the effects of all the double scatterings. However, only the forward recoil peak was used to obtain the total deuteron integral and the rescattering corrections which apply to this region of the integral are negligible.

This is so because the forward recoil peak is localized at the upper end of the energy distribution. Neutrons from a first interaction are usually degraded in energy so that

Table 5.3

Rescattering corrections

	First Interaction	Second Interaction	Correction to: Breakup Protons	Recoil Deuterons
A1	$^{12}C(n,n')X$	D(n',n")D	none	-ve
2		D(n',2n")'H	-ve	-ve
B1	D(n,n')D	D(n',n")D	none	+ve
2		D(n',2n")'H	-ve	+ve
3		$^{12}C(n',X)Y$	none	+ve
C1	D(n,2n')'H	D(n',n")D	+ve	-ve
2		D(n',2n")'H	+ve	-ve
3		$^{12}C(n'X)Y$	+ve	-ve

spurious contributions from processes A and C (see Table 5.3) are concentrated at lower L-values. Process B occurs with a high probability since the neutrons corresponding to deuterons recoiling in the forward direction have low energy and, consequently, a short mean free path. The probability of an event in the forward recoil peak being displaced to higher S-values by rescattering is typically 10%. However, events displaced in this manner from the forward recoil peak usually determine the locus of the energy distribution beyond the end-point for single scatterings and are consequently easily included (see fig. 5.9).

In correcting the proton energy distribution for re-scattering, only processes A2, B2 and C need be considered. Process C2 is negligible. The interactions denoted $^{12}C(n,n)X$ and $^{12}C(n,X)Y$ comprise both elastic and inelastic interactions of neutrons with carbon. However, since the energy of reaction products is generally too low to concern us, only elastic scattering was considered.

Calculations were simplified by assuming the mean interaction point at the center of the scintillator. The probability of subsequent re-scattering was calculated in spherical geometry. From the locus of rescattered events beyond the deuteron distribution end-point and from that representing escape from the forward recoil peak, an energy interval δ was estimated. If a charged particle other than a proton was motivated with energy E by rescattering, the event was either excluded from or included in the proton distribution depending on whether E was larger or smaller than δE. In accordance with our observations at the beginning of this section, $\frac{dS}{dL}$ for rescattering was considered the same

for all particles. The mean neutron energy corresponding to a proton energy E MeV was taken to be $\frac{1}{2}(E_o-E-2.225)$ MeV (where E_o is the incident neutron energy).

The results of these calculations at lower incident energies with δ = 2 MeV are presented in fig.5.11. In view of the smallness of the corrections, it was decided not to complicate the calculations any further. However, an uncertainty of 100% is assigned arbitrarily in view of the simplifications assumed.

Measurements with scintillators of different dimensions show that the results are insensitive to multiple scattering effects. This observation is consistent with the results of our rough calculation which show that the correction is small.

(c) Correction for n-p scattering

Since the proportion of hydrogen to deuterium in the scintillator is known (1.39%), the fraction of events in the proton distribution due to n-p scattering can be calculated.

The total number of n-p scattering events is obtained as follows

$$I_{np} = \frac{0.0139\ (\sigma_{np})S}{\sigma_{nd}}\ I_{peak} \qquad (5.35)$$

where σ_{nd} is the total n-d cross section

σ_{np} is the total n-p cross section

and the other quantities have been defined above.

To calculate the proportion of recoil proton events under the measured distribution, a rectangular n-p elastic distribution was assumed.

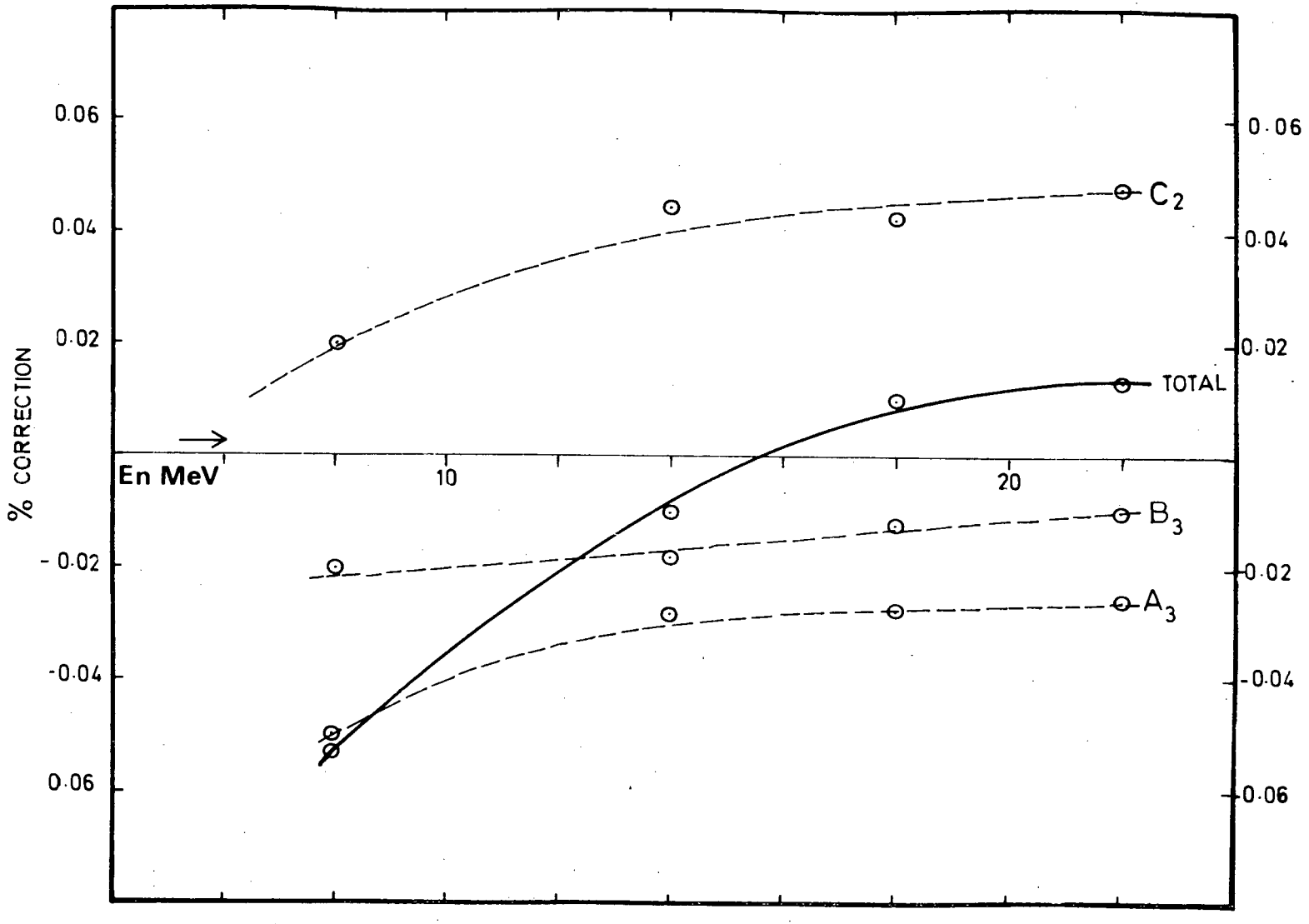

Fig. 5.11. Percentage correction for rescattering. The correction is averaged over proton energies greater than 4 MeV and is applied to the integrated proton spectrum.

Since the maximum proton energy from n-p scattering is 2.2 MeV larger than that from breakup, the end-point of the recoil proton distribution extends beyond that of the breakup distribution. Therefore, another way of estimating the contribution from n-p scattering is to normalise a rectangular recoil proton distribution to that part projecting out beyond the breakup protons.

Corrections obtained in this manner were usually larger (by $\sim$20%) than those obtained with the alternative method. Some of this discrepancy may be accounted for by multiple scattering effects. Since this correction is of the order of 6%, the discrepancy introduces an uncertainty of $\sim$1% in the final result.

CHAPTER 6

RESULTS AND CONCLUSION

6.1 Results

Pulse-height distributions for recoil deuterons and breakup protons were measured at eleven incident energies between 8 and 22 MeV. At some energies, more than one measurement was made, while at 22 MeV, several measurements, with scintillators of three different sizes (see Chapter 4) were recorded.

All pulse-height distributions were analysed as described in Chapter 5 to obtain the total breakup cross section σ_B. At all energies, both methods A and B were used. The results of these analyses are listed in table 6.1 and plotted in fig. 6.1, together with previous measurements and calculations.

A quantity δ (see Chapter 5, section 5) which represents the enhancement of phase space due to the n-n FSI at the high energy end of the proton spectra is plotted in fig. 6.2. The values obtained in this analysis are compared with those obtained by integrating the upper end of the proton energy spectra, obtained (De66) as functions of the angle of emission, over energy and angle.

Proton energy distributions may be obtained by correcting each point in the pulse-height spectra for the effect of non-linear pulse-height response and edge effects. The energy distribution at 22 MeV incident energy is plotted in fig. 6.3. No attempt was made to account for multiple scattering effects since the energy distributions of these corrections are not known. However, these effects are expected to be small (see

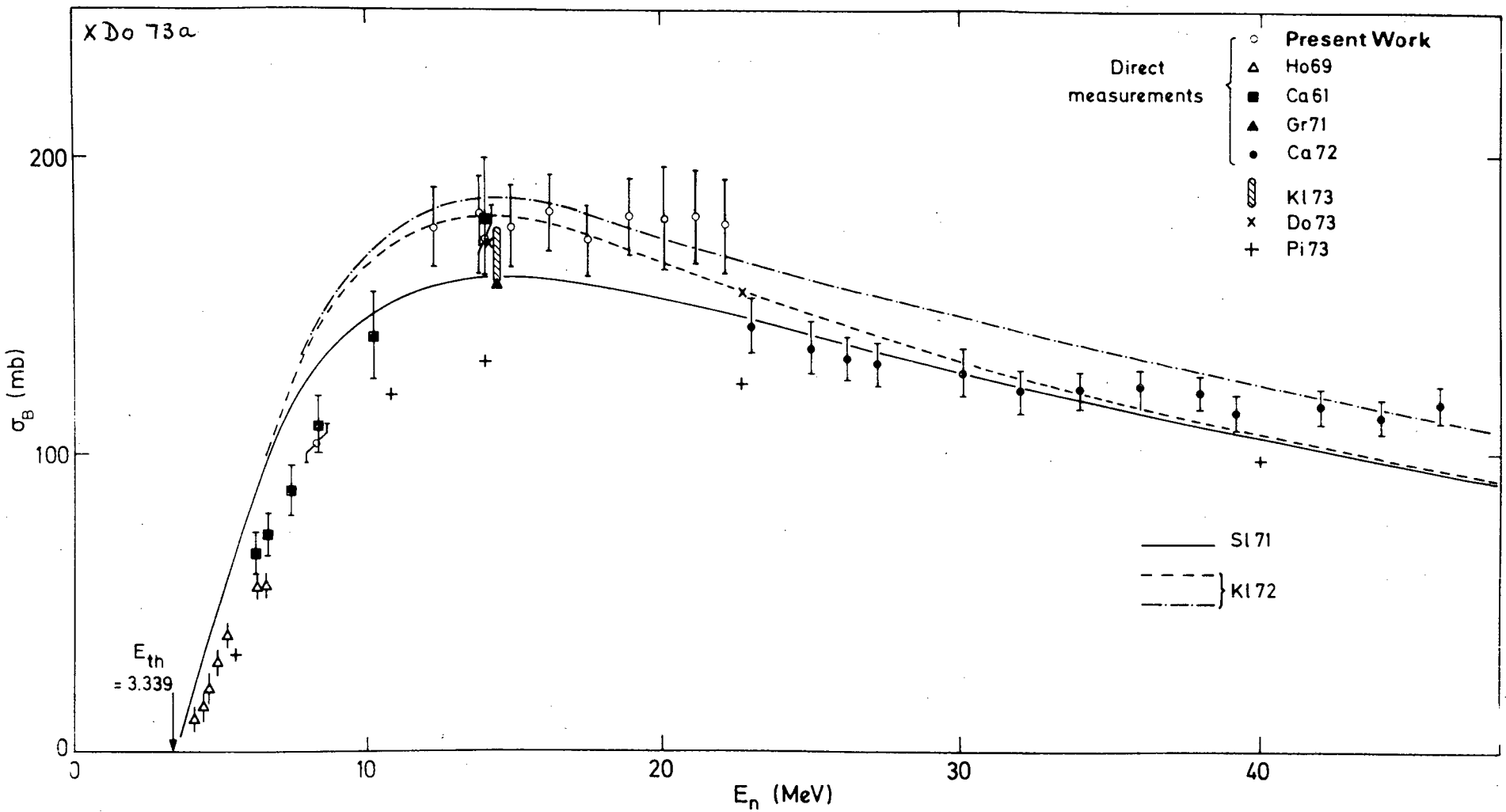

Fig. 6.1. The N-d breakup cross section for incident energies less than 50 MeV.

Chapter 5, section 7). The spectrum is not corrected for the effect of finite energy resolution. However, the resolution width was determined from an analysis of the corresponding deuteron energy spectra (see Chapter 5, section 2) for eventual comparison with theory. At proton energies $\lesssim$ 9.2 MeV, the spectrum has been corrected for contributions from the $^{11}C(n,p)^{11}B$ reaction. It was assumed that a cross section of 5mb (see Chapter 5, section 6) is distributed evenly over proton energies 5 to 9 MeV.

6.2 Estimates of Uncertainty

(a) Statistical errors

Errors due to counting statistics are negligible since the total number of counts in the integrated spectra is typically greater than 10^4.

The principal sources of statistical uncertainty are in the analyses, that is, the projection of the ridges in the (LS) two para meter spectra to obtain pulse-height distributions, the energy calibration, (see Chapter 5, section 2) the normalization of a phase space distribution to a part of the proton spectrum, and in correcting for edge effects and rescattering.

All these stages in the analysis are subject to statistical variations which influence the result in a complex manner and which are difficult to assess. The best way to do this is to repeat measurements and observe the statistical fluctuation in the result. This has been done at several energies. In particular, a total of five independent measurements were

analysed at 22 MeV. The fluctuation was less than 2% (see table 6.1) for those taken with the same scintillator. Independent measurements at other energies were also stable to within 3% (see table 6.1). Consequently, a statistical uncertainty of 2% is assigned.

(b) Systematic errors

The following should be considered as possible sources of systematic error:

(a) Errors in the relative response curve (see fig. 5.4); If, judging by the difference between our measurements and those of Smith and Polk (Sm68), we assume an uncertainty of 5% in converting pulse-height to energy, the uncertainty in the final result will depend on the fraction of the total proton integral which lies below the cutoff. Taking a typical figure of 0.4, the error in the final result, due to a 5% error in the cutoff energy, would be $\sim 5\% \times 0.4 \simeq 2\%$. The procedure whereby a phase space distribution is normalised to part of the energy spectrum is also sensitive to errors in the energy calibration. An error of 5% in E_1 and E_2 (see section 5.5) will lead to an error of $\sim 2.5\%$ in the final result This error will be in the same sense as that due to an error in determining the energy corresponding to the cutoff.

(b) Errors in correcting for edge and rescattering effects; Corrections for edge effects are all thought to be accurate to less than 10%. Those for rescattering on the other hand, have been assigned an arbitrary uncertainty of 100%. However, since they are small

TABLE 6.1

RESULTS OF MEASUREMENTS OF THE TOTAL n-d BREAKUP CROSS SECTION (σ_B) PERFORMED IN THIS WORK

E_n (MeV)	Size of Scintillator R(cm)	D(cm)	σ_B (mb) A	σ_B (mb) B	mean σ_B (mb)
22.00	1.35	2.5	186±17	184±17	
"	"	"	188±17	183±17	
"	"	1.2	178±16	167±16	176±16
"	"	2.5	179±16	179±16	
"	"	3.7	165±15	168±15	
"	"	3.7	165±15	169±15	
21.07	"	2.5	184±17	177±16	180±17
20.02	"	"	181±16	176±16	179±16
18.80	"	"	176±16	173±16	180±17
"	"	"	184±17	185±17	
17.40	"	"	175±12	168±12	172±12
16.05	"	"	183±13	178±12	181±12
"	"	"	184±13	184±13	
14.80	"	"	177±13	176±12	176±14
14.00	"	3.7	174±13	171±12	172±12
13.66	"	2.5	181±13	181±13	181±13
12.17	"	"	172±14	172±14	176±14
"	"	"	179±14	182±14	
8.20	"	"	104±10	103±10	103±10

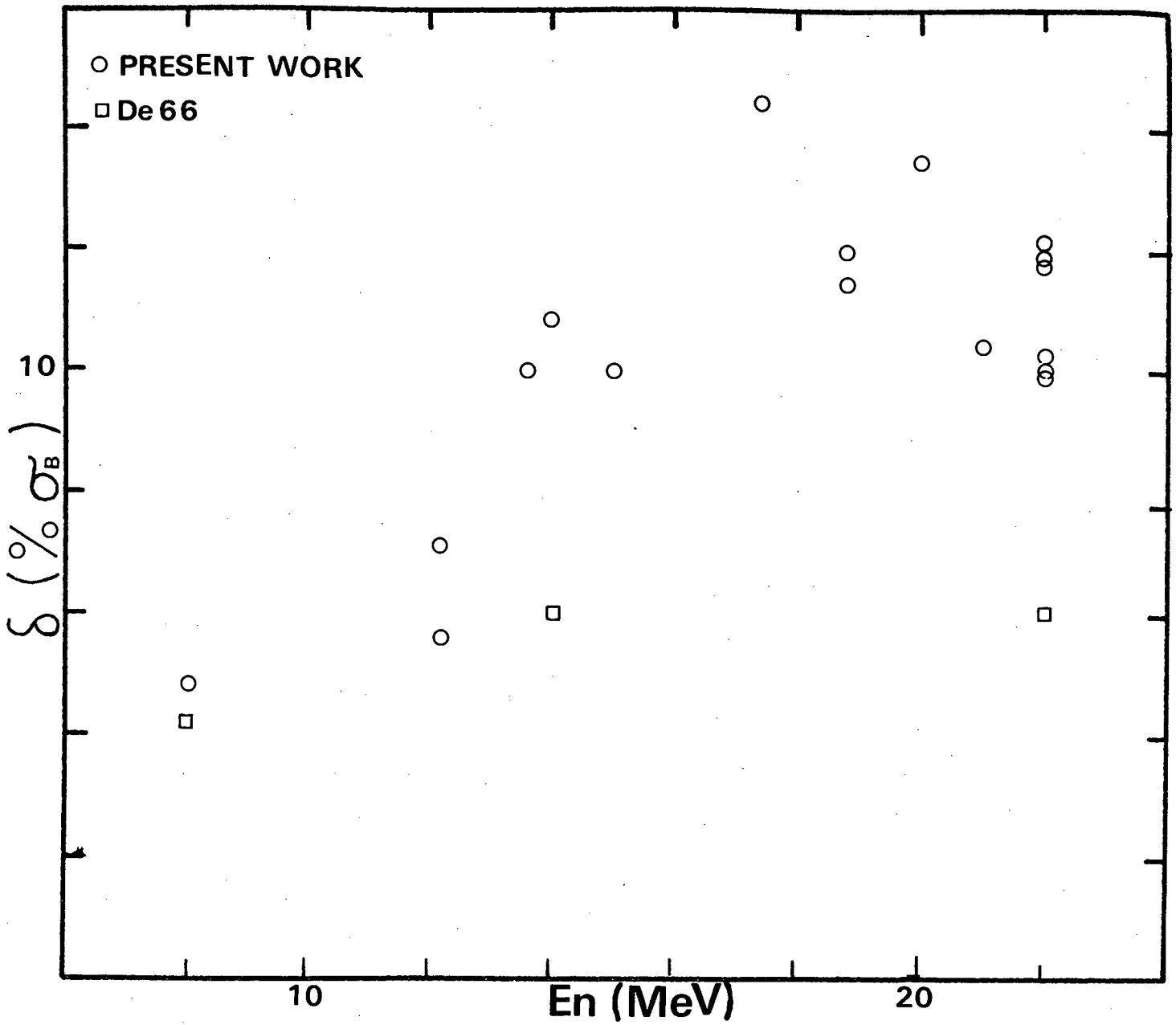

Fig. 6.2. The deviation from phase space δ attributed to the n-n FSI as a percentage of σ_B. Three values of the integral under the n-n FSI obtained from the data of Debertin (De66) are also included.

(typically less than 3%) (see fig. 5.13), they will contribute an uncertainty of less than 3% in the final result. The differences between results obtained with scintillators of different sizes are of that order (see table 6.1)

(c) Error in the method of extrapolation

The assumption of a phase space distribution to correct for the counts lost below cutoff will be considered in greater detail in the next section. The uncertainty introduced by this method has been estimated on the basis of the deviation from phase space just below the cutoff. The shaded region in fig. 6.3 represents an uncertainty of ∿5%.

(d) Uncertainty in S and σ_{peak} (see Chapter 5, section 5)

The scatter about the curves which are thought to represent the mean values as functions of incident energy is typically less than 5% for σ_{peak}, while for S, it is larger (10% in a few cases). However, the curves represent mean values and the uncertainty in the mean is smaller but difficult to assess. It has been taken to be the difference between results obtained with methods A and B (see Chapter 5, section 5) which is typically less than 2%.

(e) Error in accounting for competing reactions

At incident energies >17 MeV the $^{12}B(n,p)^{11}B$ reaction contributes to the energy distributions above cutoff. This contribution has been subtracted on the basis of the cross sections given by Rimmer and Fisher who quote an uncertainty of 25% in their results. These measurements include contributions from the reaction proceeding

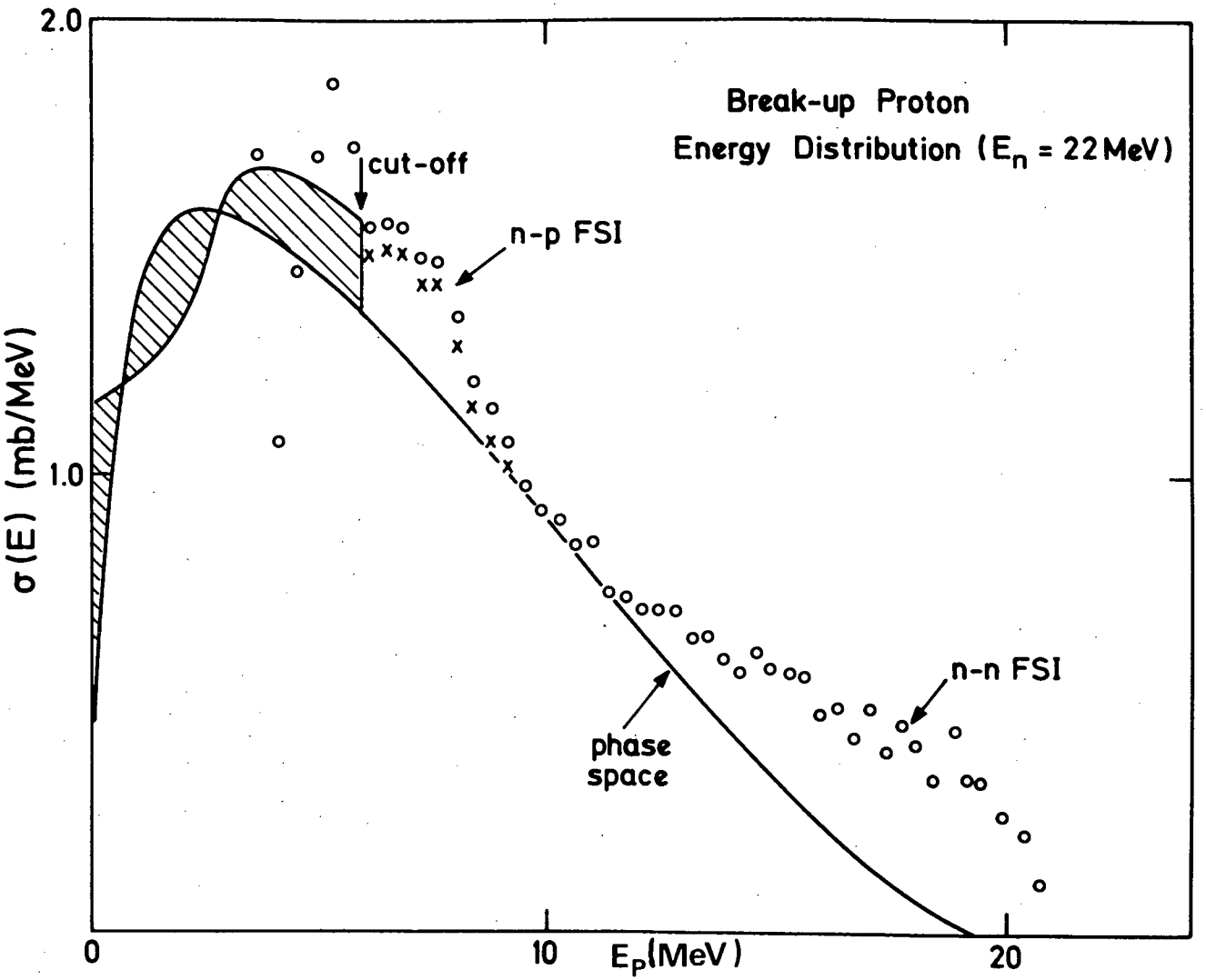

Fig.6.3. The energy distribution of breakup protons at 22 MeV incident energy. The normalised phase space distribution used to correct for the counts lost below the cutoff is shown. The area in the shaded region was used as an estimate of uncertainty in this correction. The crosses at low proton energy were obtained by subtracting the contribution from $^{12}C(n,p)^{11}B$.

to the ground and first four excited states of ^{12}B (see Chapter 5, section 6) since they are stable with respect to particle emission. However, at energies $\gtrsim$ 21 MeV, some contribution resulting from the transition to higher excited states is possible and has not been accounted for.

There is also an uncertainty in estimating the fraction of protons which are excluded from the proton distribution by the (LS) analysis (see Chapter 5 ,section 7).

Since the cross section for $^{12}C(n,p)^{11}B$ varies between 8 mb at 22 MeV and 18 mb at 18.5 MeV (see Chapter 5, section 6) an error of 50% will introduce a corresponding error of between 2% and 5% in the final result.

The total percentage uncertainty $\Delta\sigma_B$ in the values for the total breakup cross section has been taken to be a statistical combination of the errors described above, that is

$$\Delta\sigma_B = \sqrt{\Sigma\Delta_i^2}$$

6.3 Phase space as an Approximation

A general expression for the differential cross section for n-d breakup is

$$\frac{d\sigma^3}{d\Omega_1 d\Omega_2 dE_1} \propto |T|^2 \rho \qquad (6.1)$$

where ρ is the density of final states or phase space factor (see Appendix B). The differential cross sections are therefore determined in combination by the phase space factor and the transition matrix T. If T is independent of the momentum

transfer variables, the shape of the differential cross section will be determined by ρ alone.

It has generally been observed that the most pronounced enhancements of phase space are those due to FSI and QFS (see Chapter 2 and e.g. Mc73, Sl73). Outside the kinematical regions favouring these processes, enhancements are relatively small and the distributions are generally characterized by the phase space distribution. This is best illustrated by the recent work at IKO (Instituut voor Kernphysich Onderzoek, Amsterdam) (Wi72). The whole of the phase space for the H(d,2p)n reaction was explored and the result was presented as a Dalitz plot (see fig. 6.4b). The enhancements due to FSI and QFS are easily recognisable. No other effects of comparable magnitude can be distinguished outside the kinematical regions favouring these processes.

It is therefore possible to obtain a qualitative representation of a differential cross section with an expression of the type 2.60 (see Chapter 2) viz.

$$\frac{d^3\sigma}{dE_1 d\Omega_1 d\Omega_2} \propto \left(\sum A_i^2 \, T_{FSI}^2 + \sum B_i^2 \, T_{SM}^2 + C^2 \right) \rho \qquad (2.60)$$

To obtain the proton energy distribution $\frac{d\sigma}{dE}$, this expression must be integrated over the angular variables. The summation is over both triplet and singlet FSI's. However, since the triplet N-N scattering length is much smaller than the singlet one, this FSI has a much smaller effect and need not be considered for qualitative purposes.

Let us consider the terms in (2.60). These have been given in Chapter 2. We recall that T_{FSI} is given by the Watson Migdal theory as

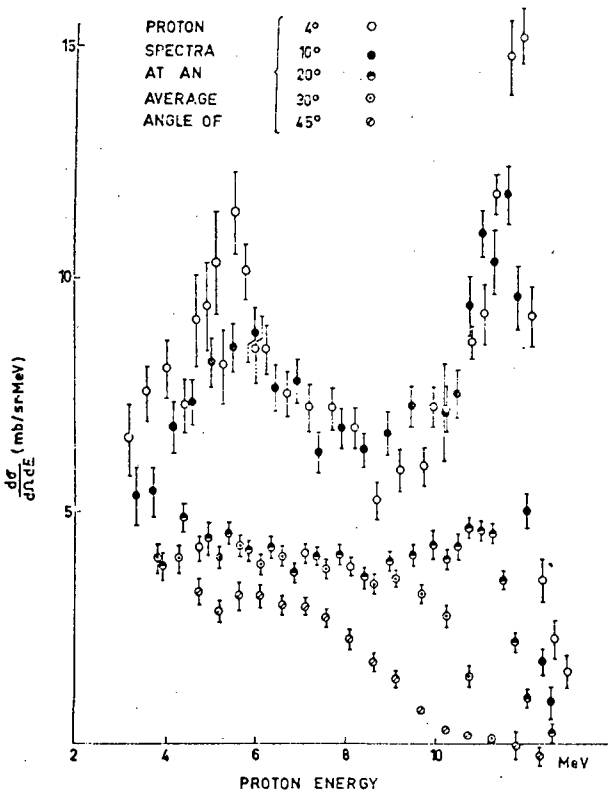

(a)

Fig.6.4(a) Proton energy spectra from $^{2}H(n,p)2n$ at 14.1 MeV for various angles of proton emission (I163)

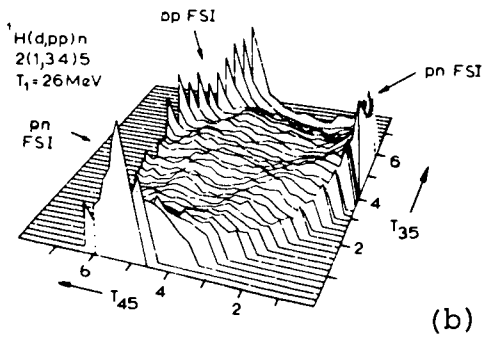

(b)

Fig.6.4(b) Dalitz spectrum for the p+d →p+p+n reaction. (Taken from the 1971/72 IKO progress report.)

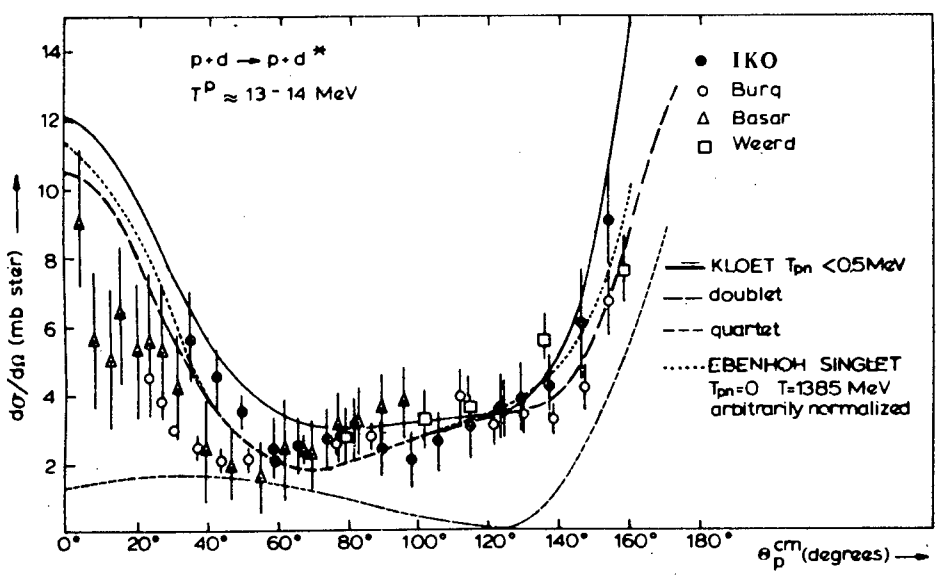

(c)

Fig.6.4(c) Angular distribution of d* (Taken from the 1971/72 IKO progress report)

$$T_{FSI} = \frac{|f(\theta)|^2}{(1 - r_o/a)(k'^2 + \alpha^2)} \qquad (6.2)$$

The energy dependence e of T_{FSI} is given by the above expression. For the D(n,2n)p reaction, $\frac{d\sigma}{dE}$ for protons due to an n-n FSI is enhanced sharply at maximum proton energy (see fig. 6.4), the shape of the peak depending on the low-energy n-n scattering parameters. However, the angular dependence $f(\theta)$ is not so easily determined. Experiment has shown (Bo68)(De66)(Il63)(Vo65)(Bu73) and (fig. 6.4.) that the FSI enhancements decrease rapidly with increasing angle of emission. As for the measurement of Ilakovac at 14 MeV (see fig. 6.4a), all measurements show that at 40^o (lab. angle) the peak has practically disappeared.

Attempts at theoretical analysis in Born approximation (see Chapter 2) have been made by Ilakovac et al. (Il63) and by Koehler (Ko64)(Ko65). Only those of Ilakovac predict a decrease in the n-d FSI with increasing angle of proton emission, in agreement with experiment. Experiments with the D(p,2p)n (Cr59) reaction show that the charge symmetric p-p FSI decreases monotonically to as far as the measurements extend (100^o lab.angle).

Much more is known about tha angular dependence of the n-p FSI from experiment and calculations on the charge symmetric reaction ^{1}H(d,pp)n. Many experiments (Bu72)(Va71)(Br70)(Wi72)(Ba70a) have been performed to determine the angular dependence of the n-p FSI. These, together with the results of exact calculations are shown in fig. 6.4(c). (This and fig. 6.4.(b) were taken from the 1971/72 IKO progress report.) It is seen that the anglar dependence is sharply peaked for the (n-p)

pair proceeding in the forward direction with a comparatively smaller peaking at back angles.

If, on the weight of the evidence mustered above, it is assumed that the FSI's produce enhancements for protons proceeding in the forward direction and that these enhancements decrease rapidly with increasing angle of emission (decreasing maximum proton energy), one expects the enhancements in the proton energy distribution integrated over all angles to be concentrated at the upper energies at which each of the n-p and n-n FSI's contribute, that is, at the maximum proton energy E_{max} and at slightly less than 4/9 E_{max}. (See fig. 6.5) This is in fact what is observed (see fig. 6.3).

The enhancement due to QFS may be understood qualitatively by considering the expression from the spectator model of Kuckes, Wilson and Cooper (Ku61) (see Chapter 2, section 5)

$$\frac{d^2\sigma}{dE_1^{\ell} d\Omega_1^{\ell} d\Omega_2^{\ell}} = \left(\frac{d\sigma}{d\Omega}\right)_{free}^{cm} \frac{4\sqrt{2}}{\pi^2} (E_o)^{-\frac{1}{2}} \frac{(E_\beta E_B)^{\frac{1}{2}} (E_B^{\frac{1}{2}} + E_\beta^{\frac{1}{2}})}{(E_B + 2E_3^{\ell})^2 (E_\beta + 2E_3^{\ell})} \frac{h^6}{m^3} \rho \qquad (2.51)$$

We take E to be the proton energy in the laboratory system. Then, for an n-n QFS, $E_3^{\ell} = o$ and, as was explained in Chapter 2, there will be an enhancement near $E_3^{\ell} = o$ because of the influence of a second-order pole in the unphysical region at $E_3^{\ell} = -\frac{E_B}{2}$ Therefore the n-n QFS leads to an enhancement which is localised at zero proton energy, while the n-p QFS is distributed over the whole proton energy range. However, QFS processes are known to be smaller than FSI ones. (S173). This is also evident from the fig. 6.4(b). Some enhancement at low energies is also expected owing to the comparatively smaller backward peaking of the n-p FSI. This will occur at zero energy. If

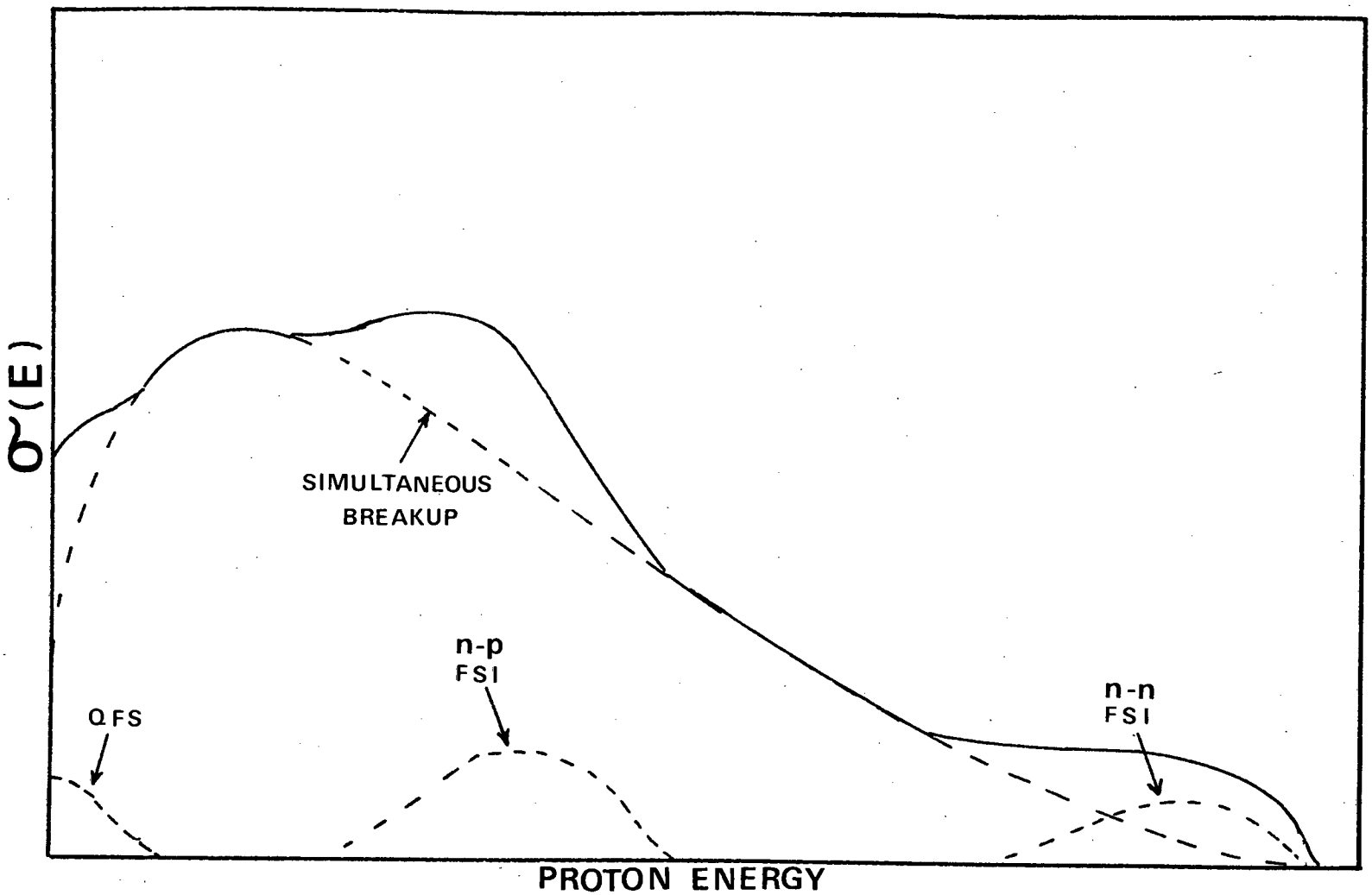

Fig. 6.5 A schematic diagram indicating the expected position of the enhancements due to various reaction mechanisms

the n-n FSI causes any enhancement in the energy spectrum of protons emitted in the backward direction this will occur at low proton energies as indicated in fig. 6.5.

In conclusion, it may be said that the part of the proton energy distribution which has been measured is characteristic of an expression of the type 2.60. The enhancements of phase space due to FSI occur at the expected energies and are in qualitative agreement with the known angular dependence of the FSI's. In particular, since they are concentrated at medium and maximum proton energies it is reasonable to expect the intermediate region to be characteristic of the phase space distribution. At low proton energies, deviations from phase space are expected to be smaller.

6.4 Discussion

As a result of this work, the n-d breakup cross section has been determined at 11 energies between 8 and 22 MeV. For most of these values, the uncertainty is estimated at ∿7%, but for the measurements at 21 and 22 MeV, it is thought to be larger (∿9%) because of the uncertainty in correcting for contributions from the $^{12}C(n,p)^{11}B$ reaction (see section 6.2).

The values obtained at energies near 14 MeV are consistent with those obtained by other measurements (As58)(Ca61) except for a value at 14.6 (Gr71) which was obtained using a method similar to the one used in this work. The essential difference between these two results, obtained using the same experimental method, is that Graves (Gr71) used a modified phase space distribution to extrapolate the proton spectrum to zero energy.

This modification was suggested by the fact that, for an incident energy lf 14 MeV, the proton energy distribution was observed to decrease at proton energies ∿3.5 MeV whereas the phase space distribution only begins to decrease at ∿1.5 MeV. No conclusive evidence for this effect was observed in this work since for energies smaller than ∿3.5 MeV protons could not reliably be separated from deuterons.

At higher incident energies, this effect should occur at comparably higher proton energies. However, here the issue is clouded by contributions from competing reactions. Nevertheless, at 22 MeV (see fig. 6.3) there is evidence that the rate of increase of the $d\sigma/dE$ is dropping at 5 MeV proton energy.

Such an effect is attributed to the n-p FSI. As explained in the previous section, a peak near 4/9 E_{pmax} (where E_{pmax} is the maximum breakup proton energy) is consistent with the known angular dependence of the n-p FSI. However, judging from the effect of the n-n FSI at high proton energy, the effect should not cause a departure from phase space of the magnitude assumed by Graves. Hence it would seem more appropriate to approximate the distribution below cutoff by means of a (normalised) phase distribution.

It would be interesting to fit a theoretical distribution to the measured part of the proton spectrum, both from the point of view of testing the theory, and to obtain a better idea of the behaviour of the distribution at low proton energies.

The measurements at the upper end of the range deviate markedly from measurements of the p-d breakup cross section at energies above 23 MeV. For energies above 21 MeV there

exists a larger uncertainty in the contribution of the $^{12}C(n,p)^{12}B$ reaction so that a least part of the discrepancy may be accounted for by an error in our measurement from this source. On the other hand, the technique used to measure the p-d breakup cross section is also subject to a greater uncertainty at these energies (Ca72).

For comparison, calculations of the breakup cross section based on the exact formalism of Faddeev (Fa61-68) and Amado (Am63) have also been included in fig. 6.1.

The calculations of Kloet and Tjon were performed using local potentials whereas in all the others, separable ones were used. Apart from those used in the calculations of Doleschall (Do73) and Pieper (Pi73a), all potentials are S-wave ones.

It was emphasized in the introductory chapters that the breakup cross section σ_B is an interesting quantity since calculations of it are sensitive to the difference in potentials used. This is evident from fig. 6.1. The difference is particularly marked between calculations with local and separable potentials. Our measurements seem to favour the calculations of Kloet and Tjon. These were performed with local potentials of the Yukawa type, incorporating hard cores. The upper curve was obtained with a hard core in only the singlet N-N potentials (potential I-IV), whereas the lower one is the result of calculations using a potential with cores in both the singlet and triplet states (potential I-III) (Ma69).

The uncertainty in these measurements is not small enough to permit selection between these two potential forms. In particular, for energies above 20 MeV, these measurements

deviate from the calculated cross sections. Part of the difference may be accounted for by the uncertainty in the contribution from $^{12}C(n,p)^{11}B$ reaction (see section 6.2).

Values of 171 mb at 14.1 MeV and 155 mb at 22.7 MeV were obtained by (Do73a) by including separable P-wave nuclear interactions exactly in the Faddeev formalism (see Chapter 2 and (Do73)). These are in agreement with calculations using S-wave local potentials (Kl72) and with our measurements near 14 MeV.

A perturbative treatment was used by Pieper (Pi72)(Pi73) to include separable P and D-wave N-N interactions in calculations of n-d scattering and polarization. The total breakup cross section obtained from these calculations (Pi73a) is also plotted in fig. 6.1. It deviates markedly from exact calculations since (Do73a) the approximation used in the calculation does not guarantee unitarity.

In conclusion, it may be said that these measurements of the total breakup cross section favour the calculations with local S-wave potentials over those with S-wave separable ones. However, the inclusion of higher partial-waves in calculations with separable potentials yield values similar to those with S-wave local potential. (Do73a) It will be interesting to see the effect of including higher partial waves in calculations with local potentials.

Recently, (Kl73) Kloet and Tjon published the results of calculations at 14 MeV with several potential forms. The range of values obtained is represented by the shaded region in fig. 6.1. It should be noted that there appears to be a discrepancy between these values for σ_B obtained with potential forms I-IV and I-III and those represented

by the curves which were obtained from previous graphical representations (Ca72). If these curves are in error, the conclusions drawn above should be altered. Shifting the curves down to correspond to the shaded area would make our measurements higher by comparison. In this case, they would favour calculations with the I-IV (Ma69) potential which yields the upper curve.

6.5 Further work

Most ot the uncertainty in the present results is due to uncertainty in

(1) The method of extrapolating the proton integral to energies below cutoff

(2) The multiple scattering corrections

(3) Accounting for competing reactions

Method C was considered in order to test our assumption that, at energies below the cutoff, the proton distribution is well approximated by phase space. In order to do this, it is necessary to reduce the cutoff to energies where the events due to different ionising particles can not be separated. This may be done as follows:

Instead of estimating the fraction of protons lost below a cutoff A (see fig. 6.6), the fraction f_T of the total number of counts (I_T) due to all contributing processes is estimated for a comparatively lower cutoff B (see fig. 6.6). The deuteron integral I_D can be obtained reliably from the measured part of the energy distribution as described in Chapter 5, section 5. Then the elastic cross section is given by

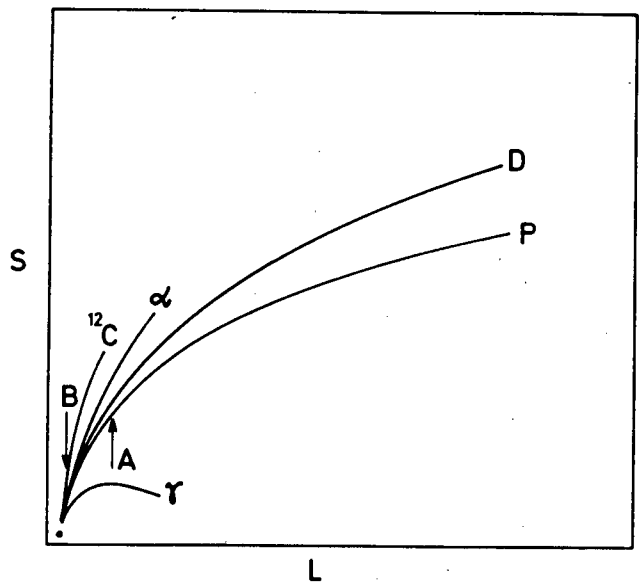

Fig. 6.6. Schematic diagram of an (LS) spectrum showing the region (A) in which the cutoff is usually taken in for methods A and B and the region (B) in which it would be taken for method (C).

and $I_T = I'_T / (1 - f_T)$ where I'_T is the sum of all observed counts,

$$\frac{I_D}{I_T} = \frac{\sigma_e}{\Sigma_n \sigma}$$

where $\Sigma_n \sigma$ is the sum of all reactions contributing to I_T and the inelastic cross section is given by $\sigma_B = \sigma_T - \sigma_e$

f_T may be obtained from

$$f_T = \frac{\sum_i (<\sigma_i/\sigma_i) n_i \sigma_i}{\sum_i n_i \sigma_i}$$

where σ_i are the reactions contributing to I_T and $<\sigma_i$ is the fraction of the contribution below cutoff B.

If f_T can be made small, an uncertainty in f_T will not have a large influence on the result. However, this procedure depends on an accurate knowledge of $\Sigma_n \sigma$.

If the low energy experimental biases are low enough to include all the products of neutron interaction with carbon, (e.g. α's from $^{12}C(n,\alpha)$ and in particular recoil ^{12}C ions), $\Sigma_n\sigma$ is given by the sum of the total ^{12}C and ^{2}H neutron cross sections, both of which are well known.

Unfortunately, the bias levels in this experiment were not low enough to include the carbon recoils from elastic scattering and the lack of detailed neutron cross section data of carbon prevented obtaining σ_n by summing the relevant partial neutron cross section for reactions on carbon (namely $^{12}C(n,\alpha)^{9}Be$, $^{12}C(n,n)3\alpha$, $^{12}C(n,p)^{12}B$, $^{12}C(n,d)^{11}B$). Experiments will be repeated with low bias levels and an extensive literature survey for measurements and evaluations of neutron cross sections on carbon is now being undertaken in order to obtain f_T accurately.

This alternative method also has the incidental advantage of obviating most of the tedious corrections needed to account multiple scattering and edge effects, since the whole area of (LS) analysis is included in obtaining I_T . If the forward recoil peak is used to obtain I_D, that is,

$$I_D = \Sigma I \text{ peak} \quad \text{(see Chapter 5, section 5)}$$

only the forward recoil peak need be corrected for these effects and this has been seen to be relatively easy (see Chapter 5, section 5).

In the absence of cross sections for competing $^{12}C(n,p)^{12}B$ and $^{12}C(n,np)^{11}B$ reactions, the possibility exists of using deuterated scintillators with different proportions of carbon to deuterium to observe the differences in contributions and thereby estimate their magnitude. A recently produced deuterated scintillator (Nuclear Enterprises NE232 - $^{6}C^{12}D$) would

be ideally suited for the purpose, but it has been noted (Bo72) that its pulse shape discrimination properties are inferior to those of NE230 C_6D_6 used in this experiment.

Another possibility is to use a deuterated anthracene ($C_{14}D_{12}$) scintillation crystal. Such a crystal is available in our laboratory. Although the proportion of deuterium to carbon atoms is not as different as for C_6D_6 its pulse shape discrimination properties have been observed to be good by other members of our group (see fig. 6.7).

In conclusion, it should be noted that the ability to separate recoil deuterons from breakup protons in deuterated scintillators offers several experimental possibilities. With additional corrections for edge effects and multiple scattering to the deuteron energy spectra, n-d elastic differential cross sections may be obtained. This has already been attempted without discriminating against breakup protons (Bl64).

Pulse shape discrimination could also be used to reduce background in kinematically complete experiments where a second detector is used to detect the breakup neutron.

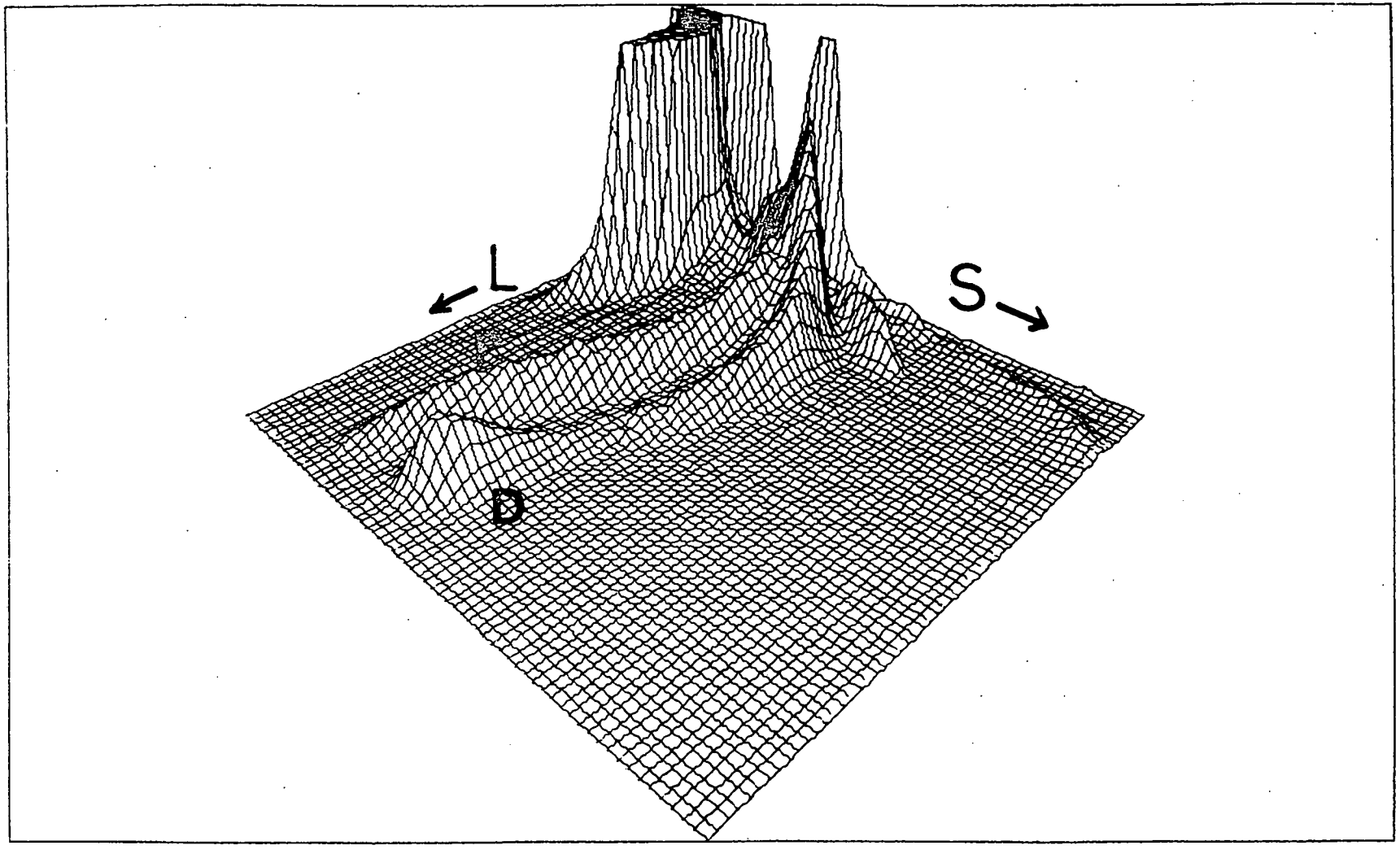

Fig. 6.7. An isometric representation of an (LS) spectrum obtained with deuterated anthracene.

REFERENCES

Aa64 R. Aaron, R.D. Amado and Y.Y.Yam, Phys. Rev., 136 (1964) B650

Aa65 R. Aaron, R.D. Amado and Y.Y. Yam, Phys. Rev., 140 (1965) B1291

Aa66 R.Aaron, and R.D. Amado, Phys. Rev., 150 (1966) 857

Aa72 J.C. Aarons and I.H. Sloan, Nucl. Phys., A182 (1972) 369

Aa72a J.C. Aarons and I.H. Sloan, Phys. Rev., C5 (1972) 582

Ah65 A. Ahmadjadeh and J.A. Tjon, Phys. Rev., 139 (1965) B1085

Al52 J.C. Allred, A.H. Armstrong, R.O. Bondelid and L. Rosen, Phys. Rev. 88 (1952) 433

Al53 J.C. Allred, A.H. Armstrong and L. Rosen, Phys. Rev., 91 (1953) 90

Al61 T.K. Alexander and F.S. Goulding, Nucl. Instr. and Meth., 13 (1961) 244

Al67 E.V. Alt, P. Grassberger and W. Sandhas, Nucl. Phys., B2 (1967) 167

Am63 R.D. Amado, Phys. Rev., 132 (1963) 485

Am69 R.D. Amado, Ann. Rev. Nucl. Sc., 19 (1969) 61

Am72 R.D. Amado, Proc. Conf. on Few Particle Problems in the Nuclear Interaction, ed. I. Slaus (North-Holland Publishing Co., and American Elsevier Publishing Co., 1972)

Ar67 J. Arvieux and J. Raynal, Nucl. Phys., A100 (1967) 473

Ar67a J. Arvieux, Nucl. Phys., A102 (1967) 513

Ar70 J. Arvieux, J.L. Durand, A. Papineau and A. Tarrats, Conf. on "Three-Body Problem in Nuclear and Particle Physics", ed. J.S.C. McKee and P.M. Rolph (North-Holland Publishing Co., Amsterdam (1970) p.213

As53 V.J. Ashby, U.C.R.I. (1953) unpublished

As58 V.J. Ashby, H.C. Catron, L.L. Newkirk and C.J. Taylor, Phys. Rev.,111 (1958) 616

Av69 Y. Avishai, M.Ebenhöh and A.S. Rinat-Reiner, Ann. Phys. (N.Y.), 55 (1969) 341

Av71 Y. Avishai and A.S. Rinat, Phys. Lett., 37B (1971) 487

Ba70 G.A. Baker,Jr., and J.L. Gammel, "The Pade Approximant in Theoretical Physics" (Academic Press, N.Y., 1970)

Ba70 P. Baumann, A. Huck and G.P. Walker, Bull. Am. Phys. Soc., 15 (1970) 567

Ba70a I. Basar et al., Conf. on "Three-Body problem in Nuclear and Particle Physics", Ed. J.S.C. McKee and P.M. Rolph (North-Holland Publishing Co., Amsterdam (1970)

Be63 G. Bellettini, C. Bemporad, C. Cerri and L. Foa, Nucl. Instr. and Meth., 21 (1963) 106

Be68 B.A. Benetskii, E.M. Burymov and I.M. Frank, Soviet J. Nucl. Phys., 8 (1968) 534

Be68 A.C. Berick, R.A. Riddle and C.M. York, Phys. Rev., 174 (1968) 1105

Be72 W. Bertl, W. Breunlich, A. Chalupka and J. Tageen, N.I.M. 104 (1972) 205-207

Bh63 B. Bhakar, Nucl. Phys., 46 (1963) 572

Bh64 V. Bhashin, Nucl. Phys., 58 (1964) 636

Bh65 V. Bhashin,G. Schrenk and A. Mitra, Phys. Rev.,137 (1965) B398

Bh65a B. Bhakar and A. Mitra, Phys. Rev. Lett., 14 (1965) 143

Bh72 S.C. Bhatt, J.S. Levinger and E. Harms, Phys. Lett., 40B (1972) 23

Bi64 J.B. Birks, "Theory and practice of scintillation counting", Pergamon Press, 1964

Bi68 G.E. Bixby and R. Smythe, Phys. Rev. 166 (1968) 946

Bl52 J.M. Blatt and V.F. Weisskopf, "Theoretical Nuclear Physics", (John Wiley and Sons Inc., 1952)

Bl64 D. Blanc, F. Cambov and G. Vedrenne, J. du Physique, 25 (1964) 678

Bo68 A. Bond, Nucl. Phys., A120 (1968) 183-192

Bo69 B.E. Bonner, E.B. Paul and G.C. Phillips, Nucl. Phys., 128 (1969) 183

Bo72 E. Bovet, P. Boschung and J. Rossel, Nucl. Instr. and Meth.,101 (1972) 315

Bo73 R. Bouchez, Acta Phys. Acad. Sci. Hung., 33 (1973) 151

Br59 F.D. Brooks, Nucl. Instr. and Meth., 4 (1959) 151

Br60 J.E. Brolley, Jr., T.M. Putnam, L. Rosen and L. Stewart, Phys. Rev., 117 (1960) 1307

Br66 B. Brunfelter, J. Kockum and H.D. Zetterstrom, N.I.M. 40 (1966) 84-88

Br70 H. Bruckmann, W. Kluge, H. Mathäy, L. Schänzler and K. Wick, Nucl. Phys., A157 (1970) 209

Br71 R. Brunig, B. Zeitnitz and J. Arvieux, Proc. Int. Symp. on Polarization Phenomena in Nuclear Reactions, ed. H.H. Barschall and W. Haeberli

Bu68 S.M. Bunker, J.M. Cameron, R.F. Carlson, J. Reginald Richardson, P. Tomas, W.T.H. Van Oers and J.W. Verba, Nucl. Phys., A113 (1968) 461

Bu72 J.P. Burq, J.C. Cabrillat, M. Chemarin, B. Ille and G. Nicolai, Nucl. Phys., A179 (1972) 371

Bu73 T.W. Burrows, Submitted to Phys. Rev.

Ca55 D.O. Caldwell and J. Reginald Richardson, Phys. Rev., 98 (1955) 28

Ca61 H.C. Catron, M.D. Goldberg, R.W. Hill, J.M. Le Blanc, J.P. Stoering, C.J. Taylor and M.A. Williamson, Phys. Rev., 123 (1961) 218

Ca70 R.T. Cahill and I.H. Sloan, "Three Body Problem in Nuclear and Particle Physics", ed. J.S.C. McKee and P.M. Rolph (North-Holland Publishing Co.)

Ca71 R.T. Cahill and I.H. Sloan, Nucl. Phys., A165 (1971) 161-179

Ca71 T.A. Cahill, J. Greenwood, H. Willmes and D.J.Shadoan, Phys. Rev., C4 (1971) 1499

Ca72 R.F. Carlson, Conf. Proc. on Few Particle Problems in the Nuclear Interaction, ed. I. Slaus et al. (North-Holland Publishing Co. and American Elsevier Publishing Co., 1972)

Ch50 G.F. Chew, Phys. Rev., 80 (1950) 196

Ch52 G.F. Chew and G.C. Wick, Phys. Rev., 85 (1952) 636

Ch59 C.N. Chou, Phys. Rev., 87 (1952) 904

Ch52a G.F. Chew and M.L. Goldberger, Phys. Rev., 87 (1952) 778

Ch53 R.S. Christian and J.L. Gammel, Phys. Rev., 91 (1953) 100

Ch59 G.F. Chew, Phys. Rev., 113 (1959) 1640

Cl72 J.M. Clement, P. Stoler, C.A. Goulding and R.W. Fairchild, Nucl. Phys., A183 (1972) 51

Co63 R. Courant and D. Hilbert, "Methods of Mathematical Physics", (Interscience Publishers, Inc., 1963)

Cr59 L. Cranberg and R.K. Smith, Phys. Rev., 113 (1959) 587

Cr63 A.H. Cromer and E.H. Thorndyke, Phys. Rev., 131 (1963) 1680

Cr63a A.H. Cromer, Phys. Rev., 129 (1963) 1681

Cr70 R.L. Craun and D.L. Smith, Nucl. Instr. and Meth., 80 (1970) 239

Cz70 J.B. Czirr, Nucl. Instr. and Meth., 88 (1970) 321

Da71 J.C. Davis and H.M. Barschall, Phys. Rev., C5 (1971) 1798

De62 L.J. De Vries and F.V. Udo, Nucl. Elec.,2 (IAEA, Vienna, 1962) 265

De66 K. Debertin, K. Hofmann and E. Rössle, Nucl. Phys., 81 (1966) 220

De69 I.M. Delves and A.C. Phillips, Rev. Mod. Phys., 41 (1969) 497

De71 I.M. Delves and M.A. Hennel, Nucl. Phys., A168 (1971) 347

Do72 P. Doleschall, Phys. Lett., 40B (1972) 443

Do72a P. Doleschall, J.C. Aarons and I.H. Sloan, Phys. Lett. 40B (1972) 605

Do72b P. Doleschall, Phys. Lett., 38B (1972) 298

Do73 P. Doleschall, Nucl. Phys., A201 (1973) 266

Do73a P. Doleschall, Private Communication

Du68 I. Duck, "Advances in Nuclear Physics", ed. M. Baranger and E. Vogt, 1968, page 343

Eb69 W. Ebenhöh, A.S. Rinat-Reiner and Y. Avishai,Phys. Lett., B29 (1969) 638

Eb72 W. Ebenhöh, Nucl. Phys., A191 (1972) 97

Ek56 H. Ekstein, Phys. Rev., 101 (1956) 880

El69 E.El Baz, C. Fayard, G.H. Lamot and J. Lafoucriere, Nuovo Cimento,A64 (1969) 13

El73 E. El Baz, C. Fayard, G.H. Lamot and J. Pigeon, Acta Phys. Acad. Sci. Hung., 33 (1973) 243

Fa61 L. Faddeev, Soviet Physics JETP, 12 (1961) 1014

Fa61a L. Faddeev, Soviet Physics "Doklady", 6 (1961) 384

Fa63 L. Faddeev, "Mathematical Problems in Quantum Theory for a Three-particle System", (Publ. Steklov Math. Inst., 1963)

Fa63a L. Faddeev, Soviet Physics "Doklady", 7 (1963) 600

Fe63 F. Ferroni and V. Wataghin, Nuovo Cimento, 28 (1963) 1342

Fi67 H. Fiedeldey, Theoretical Physics Seminar, University of Cape Town, (1967) (unpublished)

Fo62 M. Forte, A. Konsta and C. Maranzana, Nucl. Elec., 2 (IAEA, Vienna, 1962) 277

Fr54 R.M. Frank and J.L. Gammel, Phys. Rev., 93 (1954) 463

Fu69 M.G. Fuda, Phys. Rev., 186 (1969) 1078

Ga62 E. Gatti and F. De Martini, Nucl. Elec., 2 (IAEA, Vienna, 1962) 265

Gl51 R.L. Gluckstern and H.A. Bethe, Phys. Rev., 81 (1951) 761

Gl67 D.W. Glasgow and D.G. Forster, Jr., Phys. Rev., 157 (1967) 764

Go63 M.D. Goldberger, in "Progress in Fast Neutron Physics", ed. G.C. Phillips, J.B. Marion, J.R. Risser (The University of Chicago Press, 1963) page 3

Go70 M. Gouanère, M. Chemarin, G. Nicolai and J.P. Burq, Nucl. Phys., A144 (1970) 607

Gr70 R. Grubman and T. Witten, Jr., Nucl. Phys. A158 (1970) 289

Gr71 E.R. Graves and J.D. Seagrave, NCSAC 38 (1971) 116

Ha62 T. Hamada and I.D. Johnston, Nucl. Phys.,34 (1962) 382

Ha65 T. Hamade, Y. Makamura and R. Tamagaki, Progr. Theor. Phys. (Kyoto), 33 (1965) 769

Ha70 E. Harms, Phys. Rev., C1 (1970) 1667

Ha70a E.P. Harper, Y.E. Kim and A. Tubis, Phys. Rev.,C5 (1970) 877

Ha70b W. Haeberli, Proc. Conf. on the Three Body Problem in Nuclear and Particle Physics, ed. J.S.C. McKee and P.M. Rolph (North-Holland Publ. Co., 1970) page 189

Ha71 E.P. Harper, Y.E. Kim and A.Tubis, Phys. Rev. Lett., 28 (1972) 1533

Ha72 A. Hadjmichael and A.D. Jackson, Nucl. Phys., A180 (1972) 217

He72 M.A. Hennel and L.M. Delves, Phys. Lett., 40B (1972) 20

Ho69 M. Holmberg, Nucl. Phys. A129 (1969) 327-330

Ho68 A. Horsley, Nucl. Data Tables, A4 (1968) 321

Hu57 L. Hulthen and M. Sugawara, "Handbuch der Physik", ed. S. Flügge (Springer-Verlag, 1957) page 1

Hy64 L.G. Hyman, R.M. Schwarz and R.A. Schluter, Rev. Sci. Instr., 35 (1964) 393

Il61 K. Ilakovac, L.G. Kuo, M. Petravic and I. Slaus, Phys. Rev., 124 (1961) 1923

Il61a K. Ilakovac, L.G. Kuo, M. Petravic, I. Slaus and P. Tomas, Phys. Rev. Lett., 6 (1961) 356

Il63 K. Ilakovac, L.G. Kuo, M. Petravic, I. Slaus and P. Tomas, Nucl. Phys.,43 (1963) 254

Iw56 J. Iwadore, S. Otsuki, R. Tamagaki and W. Watari, Progr. Theor. Phys. (Kyoto) 3 (1956) 32

Ja69 D.F. Jackson, "Nuclear Reactions", (Methuen and Co. Ltd., 1970)

Ja70 A.D. Jackson, and J.A. Tjon, Phys. Lett., 32B (1970) 9

Ja71 A.D. Jackson, A. Lande and P.V. Sauer, Phys. Rev. Lett., 28 (1972) 1533

Ki60 S. Kikuchi, J. Sanada, S. Suwa, I. Hayashi, K. Nisimura and K. Fukinaga, J. Phys. Soc. Japan, 15 (1960) 9

Ki64 C.C.Kim, Nucl. Phys., 58 (1964) 32

Kl71 W.M. Kloet and J.A. Tjon, Phys. Lett., 37B (1971) 460

Kl72 W.M. Kloet and J.A. Tjon, Proc. Conf. on Few Nucleon Problems in the Nuclear Interaction, ed. I. Slaus et al. (North-Holland Publ. Co. and American Elsevier Publ. Co. Inc.) 380

Kl72a W.M. Kloet and J.A.Tjon, Proc. Conf. on Few Particle Problems in the Nuclear Interaction, ed. I. Slaus et al. (North-Holland Publ. Co. and American Elsevier Co. Inc., 1972) 376

Kl73 W.M. Kloet and J.A. Tjon, Nucl. Phys., A120 (1973) 380

Ko63 K. Kowalski and D. Feldman, Phys. Rev., 130 (1963) 276

Ko64 D.R. Koehler and R.A. Mann, Phys. Rev., 135 (1964) B91

Ko64a V.V. Komarov and A. Popova, Nucl. Phys., 54 (1964) 278

Ko65 D.R. Koehler, Phys. Rev., 138 (1965) B607

Ko71 L.A. CH. Koerts et al., Nucl. Instr. and Meth., 92 (1971) 157

Ko72 K. Kowalski and S.C. Pieper, Phys. Rev., C5 (1972) 324

Kr59 W.E. Kreger and B.D. Kern, Phys. Rev., 113 (1959) 890

Kr70 J. Krauss and K.L. Kowalski, Phys. Rev., C2 (1970) 1319

Kr70a J. Krauss and K.L. Kowalski, Phys. Lett., 31B (1970) 263

Ku61 A.F. Kuckes, R. Wilson and P.F. Cooper, Ann. Phys., 15 (1961) 193

Le73 J.S. Levinger, Acta Phys. Acad. Sci. Hung., 33 (1973) 135

Li63 J. Lindhard, M. Scharff and H.E. Schiøtt, Kgl. Danske Videnskab Selskab, Mat. -Fys. Meeld., 33 (1963) 14

Li37 M.S. Livingstoneand H.A. Bethe, Rev. Mod. Phys., 9 (1937) 245

Lo64 C. Lovelace, Phys. Rev., 135 (1964) B1225

Lo64a C. Lovelace, "Strong Interactions in Nuclear Physics", ed. R.G. Moorehouse, (Oliver and Boyd, London, 1964)

Lu70 R.L. Ludin, B.A. Wooten, R. Goloskie and R.G. La Montague, Phys. Rev., C5 (1970) 1740

Ma58 K.B. Mather and P. Swan, in "Nuclear Scattering", (University of Cambridge Press, 1958)

Ma69 R.A. Malfiet and J.A. Tjon, Nucl. Phys., A127 (1969) 161

Ma70 R.A. Malfiet and J.A. Tjon, Ann. Phys., 61 (1970) 425

Mc73 J.S.C. McKee, Acta Phys. Acad. Sci. Hung., 33 (1973) 167

Me65 A. Messiah, "Quantum Mechanics", (North-Holland Publ. Co., Amsterdam, 1965)

Mi55 A.B. Migdal, JETP, 28 (1955) 113

Mi62 A. Mitra, Nucl. Phys., 32 (1962) 529

Mi63 A. Mitra and V. Bhashin, Phys. Rev., 131 (1963) 1265

Mi66 A. Mitra, G. Schrenk and V. Bhashin, Ann. Phys., 40 (1966) 357

Mi69 A. Mitra, in "Advanced Nuclear Physics ", 3 (1969) 1

Na64 J.H. Naqvi, Nucl. Phys., 58 (1964) 289

Ni61 K. Nisimura, J. Phys. Soc. Japan, 16 (1961) 2097

No70 H.P. Noyes, Proc. Conf. on Three Body Problem in Nuclear and Particle Physics, ed. J.S.C. McKee and P.M. Rolph, (North-Holland Publ. Co., 1970) page 2

No70a L.C. Northcliffe and R.F. Schilling, Nucl. Data., 7 (1970) 233

No72 H.P. Noyes, Proc. Conf. on "Few Particle Problems in the Nuclear Interaction", ed. I. Slaus et al., (North-Holland Publ. Co. and American Elsevier Publ. Co., 1972) 122

Oh65 G.G. Ohlsen, Nucl. Inst. and Meth., 37 (1965) 240

Ok71 K. Okamoto and C. Pask, Ann. Phys., 68 (1971) 18

Om64 R.L. Omnes,Phys. Rev., 134 (1964) B1358

Os66 T.A. Osborn, and H.P. Noyes, Phys. Rev. Lett., 17 (1966) 215

Os69 T.A. Osborn, Nucl. Phys., A138 (1969) 305

Ow58 R.B. Owen, I.R.E. Trans. Nucl. Sci. NS-5 (1958) 198

Ph60 G.C. Phillips, T.A. Griffy and L.C. Biedenharm, Nucl. Phys., 21 (1960) 327

Ph62 R.J.M. Phillips, Nucl. Phys., 31 (1962) 643

Ph64 R.J.M. Phillips, Nucl. Phys., 53 (1964) 650

Ph66 A.C. Phillips, Phys. Rev., 142 (1966) 984

Ph66a A.C. Phillips, Phys. Rev. Lett., 20 (1966) 50

Ph68 A.C. Phillips, Nucl. Phys. A107 (1968) 209

Ph70 The "Philips Application Book for Photomultipliers" by J.M. Schonkeren, ed. H. Koter and L.J. Thompson, (supplied by "South African Philips (Pty) Ltd., 1970)

Pi72 S.C. Pieper, Nucl. Phys., A193 (1972) 529

Pi72a S.C. Pieper, Nucl. Phys., A193 (1972) 519

Pi72b S.C. Pieper and K.L. Kowalski, Phys. Rev., C5 (1972) 306

Pi72c S.C. Pieper, Phys. Rev., C6 (1972) 1157

Pi73 S.C. Pieper, Private Communication and to be published (1973)

Pu68 R.D. Purrington and J.L. Gammel, Phys. Rev., 168 (1968) 1174

RCA70 "The RCA Photomultiplier Manual", 1970 (supplied by the R.C.A. Corporation),

Re68 R.V. Reid, Ann. Phys., 50 (1968) 411

Ri68 E.M. Rimmer and P.S. Fisher, Nucl. Phys., A108 (1968) 567

Ro64 L. Rosenberg, Phys. Rev., 135 (1964) B715

Ro70 J.L. Romero, J.A. Jungerman, F.P. Brady, W.J. Knox and Y. Ishizaki, Phys. Rev., C2 (1970) 1153

Ro70 J.L. Romero, J.A. Jungerman, F.P. Brady, W.J. Knox and Y. Ishizaki, Phys. Rev., C2 (1970) 2134

Sa73 W. Sandhas, Acta Phys. Acad. Sci. Hung., 33 (1973) 109

Sc61 L. Schick, Rev. Mod. Phys., 33 (1961) 608

Sc67 G. Schrenk and A. Mitra, Phys. Rev. Lett., 19 (1967) 530

Se55 J.D. Seagrave and R.L.Henkel, Phys. Rev., 98 (1955) 666

Se55a J.D. Seagrave, Phys. Rev., 97 (1955) 757

Se70 J.D. Seagrave, Proc. Conf. on Three Body Problems in Nuclear and Particle Physics, ed. I.S.C. McKee and P.M. Rolph, (North-Holland Publ. Co., 1970)

Se72 J.D. Seagrave, J.C. Hopkins, D.R. Dixon, P.W. Keaton, Jr., E.C. Kerr, A. Hüler, R.H. Sherman and R.K. Walter, Ann. Phys., 74 (1972) 250

Sh68 S. Shirato and N. Koori, Nucl. Phys., A120 (1968) 387

Sh70 D. Shackleton, Thesis, University of Cape Town, (unpublished) 1970

Si63 A.G. Sitenko and V.F. Karchenko, Nucl. Phys., 49 (1963) 1265

Si65 A.G. Sitenko and V.F. Karchenko, Soviet J. Nucl. Phys., 1 (1965) 708

Si72 P. Signell, Proc. Conf. on "Few Particle Problems in the Nuclear Interaction", ed. I. Slaus, (North-Holland Publ. Co. and American Elsevier Publ. Co.)

Sl68 I.H. Sloan, Phys. Rev., 165 (1968) 1587

Sl69 I.H. Sloan, Nucl. Phys., A139 (1969) 337

Sl69a I.H. Sloan, Phys. Rev., 185 (1969) 1361

Sl71 I.H. Sloan, Nucl. Phys., A168 (1971) 211-224

Sl72 I.H. Sloan, Nucl. Phys., A182 (1972) 549

Sl72a I.H. Sloan, Nucl. Phys., A188 (1972) 193

Sl72b I.H. Sloan, Nucl. Phys., A198 (1972) 321

Sl73 I. Slaus, Acta Phys. Acad. Sci. Hung., 33 (1973) 191

Sm68 D.L. Smith, R.G. Polk and T.G. Miller, Nucl. Instr. and Meth., 64 (1968) 157

Sp70 D.W.L.Sprung and M.K. Srivastava, Proc. Int. Conf. on "The Properties of Nuclear States", 1970

St70 M. Stingl and A.S. Rinat, Nucl. Phys., A154 (1970) 613

Ta64 F. Tabakin, Ann. Phys., 30 (1964) 51

Ta65 F. Tabakin, Phys. Rev., 137 (1965) B75

Ta68 F. Tabakin, Phys. Rev., 174 (1968) 1208

Tj70 J.A. Tjon, B.F. Gibson and J.S. O'Connel, Phys. Rev. Lett., 25 (1970) 560

Tj70a J.A. Tjon, Phys. Rev., D1 (1970) 2109

Tr67 W. Trächslin, L. Brown, T.B. Clegg and R.G. Seyler, Phys. Lett., 25B (1967) 585

Va66 W.T.H. Van Oers and K.W. Brockman, Jr., Nucl. Phys., 21 (1960) 189

Va67 W.T.H. Van Oers and R.W. Brockmann, Jr., Nucl. Phys., A92 (1967) 561

Va67a W.T.H. Van Oers and J.D. Seagrave, Phys. Lett., B24 (1967) 562

Va71 R. Van Dantzig et al., Nucl. Instr. and Meth., 92 (1971) 199

Va71a R. Van Dantzig et al., Nucl. Instr. and Meth., 92 (1971) 205

Va71 J.C. Van der Weerd, T.R. Canada, C.L. Fink and B.L. Cohen, Phys. Rev., C3 (1971) 66

Ve57 M. Verde, in "Hundbuch der Physik", ed. S. Flügge, (Springer-Verlag, 1957)

Ve62 G. Vedrenne, D. Blanc and F. Cambou, J. de Phys., 24 (1963) 801

Vo65 V.K. Voitovetskii, I.L. Korsinskii and Yu F. Pazhin, Nucl. Phys., 69 (1965) 531

Vo65a V.K. Voitovetskii, I.L. Korsinskii and Yu F. Pazhin, Nucl. Phys., 69 (1965) 513

Wa52 K.M. Watson, Phys. Rev., 88 (1952) 1163

We63 S. Weinberg, Phys. Rev., 131 (1963) 440

We64 S. Weinberg, Phys. Rev., 133 (1964) B232

Wh58 W. Whaling, in "Hundbuch der Physik", ed. S. Flügge, (Springer-Verlag, 1958)

Wi43 G.C. Wick, Atti Acad. d'Ital., 13 (1943) 1203

Wi58 J. Williams, Phys. Rev., 110 (1958) 136

Wi72 B.J. Wielinga, G.J.F. Blommestijn, R. Van Dantzig, K. Mulder, A.D. Ijpenberg, I. Slaus, W.M. Kloet and J.A. Tjon, Proc. Conf. on "Few Particle Problems in the Nuclear Interaction", ed. I. Slaus et al., (North-Holland Publ. Co. and American Elsevier Publ. Co., 1972)

Ya54 Y. Yamaguchi, Phys. Rev., 95 (1954) 1628

Ya54a Y. Yamaguchi and Y. Yamaguchi, Phys. Rev., 95 (1954) 1635

Yu71 C.Y.Hu, Phys. Rev., C3 (1971) 2151

APPENDIX A

TWO-NUCLEON SCATTERING THEORY

Collected in this Appendix are some theoretical aspects of two-nucleon scattering theory necessary for the understanding of three-nucleon theory.

In particular, the Lipmann-Schwinger equation and some operator relationships are introduced.

For complete discussions we refer to (Ja69), (Me65), and (Du68).

A.1 The Lipmann-Schwinger Equation

We deal with spherically symmetric potentials and spinless non-identical nucleons. After separating out the centre-of-mass motion, the two-nucleon scattering problem reduces to the solution of the Schrödinger equation for one particle with reduced mass m.

$$(E-H)\psi = 0 \qquad A(1)$$

where ψ is the wave function of relative motion and H the hamiltonian

$$H = -\frac{\hbar^2}{2m}\nabla^2 + V \text{ and } E = \frac{\hbar^2 k_o^2}{2m} \qquad A(2)$$

$$= H_o + V$$

where H_o is known as the free-particle hamiltonian.

The asymptotic behaviour of the wave function is given by

$$\psi(\underset{\sim}{r}) \underset{\infty}{\rightarrow} \phi_o(x) + f(\theta) \frac{e^{ik_o r}}{r} \qquad A(3)$$

where ϕ_o is an incoming plane wave along the z direction

$$\phi_o(r) = e^{ik_o z} \qquad A(4)$$

and $f(\theta)$ is the scattering amplitude.

Equation (1) may be solved for ψ and the scattering amplitude obtained by matching the actual wave function to the asymptotic form at some point outside the potential.

Alternatively, by using operator algebra, the equation can be recast directly into an equation for the scattering amplitudes. Equation (1) can be written as

$$\psi = \frac{V\psi}{E-H_o} + \phi_o \qquad A(5)$$

where ϕ_o is given above. It is the solution of the homogeneous equation

$$(E - H_o)\ \phi_o = 0 \qquad A(6)$$

Equation (5) is an operator equation which is given meaning by inserting complete sets of eigenstates, e.g.

$$\langle r|\psi\rangle = \langle r|k_o\rangle + \langle r|G_o|r'\rangle\langle r'|V|\psi\rangle \qquad A(7)$$

It is an integral equation of the Fredholm type which can be written

$$\psi(\underset{\sim}{r}) = \phi_o + \int G_o(r,r')V(r')\ (r')dr' \qquad A(8)$$

where $G_o = \frac{1}{E-H_o}$

G_o is known as the free-particle Green's function. It contains a singularity at $k = \sqrt{2mE}$ which is avoided by giving E a

This is an integral equation for the scattering amplitude and is known as the Lipmann-Schwinger equation.

A.2 Off-shell Elements of the T-matrix

Elements of the T-matrix define the scattering amplitudes

$$-\frac{m}{2\pi\hbar^2}\ \langle k|T|k_o\rangle\ =\ f(\theta)$$

If energy is conserved, i.e.

$$\frac{\hbar^2k^2}{2m}\ =\ \frac{\hbar^2k_o^2}{2m}\ =\ E$$

the matrix element is said to be on the energy shell while, if either

$$\frac{\hbar^2k^2}{2m}\ \neq\ E$$

or

$$\frac{\hbar^2k_o^2}{2m}\ \neq\ E$$

or

$$\frac{\hbar^2k_o^2}{2m}\quad\text{and}\quad\frac{\hbar^2k^2}{2m}\ \neq\ E$$

the matrix elements are said to be off the energy shell. In the first two cases above, they are said to be "half off" or "off at one end", while in the third, they are "completely off".

Clearly, such situations do not arise physically, but in employing the Lipmann-Schwinger equation, matrix elements must be defined both on, and off, the energy shell.

For transitions from a state α to a state β, the T-matrix is related to the scattering (S-) matrix by

$$S_{\beta\alpha} = \delta_{\beta\alpha} - 2\pi i\, \delta(E_\beta - E_\alpha)\, \langle\phi_\beta|V|\psi_\alpha\rangle$$

$$= \delta_{\beta\alpha} - 2\pi i\, \delta(E_\beta - E_\alpha)\, \langle\phi_\beta|T|\phi_\alpha\rangle \qquad A(16)$$

A.3 Operator Identities

By manipulating the operators according to operator algebra, some useful identities can be derived. Besides the Lipmann-Schwinger equation as given above, viz.

$$T = V + V\, G_o\, T \qquad A(15)$$

one obtains

$$T = V + T\, G_o\, V \qquad A(17)$$

and $$T = V + V\, G\, V \qquad A(18)$$

where

$$G = \frac{1}{E-H} = \frac{1}{E-H_o-V} \qquad A(19)$$

G is related to G_o by

$$G = G_o + G_o\, V\, G \qquad A(20)$$

G is known as the full Green's function. Its set of matrix elements in the complete space of all the solutions of the corresponding Hamiltonian, is known as its spectral resolution. This may be written

$$G(E) = \sum_B |\psi_B\rangle (E-E_B)^{-1} \langle\psi_B| + \int d\underset{\sim}{k}\, |k\rangle \left(E - \frac{h^2}{2m} k^2\right)^{-1} \langle k| \qquad A(21)$$

where the ψ_B's are bound state wave functions.

A.4 Methods of Solution

Equation A(15) may be formally solved by inversion, i.e.

$$T = \frac{1}{(1 + V G_o)} V \qquad A(22)$$

or by iteration, i.e.

$$T = V + V G_o V + V G_o V G_o V + \ldots\ldots\ldots \qquad A(23)$$

Equation A(23) is known as the perturbation, or multiple scattering expansion. Usually, equation A(15) is reduced to a one-dimensional integral equation by making a partial wave expansion of transition amplitude

$$\langle k|T|k_o\rangle = \sum_{\ell=o}^{\infty} (2\ell+1) \; T_\ell(k,k_o) P_\ell(\cos\theta) \qquad A(24)$$

where $P_\ell(\cos\theta)$ is a Legendre Polynomial, and

$$\cos\theta = \frac{\underset{\sim}{k}.\underset{\sim}{k}_o}{|\underset{\sim}{k}.\underset{\sim}{k}_o|}$$

then, equation A(15) for partial wave ℓ, is written

$$T_\ell(k,k_o) = V_\ell(k,k_o) + \int K_\ell(k,k') T_\ell(k',k_o) dk' \qquad A(25)$$

where

$$K_\ell(k,k') = \frac{k^2}{2\pi^2} \frac{V_\ell(k,k')}{\left(E - \frac{h^2 k'^2}{2m}\right)}$$

is known as the kernel. A condition for equation A(25) to be amenable to standard techniques of solution, is that it be square integrable (Co63)

$$\int |K_\ell(k',k)|^2 d\underset{\sim}{k} d\underset{\sim}{k}' < \infty \qquad A(26)$$

APPENDIX B

KINEMATICS AND PHASE SPACE

Collected in this appendix are some expressions for two and three-body kinematics and phase space. The coordinate system and many of the expressions are, with a few changes in notation, those of Ohlsen (Oh68). For derivations of these we refer to the original text. We consider a case where a particle is incident on the bound state system of two particles which we call the target. The subscripts 1, 2 and 3 refer to the individual particles, and the subscript t to the target. Subscripts c and c_i refer to the centre-of-mass of the total system and that of particles j and k respectively (i,j,k = 1,2 or 3 and i ≠ j or k). The coordinates referring to the incident particle are denoted by a subscript 0. Fig. B 1(a)is a velocity diagram for the special case where $m_2 = m_3$. It can also be used as a coordinate diagram by replacing the v's with r's. Fig.B1(b) is a velocity triangle for particle 1. The coordinates of each particle in the C system can be related to the lab coordinates in terms of the angles and sides of a similar triangle. For this case, we record the following expressions:

$$a = (\tfrac{1}{2}m\,V^2)^{\frac{1}{2}} = (m_1 m_0 E^{\ell})^{\frac{1}{2}}/(m_0 + m_t) \qquad (B.1)$$

$$V = (2m_0 E_0^{\ell})^{\frac{1}{2}}/(m_0 + m_t) \qquad (B.2)$$

$$E_1^C = \tfrac{1}{2}m_1 (v_1^C)^2 = E_1^{\ell} - 2a_1 (E_1^{\ell})^{\frac{1}{2}} \cos\theta_1^{\ell} + (a_1)^2 \qquad (B.3)$$

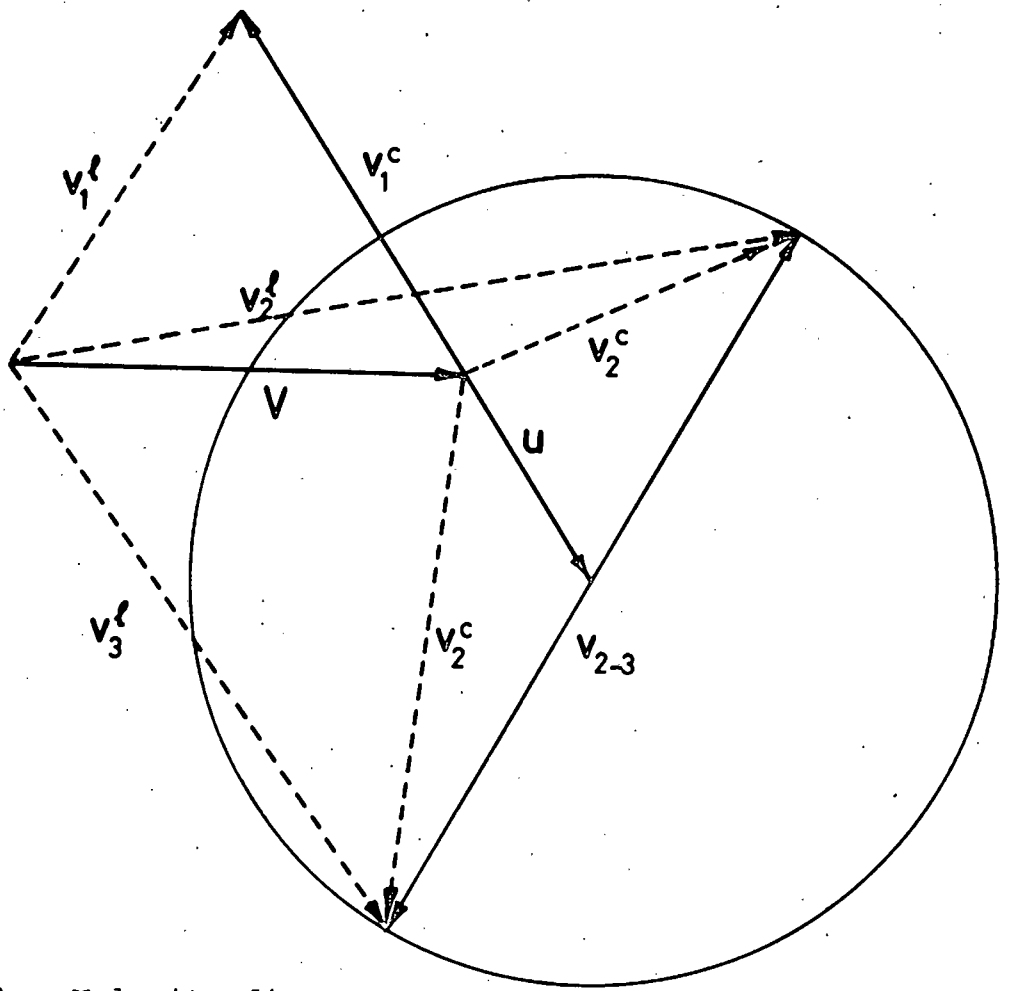

Fig.B1(a). Velocity diagram representing 3 particles in the final state for $m_1 = m_2$.

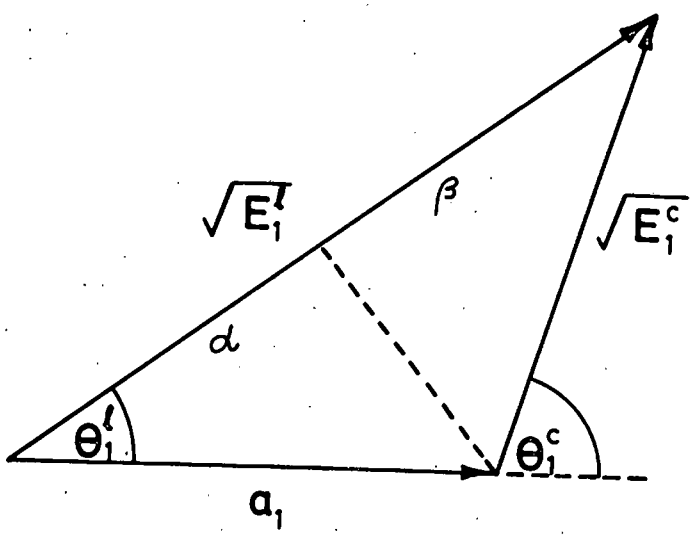

Fig.B1(b). Velocity diagram of a single particle relating the c.m. motion to the lab. motion.

$$\cos\theta_1^c = \frac{(E_1^\ell)^{\frac{1}{2}}\cos\theta_1^\ell - a_1}{[E_1^\ell - 2a_1(E_1^\ell)^{\frac{1}{2}}\cos\theta_1^\ell + (a_1)^2]^{\frac{1}{2}}} \qquad (B.4)$$

$$\phi_1^c = \phi_1^\ell \qquad (B.5)$$

The inverse relations are:

$$E_1^\ell = E_1^c + 2a_1(E_1^c)^{\frac{1}{2}}\cos\theta_1^c + (a_1)^2 \qquad (B.6)$$

$$\cos\theta_1 = \frac{(E_1^c)^{\frac{1}{2}}\cos\theta_1^c + a_1^2}{[E_1^c + 2a_1(E_1^c)^{\frac{1}{2}}\cos\ {}^c_1 + (a_1)^2]^{\frac{1}{2}}} \qquad (B.7)$$

Each particle i has a maximum energy in the c system when the energy in the c_i system is zero. In the case represented by fig. 1 this occurs when $v_{2-3} = 0$. The pair (2,3) then corresponds to a single particle of mass $m_2 + m_3$ and we can determine maximum energies and angles in terms of two-body kinematics.

$$E_1^c(\max) = \frac{(m_3 + m_2)E_{tot}^c}{M} \qquad (B.8)$$

where $$E_{tot}^c = \frac{Q + m_t E_o^\ell}{(m_o + m_t)} \qquad (B.9)$$

where Q is the reaction Q-value

and $M = (m_1 + m_2 + m_3)$

One can determine maximum energies and angles of emission in the laboratory frame in terms of the quantities α and β (see fig. B1(b)) and γ where

$$\alpha = a_1 \cos \theta_1^{\ell} \tag{B.10}$$

$$\beta = [E_{1\ max}^{c} - (a_1 \sin\theta_1^{\ell})^2]^{\frac{1}{2}} \tag{B.11}$$

$$\gamma = [E_{1\ max}^{c}]^{\frac{1}{2}}/a_1 \tag{B.12}$$

For any angle of emission θ_1^{ℓ}, the maximum and minimum laboratory energies are given by

$$E_{1\ max}^{\ell} = (\alpha + \beta)^2 \tag{B.13}$$

$$E_{1\ min} = (\alpha - \beta)^2 \quad \text{if} \quad \alpha > \beta \tag{B.14}$$

$$= 0 \quad \text{if} \quad \alpha \leq \beta$$

while the maximum laboratory angle of emission is given by

$$\theta_{1(max)}^{\ell} = \sin^{-1}\gamma \quad \text{if} \quad \alpha \leq 1 \tag{B.15}$$

$$= 180^{\circ} \quad \text{if} \quad \gamma > 1$$

It is often convenient to describe the system in terms of relative coordinates defined by

$$R = (m_1 \underset{\sim}{r}_1 + m_2 \underset{\sim}{r}_2 + m_3 \underset{\sim}{r}_3)/M \tag{B.16}$$

$$r_{1-23} = \underset{\sim}{r}_1 - \frac{(m_2 \underset{\sim}{r}_2) + (m_3 \underset{\sim}{r}_3)}{(m_2 + m_3)} \tag{B.17}$$

$$r_{2-3} = \underset{\sim}{r}_2 - \underset{\sim}{r}_3 \tag{B.18}$$

with reduced masses

$$\mu_{1-23} = \frac{m_1 (m_2 + m_3)}{M} \tag{B.19}$$

$$\mu_{2-3} = \frac{m_2 m_3}{(m_2 + m_3)}$$

and associated momenta

$$\underset{\sim}{P} = \underset{\sim}{p}_1 + \underset{\sim}{p}_2 + \underset{\sim}{p}_3$$

$$\underset{\sim}{P}_{1-23} = \mu_{1-23} \dot{\underset{\sim}{r}}_{1-23} \qquad \text{(B.20)}$$

$$\underset{\sim}{P}_{2-3} = \mu_{2-3} \dot{\underset{\sim}{r}}_{2-3}$$

$$\text{then } E_{tot} = \frac{\underset{\sim}{P}^2_{1-23}}{2\mu_{1-23}} + \frac{\underset{\sim}{P}^2_{2-3}}{2\mu_{2-3}} + \frac{\underset{\sim}{P}^2}{2M} \qquad \text{(B.21)}$$

$$\text{i.e.} \quad E^C_{tot} = E_{1-23} + E_{2-3} \qquad \text{(B.22)}$$

$$\text{A useful relation is } E_{1-23} = \frac{M E^C_1}{(m_1 + m_3)} \qquad \text{(B.23)}$$

The problem is now reduced to that for two equivalent two-body system in C and C^i. In the text the following notation is often used

$$\begin{aligned} \hbar k &= \underset{\sim}{P} = \underset{\sim}{P}_{i-jk} \\ \hbar k' &= \underset{\sim}{P}' = \underset{\sim}{P}_{j-k} \end{aligned} \qquad \text{(B.24)}$$

The density of final states, or phase space, is given by

$$\rho d\tau = \frac{1}{\hbar^6} \int d\underset{\sim}{p}_1 d\underset{\sim}{p}_2 d\underset{\sim}{p}_3 \, \delta(P - p_1 - p_2 - p_3) \delta(E - E_1 - E_2 - E_3)$$

(B.25)

In the relative coordinate system this reduces to

$$\rho d\tau = \frac{2}{h^6}\left(\frac{m_1 m_2 m_3}{M}\right)^{3/2}\left[E_{1-23}\left(E^c_{tot}-E_{1-23}\right)\right]^{\frac{1}{2}} dE_{1-23}\, d\Omega_{1-23}\, d\Omega_{2-3} \tag{B.26}$$

The variables are permuted to obtain the corresponding expression for other relative variables.

The above form is easily related to the centre-of-mass coordinates and to the laboratory coordinates by the given kinematic relations and by

$$\frac{\partial\,(E_1^c\,,\ \cos\theta_1^c\ \phi_1^c)}{\partial\,(E_1^\ell\,,\ \cos\theta_1^\ell\ \phi_1^\ell)} = \left(\frac{E_1^\ell}{E_1^c}\right)^{\frac{1}{2}} \tag{B.27}$$

One obtains

$$\rho dE_1^\ell d\Omega_1^\ell = \frac{2}{h^6} M^{\frac{1}{2}} \frac{(m_1 m_2 m_3)^{3/2}}{(m_2+m_3)}\left(E_1^\ell \frac{m_2+m_3}{M} E^c_{tot} - E_1^\ell + 2a_1 (E_1^\ell)^{\frac{1}{2}}\cos\theta_1^\ell - a_1^2\right)^{\frac{1}{2}} \tag{B.28}$$

which for convenience we write

$$\rho dE_1^\ell d\Omega_1^\ell = -a(b + \cos\theta_1^\ell)^{\frac{1}{2}}\, d(\cos\theta_1^\ell)\, d\phi_1^\ell\, dE_1^\ell \tag{B.29}$$

where

$$\begin{aligned} a(E_1^\ell) &= \frac{2}{h^6} M^{\frac{1}{2}} \frac{(m_1 m_2 m_3)^{3/2}}{(m_2+m_3)^2} (E_1^\ell)^{\frac{1}{2}} \\ b(E_1^\ell) &= \left(\frac{(m_2+m_3)}{M} E^c_{tot} - E_1^\ell - a_1^2\right) \\ c(E_1^\ell) &= 2a_1 (E_1^\ell)^{\frac{1}{2}} \end{aligned} \tag{B.30}$$

To obtain $\rho(E_1^{\ell})$, we integrate over $d\Omega_1^{\ell}$ and obtain

$$\rho(E_1^{\ell})dE_1^{\ell} = \frac{4\pi a}{3c} \left[(b + c)^{3/2} - (b + cx_m)\right]^{3/2} \qquad (B.31)$$

where $x_m = \cos\theta_{1max}$ (E_1^{ℓ}) is the upper limit of integration and is given by (B.3)

$$\cos\theta_m = - \frac{E^c_{max} + E_1^{\ell} + a_1^2}{2a_1(E_1^{\ell})^{\frac{1}{2}}} \qquad (B.32)$$

APPENDIX C

PARAMETRISED CROSS SECTIONS

(a) N-d differential cross sections

It has been proposed by Ludin (Lu70) that, in the range 1-21 MeV, the n-d differential cross sections are well represented by

$$\frac{d\sigma}{d\Omega}(\theta) = N\left|e^{\alpha\mu} - \eta\, e^{i\phi}\, e^{-\beta\mu}\right|^2 \qquad (C.1)$$

where $N = 126.5\, e^{-E/7.05}$

$\eta = 1/(\sqrt{2}E)$

$\phi = 100\, e^{-E/13.7} - 130\, e^{-E/0.436}$

$\alpha = 0.0222\, E + 0.542$

$\beta = 1.01\, \ell n\, (E/0.347)$

E = incident neutron energy

This may be written

$$\frac{d\sigma}{d\Omega}(\theta) = A\, e^{2\alpha\mu} + B\, e^{-2\beta\mu} - C\, e^{(\alpha-\beta)\mu}$$

where $A = N$

$B = \eta^2 N$

$C = 2\eta \cos\phi\, N$

This formula has been used in this work to obtain pulse-height distributions (see fig. 5.2) which are compared with the measured ones to obtain the detector resolution and the shift of the forward recoil peak due to finite detector resolution (see Chapter 5).

The formula was also used to calculate s, σ_{peak} and

$\cos \theta_m^c$ (see figs. 5.6 and 5.7). It is found that the formula is in good agreement with experiment below 14 MeV, but that it deviates at higher energies.

(b) N-d total cross section

Seagrave and Henkel (Se55) have given an expression which approximates the total n-d cross section with a 1.4% r.m.s. deviation

$$= \frac{14.35}{(E_n + 3.6)\ \text{MeV}}$$

This formula has been used to compute total n-d cross sections which are required to obtain the total breakup cross section with method B (see Chapter 5, section 5).

APPENDIX D

THE RELATION BETWEEN PROTON AND DEUTERON RESPONSE

Semi-empirical formulae for the scintillation response as a function of particle type and particle energy are based on the assumption that the light dL due to the energy deposited in an interval Δx also depends on the specific energy loss dE/dx alone. For example the Birks formula is

$$\frac{dL}{dx} = \frac{S(-dE/dx)}{[1 + kB(-dE/dx)]}$$

or

$$\frac{dL}{dE} = \frac{-SdE}{[1 + kB(-dE/dx)]} \qquad (D.1)$$

For ions having velocities large compared with the velocities of the most energetic electrons in the stopping atoms, dE/dx is well understood in terms of the Livingstone-Bethe formula†.

$$(-dE/dx) = (z^2 Zne^4/4\pi\varepsilon_o^2 m_o v^2)[\ell n(2m_o v^2/I) - \ell n(1-\beta^2) - \beta^2] \qquad (D.2)$$

where m_o is the electron rest mass

v is the velocity of the charged particle

---

†At proton energies 0.05 MeV the Livingstone-Bethe formula can not be applied in the given form. However, a departure from the assumptions based on the formula of such low energies will have a negligible effect on the conclusions drawn for protons and deuterons in the MeV range.

and z is the charge in units of e of the particle.

Since protons and deuterons both have z = 1, they will have the same dE/dx at the same velocity. Therefore

$$(dE/dx)_p(E) = (dE/dx)_D(2E) \qquad (D.3)$$

According to an expression f(dE/dx) such as (A.1), the light output L, for a proton having energy E is given by

$$L_p(E) = \int_0^E f(dE/dx)_p(E)\,dE$$

and, using (D.3), one can write this in terms of $(dE/dx)_D$ i.e.

$$L_p,(E) = \int_0^E f(dE/dx)_D(2E)\,dE$$

Changing the variables

$$L_p(E) = \tfrac{1}{2} \int_0^{2E} f(dE/dx)_D(2E)\,d(2E)$$

or

$$L_p(E) = \tfrac{1}{2} L_D(2E) \qquad (D.4)$$

APPENDIX E

COMPUTATIONAL METHODS

All raw data was stored on magnetic tape and processed on an off-line Univac 1106 Computer of the University of Cape Town.

During the first stage of analyses, two-dimensional plots (contour and isometric - see figs. 4.6 and 4.2) were obtained and the ridges corresponding to each ionising particle were projected onto the L-axis to obtain pulse-height distributions. This was done using programs which were already available.

To obtain "smeared" pulse-height distributions for comparison with the measured ones, parametrized forms of the elastic differential elastic cross section (see Appendix C and Chapter 5) were used in epxression 5.3. The numerical integration was performed by a method of Gaussian quadrature. The resolution σ (see expression 5.5), energy calibration points and peak shift were those giving a best χ^2 fit to the forward recoil deuteron peak. (see Chapter 5, section 2)

The response was calculated from Birks formula (expression 5.10) by the same method of numerical integration and KB was varied to obtain a best χ^2 fit to the response data from ($L\tau$) measurements. (see Chapter 5, section 3).

Using the value of KB thus obtained the response was calculated for a series of energies between 0.5 and 20 MeV, This table of values, together with an interpretation routine of the Aitken type were used as a standard relative response.

The specific energy loss (dE/dx) as a function of deuteron energy was specified in similar manner. In both cases, the logs of these quantities were interpolated since they have a

smoother energy dependence.

Aitken interpolation was used because it does not require the interpolation step to be constant.

Integrations over phase space to obtain corrections for edge effects (see Chapter 5, section 7) were also performed numerically.